MINISTERE DE L'ENSEIGNEMENT SUPERIEUR ET DE LA REÇHERCHESCIENTIFIQUE
****
UNIVERSITE DES SCIENCES, DES TECHNIQUES ET DESTECHNOLOGTES DE BAMAKO (USTTB)
****
ECOLE DOCTORALE DES SCIENCES ET TECHNOLOGIES DU MALI (EDSTM)

REPUBLIQUE DU MALI
****
Un Peuple - Un But - Une Foi

DOCTORATE THESIS

THEME

FIELD EXPERIMENTAL AND MODELLING ASSESSMENT OF THE EFFECTS OF DIFFERENT WATER MANAGEMENT AND N-FERTILIZER LEVELS ON CO_2 EMISSIONS, NET ECOSYSTEM CARBON BALANCE AND RICE PRODUCTION

****

A thesis, in the Rural Polytechnic Institute of Training and Applied Research (IPR/IFRA) in partnership with the West African Science Service Centre on Climate Change and Adapted Land use (WASCAL), submitted in partial fulfilment of the requirements for the Doctor of Philosophy in Climate Change and Agriculture of the University of Sciences, Techniques and Technologies of Bamako (USTTB)

Presented and defended on 19 /05/2023.

by
COFFI LEONCE GEOFROY SOSSA

JURY

President: Dr Sabaké DIARRA, Associate Professor, IPR/IFRA, Mali

Examiner: Dr Souleymane KEITA, Assistant Professor, ENI/ABT, Mali

Reporter: Dr Kaboro SAMASSE, Assistant Professor, IPR/IFRA, Mali

Reporter: Dr Adama TOURE, Assistant Professor, ENI/ABT, Mali

Director: Dr Souleymane SANOGO, Associate Professor, FST, Mali

Co-Director: Prof. Dr. Luc O. SINTONDJI, Full Professor, INE/UAC, Benin

FIELD EXPERIMENTAL AND MODELLING ASSESSMENT OF THE EFFECTS OF DIFFERENT WATER MANAGEMENT AND N-FERTILIZER LEVELS ON CO_2 EMISSIONS, NET ECOSYSTEM CARBON BALANCE AND RICE PRODUCTION

BY

COFFI LEONCE GEOFROY SOSSA

Msc. Rural Engineering and Water Management

(MATRICULE NUMBER: 10041011)

A THESIS

IN THE RURAL POLYTECHNIC INSTITUTE OF TRAINING AND APPLIED RESEARCH IN PARTNERSHIP WITH THE WEST AFRICAN SCIENCE SERVICE CENTRE ON CLIMATE CHANGE AND ADAPTED LAND USE (WASCAL), SUBMITTED TO THE SCHOOL OF POSTGRADUATE STUDIES, IN PARTIAL FULFILMENT OF THE REQUIREMENT FOR THE AWARD OF THE DEGREE OF DOCTOR OF PHILOSOPHY IN CLIMATE CHANGE AND AGRICULTURE OF THE UNIVERSITY OF SCIENCES, TECHNIQUES AND TECHNOLOGIES OF BAMAKO (USTTB), BAMAKO, MALI

MAY ,2023

CERTIFICATION

By the student:

This work has not been presented elsewhere for the award of a degree, or any other purpose.

Candidate's Name: Coffi Leonce Geoffroy Sossa

Signature: Date: 25.05.2023

b) By the supervisor(s):

I certify that this work has been carried out by M. Coffi Leonce Geoffroy Sossa under my supervision and that to the best of my knowledge, it has not been submitted elsewhere for the award of a degree.

Major supervisor: Dr. Souleymane Sanogo

Signature: Date: 25.05.2023

Co-supervisor: Dr. Jesse B. Naab

Signature: Date: 26.05.2023

Co-supervisor: Prof. Dr. Luc O. Sintondji

Signature: Date: 26.05.2023

Adviser: Dr. Mathias Hoffmann

Signature: Date: 26.05.2023

Adviser: Prof. Dr. Jürgen Augustin

Signature: Date: 26.05.2023

Table of content

DEDICATION

- ✓ To the Almighty GOD for his protection 🙏
- ✓ To my parents, *Guy Codjo SOSSA* and *Ayaba Catherine KOUDONOU* for their sacrifice and confidence
- ✓ To my wife and my children, *Nelson Geovany* and *Emma Blessing* for their love and patience
- ✓ To my sisters for their love and support

ACKNOWLEDGMENT

First, I would like to thank my committee – Dr. Souleymane Sanogo, Dr. Jesse Bonaventure Naab, Prof. Luc Sintondji, Prof. Jürgen Augustin, and Dr. Mathias Hoffmann for their invaluable guidance throughout this study.

Special thanks go to the staff of the WASCAL Graduate Research Program (GRP) in Climate Change and Agriculture (CC&Agic), led by Dr. Yacouba DIALLO, for their constant support. My thanks are also going to the amazing and lovely people from MonKsHillLab at the Leibniz Centre for Agricultural Landscape Research (ZALF), working group for Isotope Biogeochemistry and Gas Fluxes, Germany. I really enjoyed my stay while having fun in the field, and I am looking forward to meeting you all again.

I profoundly acknowledge all the people who helped me during my field work. Some of those included Mr. Charles N'Gnanou, Expedit Lomikpo, and all Koussin-Lele's farmers.

I wish to thank my colleagues from batch 3 of WASCAL GRP CC & Agric for creating a nice work atmosphere and providing mutual support.

Finally, this work could not be achieved without the financial support of certain organizations/institutions, which I would like to sincerely thank:

- ✓ The BMBF through the West Africa Science Service Center on Climate Change and Adapted Land Use (WASCAL) program,
- ✓ The IPCC Scholarship Program through the Foundation Prince Albert II of Monaco,
- ✓ The International Foundation for Science (IFS) Research Grants,
- ✓ The Climate, Food and Farming, Global Research Alliance Development Scholarships (CLIFF-GRADS).

LIST OF ACRONYMS AND ABBREVIATIONS

(N) FT-(N)SS	(Non)-Flow-Through (Non)-Steady-State
A	Basal Area
AWD	Alternate Wetting and Drying
CEC	Cation exchange capacity
CH_4	Methane
CO_2	Carbon Dioxide
CF	Continuous Flooding
D	Day
DSSAT	Decision Support System for Agrotechnology Transfer
dc	Change In Gas Concentration During Measurement.
DOM	Day Of the Measurement
DOY	Day Of the Year
E_0	Activation Energy [K]
GHG	Greenhouse Gas
GPmax	Maximum Rate of Carbon Fixation at Par Infinite
GPP	Gross Primary Production
GWP	Global Warming Potential
IPCC	Intergovernmental Panel on Climate Change
IRGA	Infrared Gas Analyzer
^{o} K	Degree Kelvin
M	Molar Mass [G C, N Mol^{-1}]
N_2O	Nitrous Oxide
NDVI	Normalized Difference Vegetation Index
NECB	Net Ecosystem Carbon Balance
NEE	Net Ecosystem Exchange
OC	Organic Carbon
OM	Organic matter
p	Air Pressure
Pa	Pascal
PAR	Photosynthetic Active Radiation
PVC	Polyvinyl Chloride
R	Ideal Gas Constant [8.3143 m^3 Pa K^{-1} Mol^{-1}]

Ra	Autotrophic Respiration
BG_Ra	Belowground Autotrophic (Root) Respiration
Ra (shoot)	Aboveground Autotrophic (Shoot) Respiration
Reco	Ecosystem Respiration
Rh	Heterotrophic Respiration
RRef	Ecosystem Respiration at Reference Temperature
Rsoil	Sol Respiration (BG_Ra + Rh)
S	Second
SOC	Soil Organic Carbon
SOM	Soil Organic Matter
SWC	Soil Water Content
T	Temperature
t	Time
T_0	Temperature Constant for start of biological process.
TRef	Reference Temperature
SD	Standard Deviation

LIST OF FIGURES

LIST OF TABLES

ABSTRACT

Accurate measurement of carbon dioxide (CO_2) emissions and water (H_2O) fluxes is crucial for reducing global greenhouse gas (GHG) emissions and mitigating climate change, especially in agricultural land systems. To explore effective ways to improve rice production in Benin while protecting the environment, an adaptive, low-cost, open-source data logger has been developed to measure CO_2, evapotranspiration (ET), and estimate the net carbon (C) balance from irrigated lowland rice cultivation in Benin. Laboratory tests and field validation on different Non-Dispersive Infrared (NDIR) sensors showed that the K30 Fr and SCD30 sensors are the most accurate compared to the Li-COR 850 IRGA. The field application aims to identify the best farming management practices that improve water and nitrogen use efficiency, grain yield, and the net ecosystem carbon balance while keeping CO_2 emissions low. It was established at Koussin-Lele, southern Benin, using a split plot design where the main plot is different water management, and the subplot is different level of nitrogen fertilizer. The water management included continuous flooding (CF) and two levels of alternate wetting and drying at 15 cm and 25 cm thresholds (AWD_{15} and AWD_{25}). The different levels of nitrogen fertilizer were: no nitrogen, N90 kg ha^{-1}, and N120 kg ha^{-1}. To measure gaseous seasonal C emissions and soil CO_2 respiration, the NFT-NSS closed chamber system is used, and results showed that both net ecosystem exchange, the net C balance, and evaporation were higher under AWD_{15} and CF even though all the treatments are sinks of carbon. The heterotrophic respiration was higher under AWD_{25}. In terms of water productivity, grain yield, and N uptake, results showed that the treatment AWD_{15} with N 90 kg ha^{-1} is the best. Consequently, this treatment should be promoted to reduce costs resulting from fertilizer inputs, conserve yield, and combat water scarcity. In addition, the calibration of the DSSAT CERES rice model was successful in simulating growth and yield, and the results illustrated that the model is a useful tool for evaluating alternative management options to maintain yields while saving water. As a recommendation, for further study, it could be interesting to add manure fertilizer and assess CH_4 emissions from each treatment. In perspective, this study will help to make decisions regarding the C balance and the optimization of water and nitrogen inputs for sustainable irrigated rice.

Key words: CO_2, Net ecosystem Carbon balance, Water, nitrogen, CERES Rice

RÉSUMÉ

La mesure précise des émissions de dioxyde de carbone (CO_2) et des flux d'eau (H_2O) est essentielle pour réduire les émissions de gaz à effet de serre (GES) et atténuer le changement climatique, en particulier dans les systèmes de terres agricoles. Afin d'explorer des moyens efficaces d'améliorer la production de riz au Bénin tout en protégeant l'environnement, un enregistreur de données adaptatif et peu coûteux a été développé pour mesurer le CO_2, l'évapotranspiration et estimer le bilan en carbone de la riziculture irriguée au Bénin. Les tests en laboratoire et la validation sur le terrain en utilisant différents capteurs ont montré que les capteurs K30 Fr et SCD30 sont plus précis et présentent des réponses comparatives au Li-COR 850 IRGA. L'utilisation de nouvel équipent sur le terrain vise à identifier les meilleures pratiques de gestion agricole qui améliorent l'efficacité de l'utilisation de l'eau et de l'azote, le rendement des céréales et le bilan en séquestration de carbone tout en réduisant les émissions de CO_2. L'essai a été installé à Koussin-Lele, dans le sud du Bénin, en utilisant le dispositif split plot où la gestion de l'eau était le facteur principal et comprenait l'irrigation continue (CF) et deux niveaux d'alternance d'humidification et de séchage à des seuils de 15 cm et 25 cm (AWD15 et AWD25). Pour les sous-parcelle, trois niveaux d'engrais (urée) ont été considérés (pas d'azote, 90 kg ha^{-1} et 120 kg ha^{-1}). Pour mesurer les émissions saisonnières du carbone et la respiration du CO_2 dans le sol, le système de chambre fermée a été utilisé. Les résultats ont montré que les échanges de CO_2, le bilan net en carbone et l'évaporation étaient plus élevés avec AWD15 et CF, même si tous les traitements étaient des puits de carbone. La respiration hétérotrophe était plus élevée sous AWD25. En termes de productivité de l'eau, de rendement en grains et d'absorption d'azote, les résultats ont montré que le traitement AWD15 avec 90 kg ha^{-1} d'azote était le meilleur avec une réduction d'eau de près de 32% par rapport à l'irrigation continue. Par conséquent, ce traitement devrait être encouragé pour réduire les coûts résultant des apports d'engrais, conserver le rendement et lutter contre la rareté d'eau. En outre, l'étalonnage du modèle DSSAT-CERES a réussi à simuler la croissance et le rendement. Les résultats ont montré que le modèle est un outil utile pour évaluer les options de gestion alternatives afin de maintenir les rendements tout en économisant l'eau. En guise de recommandation, il serait intéressant d'ajouter des engrais à base de fumier et d'évaluer les émissions de CH_4 de chaque traitement dans le cadre d'une étude plus approfondie. En perspective, cette étude aidera à prendre des décisions concernant le bilan en carbone et l'optimisation des apports d'eau et d'azote pour la production durable du riz irriguée.

Mot clés : CO_2, bilan net de l'écosystème en carbone, gestion de l'eau, azote, CERES Rice

CHAPTER ONE

INTRODUCTION

1.1 Problem and Justification

Global agriculture is currently facing the challenges of an increase in food demand to feed the rapidly growing world population and a reduction in global water resource availability (GRISP 2010; Islam et al., 2020). Water availability is likely to reduce under the projected climate change scenarios consisting of reduced rainfall and an increase in temperatures, leading to more frequent and severe events of water scarcity. Over the past few decades, water scarcity has emerged as one of the biggest challenges for sustaining rice production, which threatens irrigated lowland rice production. With the reduction of water availability for agriculture, saving water and increasing rice productivity have become major challenges for many rice producers. Facing this situation, determining the crop-water requirement is a first step in the planning, design, and operation of irrigation projects (Trajkovic et al., 2009). Therefore, it requires estimating reference crop evapotranspiration (ETo). Evapotranspiration provides a basic tool for predicting crop-water requirements and computing water balance (Attarod et al., 2005). The development of novel water saving technologies is then, an important step to help rice farmers cope with water scarcity (Liu et al., 2013). Many water-saving techniques have been developed for rice production, in response to water scarcity. The selection of water-saving methods and the optimum thresholds for obtaining maximum benefits depend mainly on soil type, management, and the environment (Yao et al., 2012; Liu et al., 2013). This diversity of water-saving methods includes saturated soil culture, aerobic rice, a system of rice intensification, non-flooded mulching cultivation, safe alternate wetting and drying irrigation (AWD) (Yao et al., 2012; Liu et al., 2013). Arif et al. (2019) found from 31 published research studies on AWD that 92% of AWD treatments led to yield decreases compared with continuously flooded treatments, while some scholars found the opposite trend under different thresholds of AWD application (Belder et al., 2004; Tuong et al., 2005; Pan et al., 2017). The differences in frequency and threshold of the drying cycles of the AWD, soil types, groundwater table depths, and rice varieties may contribute to the contrasting results. Based on a meta-analysis conducted by Carrijo et al., (2017), it has been found that the degree of soil drying during the drying events was critical to avoinding yield loss. This technology, characterized by its alternation of periods of soil submergence with periods of non-submergence during the growing season, could substantially reduce irrigation water and lead to an improvement in water use efficiency (WUE) (Yang et al., 2007; Zhang et al., 2008, Yao et al., 2012). In addition, the timing and amount of irrigation are two critical factors for improving the water use efficiency (WUE) under limited water supply conditions. Due to the lack of fixed criteria for re-watering different soil and climatic conditions, AWD often results in over- or under-irrigation. It is difficult to decide when the best time is to rewater the rice crop. However, it is still debatable if the technology could sustainably achieve the dual goal of increasing grain yield and saving water (Zhang et al., 2008; Yao et al., 2012; Liu et al., 2013).

Besides water, nitrogen (N) is another key input determining crop yield (Sun et al., 2012; Pan et al., 2017). It is one of the most important elements affecting crop growth and the most important nutrient-limiting factor for crop yield formation (Jiang et al., 2004; Thakur et al., 2013). N application can significantly improve crop yield. In our rural areas and especially in southern Benin, farmers used to apply higher rates of applied N fertilizer than the recommended amount, assuming that increasing N would always result in increasing crop yields (Dossou-Yovo et al., 2020), which can result in altering and negatively affecting the sustainability of the production system and increasing the production cost. However, the use of N fertilizer is generally inefficient, and the apparent recovery efficiency of N fertilizer is only about 33%, on average (Garnett et al., 2009). The remaining N is lost as either surface runoff, leached nitrate in groundwater, volatilization to the atmosphere, or by microbial denitrification (Liu et al., 2013; Cao et al., 2020). An adequate utilization rate of N fertilizer will not only cause a low waste of resources and financial resources but could also reduce the negative impact on the environment and the safety of agricultural products.

Water and nitrogen may interact with each other to produce a coupling effect. Some studies (Sun et al., 2012; Wang et al., 2017) indicated that there was a significant interaction between nitrogen application and water management on nitrogen absorption, utilization, and grain yield in rice. However, other studies have found no significant interaction between them (Yang et al., 2012; Yao et al., 2012). To simulate this interaction between different water management and rates of nitrogen application and rice response under various agroclimatic conditions, crop growth models have been used in various aspects of agronomic research. These models can be useful tools for estimating the growth, development, and yield of a crop in accordance with various environmental changes, including climate change (Buresh et al., 2010). In general, crop growth model reproduces the mechanisms of photosynthesis and respiration, and the production process in biological systems by simplifying the formulae based on scientific theory and hypotheses (Steduto et al., 2012).

These different management practices for rice cultivation have a substantial effect on the carbon cycle and contribute to global climate change (Ren et al., 2007). Based on FAO database, rice cultivation contributed for 10.1% of total agricultural GHG emissions worldwide. Rice cultivation is a carbon (C) sink of atmospheric CO_2 and sensitive to changes in the C pool (Alberto et al., 2014). The carbon cycle in these systems is easily affected by different water management practices and the application of nitrogen fertilizer (Alberto et al., 2014; Komiya et al., 2015). The exchange of CO_2 within the crop-atmosphere continuum plays an important role not only in the carbon cycle in agricultural ecosystems but also in the water and nitrogen cycles (Saito et al., 2005; Gilmanov et al., 2013). In the context of understanding the processes and components of net ecosystem carbon balance (NECB) in lowland rice cultivation under different water management and nitrogen application, it is important to determine whether the system is behaving as a net C sink (net C accumulation in the system) or a C source (net C depletion or loss from the system). Additionally, another important factor is the determination of the heterotrophic respiration as well as the autotrophic respiration, which take place during different stages of plant growth and cause enhanced mineralization of soil organic carbon (Patel et al., 2011). Furthermore, the radiant energy absorbed by the crop canopy is the strongest driving factor in the carbon cycle and needs to be understood because of its significant physiological and phenological effects on the crop canopy (Hoffmann et al., 2015). Some studies that have quantified net ecosystem exchange (NEE) of CO_2 from intermittently flooded paddy fields in Japan, China, and the Philippines showed significantly greater CO_2 emissions than continuously flooded paddy soils, implying higher ecosystem respiration (Liu et al., 2013; Alberto et al., 2014). Yet whether the higher ecosystem respiration was the result of increased autotrophic respiration (RA) or enhanced heterotrophic respiration (RH) is still debatable. Moreover, the mechanism of CO_2 exchange between rice paddies and the atmosphere has been explored in only few studies and is not yet fully understood, even though it is still very scarce in Africa (Alberto et al., 2012; Liu et al., 2013; Alberto et al., 2014). Therefore, it is important to understand the balance between C sequestration and GHG emissions in paddy fields, as well as enhance the C sequestration capacity, to establish water-saving agricultural production. Hence, further evaluations of CO_2 flux from rice crops are necessary for understanding the dynamics. of agroecosystems and predicting future climate change (Patel et al., 2011; Dossou-Yovo et al., 2020).

CO_2 measurement uses different methods and techniques that are not accessible in all parts of the world, especially in Africa, where there is a significant lack of materials (Sossa et al., 2022). Recent efforts in developing low-cost measurement devices focus on solving the financial and portability constraints that limit scientific CO_2 emission and water flux measurements. This development was catalyzed by the increasing availability of relatively inexpensive microcontrollers used for scientific research (Blackstock et al., 2019; Capri et al., 2021) combined with the improvement in accuracy and precision of low-cost non-dispersive infrared (NDIR) CO_2 sensors. Evaluation of commercially available NDIR CO_2 sensors (Pandey et al., 2007; Yasuda et al., 2012; Martin et al., 2017; Keimel et al., 2019) shows that they have acceptable accuracy, especially when a proper calibration method is applied. Though they are usually applied for air quality monitoring (Wastine et al., 2022), there are now low-cost CO_2 measurement systems that are being adapted for environmental studies (Bastiken et al., 2015; Brändle et al., 2019; Curcoll et al., 2022). Some studies were also able to demonstrate that these low-cost NDIR CO_2 sensors show good agreement when compared to more accurate CO_2 analyzers, such as the LI-6262 (Yasuda et al., 2012), or with currently available instruments (e.g., Los Gatos Research, Picarro, LI-COR, PP Systems, and Quantek Instruments) used for CO_2 measurements in environmental science (Brown et al., 2020). Considering all these constraints, it is very important to test these low-cost systems that still face challenges in terms of data quality and reliability when compared to commercial CO_2 and H_2O flux systems, especially when deployed for long-term field measurements. Therefore, the development, the field validation, and the field trial application of a low-cost and open-source data logger integrated with NDIR-based CO_2 and environmental parameter sensors (such as a RH sensor) applied at field-level using closed chamber CO_2 exchange measurements is prior very crucial.

1.2 State of the knowledge

Global warming and increased emissions of anthropogenic greenhouse gases (GHGs) have become an international issue of great concern. Comprehending the dynamics of global climate change requires a deep understanding of the exchange of greenhouse gases between terrestrial ecosystems and the atmosphere (Smith et al., 2007). Carbon dioxide (CO_2) is one of the major contributors to anthropogenic GHGs, accounting for 76% of total emissions in 2010 (IPCC, 2014). Rice fields are one of the important agricultural land uses, having a substantial effect on the carbon cycle, and they are a carbon (C) sink for atmospheric CO_2. The carbon cycle in these systems is easily affected by different management practices that include water management and N fertilizer application. In terms of water management, due to its scarcity, several methods of water saving have been introduced to save water while limiting irrigation costs and protecting the environment. One of the recent methods is alternate wetting and drying (AWD). This method is also known as alternating between submergence and non-submergence. AWD represents the alternating irrigation of rice fields with periods of standing water and damp or dry soil conditions, which is approximately 15 days after transplanting or planting of rice plants up to harvesting. It creates an aerobic and anaerobic condition and is the best option compared to normal flooding conditions for reducing CH_4 emission by rice fields (Wassmann et al., 2009). Simultaneously, increased oxygen availability can increase total microbial activity and, as such, the decomposition of organic soil matter. Consequently, changes in water management in rice agriculture were reported to alter the soil organic carbon (SOC) balance and soil fertility (Ye et al., 2015). Application of nitrogen fertilizer may increase crop yield and the SOC stock as well. Although the application of nitrogen fertilizer typically increases crop biomass, its impact on soil carbon content may vary with the soil type and different climatic conditions (Quansah et al., 2015).

Until now, only few studies have evaluated the combined effects of different water management and nitrogen fertilizer on CO_2 emissions in rice fields. Therefore, it is important to understand the balance between crop water requirements and CO_2 emissions in paddy fields to enhance the C sequestration capacity and establish water-saving agricultural production. A lot of work has been done in this context in Asia and Europe but remains very scare in West Africa, where the climate change impacts agricultural production severely. According to Kim et al. (2013), only 2 out of 73 rice production studies exposed the available data on GHG emissions from sub-Saharan African agricultural lands. Therefore, it is crucial to reinforce the need for continuous research and knowledge generation since rice cultivation contributes significantly to food security in Africa. The limited literature that is available employs mathematical modelling and qualitative research approaches in studying and predicting the levels of GHG emissions from rice cultivation systems (Boateng et al., 2017). This lack of research in Africa is related to the fact that most of the equipment to measure in general the GHG emissions from agricultural land is very expensive and therefore, not accessible to African researchers (Sossa et al., 2022). The development of a low-cost device could be an option to investigate CO_2 emissions from agricultural land in a developing country such as Benin. In addition, different crop models, such as the DSSAT CERES rice model, have been developed to explore the yield and growth response to various climate conditions and management practices for sustainable rice cultivation.

1.3 Research hypothesis

For this study, we hypothesized that:

- (H1): The development of an adaptive, low-cost, open-source data logger for NDIR-based closed chamber CO_2 exchange and ET measurements is a valuable tool in assessing the global C budget and evapotranspiration research, which are both critical for climate change mitigation,
- (H2): CO_2 emissions from rice cultivation increase with the increase in irrigation dose and the high amount of nitrogen for irrigated rice cultivation,
- (H3): The net ecosystem carbon balance (NECB) and the evapotranspiration (ET) are higher under a high amount of nitrogen application and continuous flooding irrigation,
- (H4): The combination of alternate wetting and drying (AWD) as water management and an optimum amount of N fertilizer improves water productivity, nitrogen use efficiencies, and grain yield from irrigated rice cultivation,
- (H5): The DSSAT CERES-Rice crop growth model is capable of simulating rice growth and irrigated rice yield under different water management practices and rates of nitrogen (N) fertilizer in Benin.

1.4 Objectives

1.4.1 Overall objective

The overall objective of this study is to identify the best farming management practices that improve water and nitrogen use efficiency, grain yield, and the net ecosystem carbon balance while keeping CO_2 emissions low in off season rice production in Benin.

1.4.2 Specific objectives

Specifically, the research attempts to

1. Develop an adaptive, low-cost, open-source data logger for NDIR-based closed chamber CO_2 exchange and evapotranspiration (ET) measurements,
2. Determine the effects of different water management and N fertilizer levels on CO_2 seasonal dynamics and soil CO_2 respiration,
3. Determine the effects of different water management and N fertilizer levels on net ecosystem carbon balance and evapotranspiration,
4. Determine the effects of water management and N fertilizer levels on growth, water productivity, N uptake, and grain yield of irrigated rice,
5. Calibrate and evaluate the DSSAT CERES-Rice model to simulate rice growth and rice yield under different water management and rates of nitrogen (N) fertilizer.

CHAPTER TWO

LITERATURE REVIEW

2.1 Rice Production from a global perspective in Benin

Rice (Oryza sativa) has always been a common staple and one of the most rapidly growing food resources in Benin, mainly due to urbanization. In Benin, rice is the third most stable food and the most consumed cereal crop after maize and wheat. Approximately, 48% of the active population earns their income from farming, notably rice cultivation, and its production is far below the demand needed to cope with the needs of the population (Seck et al., 2013). The rice self-sufficiency rate was about 23% in 2020, resulting in the need for annual imports to meet the growing rice demand (Index-Mundi, 2020).

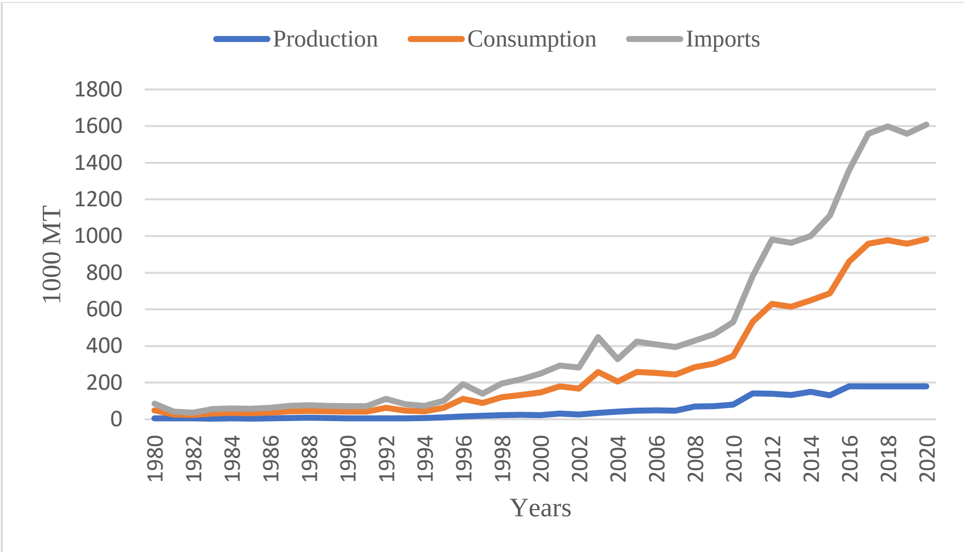

Figure 1: Rice production, consumption, and importation from 1980 to 2020 in Benin

Source: Indexmundi, 2021.

The rice consumption and the rice importation have increased over the years despite the increase in production. For the year 2020, a large quantity of rice was imported from the international market (625000 metric tons); that is more than the total of the potential production (179000 metric tons). In Benin, rice can grow under specific conditions of water regimes (in dry and wetland conditions) and temperatures (at low and high altitudes and latitudes) (Seck et al., 2012). Taking these environmental factors into account, a more detailed classification of rice environments is possible; for instance, 'high-altitude rainfed upland rice' versus 'low altitude rainfed upland rice. This has led to the characterization of three major rice-growing environments in Benin (Figure 2) that include upland, rainfed lowland, and irrigated lowland.

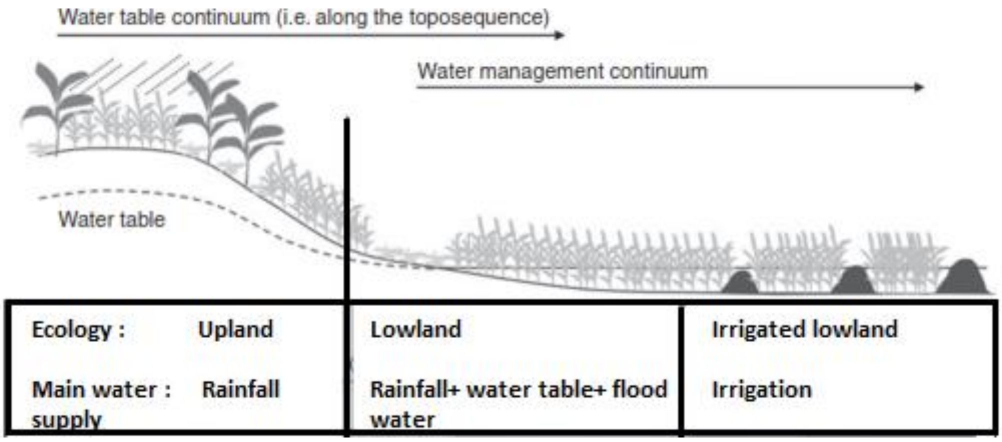

Figure 2: Major rice growing environments and their attributes in Benin.

Source: Ministry of Agriculture of Benin, 2005.

2.2 Water Management as a key to sustainable rice production

Water is an important natural resource that is rapidly becoming scarce, mainly due to climate change, the growing population, and agriculture intensification. The ability of the world to meet the increasing food demand is challenged by water scarcity (Hanjra and Qureshi, 2010). Proper water management is essential for rice production. When rainfall is not sufficient, additional water supply in the form of irrigation is necessary (Yang et al.,2012). Regarding the different systems of water management for rice production, we can generally distinguish between the continuous flooding irrigation system and the alternate wetting and drying irrigation system.

The continuous flooding irrigation system is generally used in Benin, where rice plants are grown in flat areas of land and can stand in wet or waterlogged conditions. It is a commonly used practice in traditional irrigation for rice production but is now regarded as water-consuming (Yang et al., 2016). In flood irrigation systems, water is commonly very unevenly distributed and can either be in excess or in deficit. Due to anaerobic conditions, this method has been linked with methane production since the more methane-producing bacteria grow, the more they generate methane.

The alternate wetting and drying irrigation system is also known as controlled irrigation or multiple irrigations. It aims to reduce water use in irrigated rice fields without lowering productivity (Dill et al., 2013). In this practice, rice fields are alternately flooded and unflooded rather than kept continuously submerged like in a continuous flooding system. This practice involves repeatedly flooding a farm field, typically to a water depth of around 5 centimeters above the soil surface when the water level drops to around 15 cm below the soil surface (Uphoff et al., 2015). The depth of water is monitored by using a perforated field water tube, which is made of a 40 cm long plastic pipe or bamboo and has a diameter of 15 cm or more so that the water table is easily visible (Pan et al., 2017). This cycle can continue from 20 days after sowing until 2 weeks before flowering. The number of non-flooded days between irrigations varies between one and ten days depending on the plant's development stage and water availability (Dill et al., 2013; IRRI, 2009). This system saves water and reduces greenhouse gas (GHG) emissions while increasing rice productivity (Richards and Sander, 2014). In addition, alternate wetting and drying (AWD) can reduce water use by up to 30% due to a reduction in the number of irrigation events (Richards and Sander, 2014). It reduces seepage and percolation during production, thereby helping to increase water use efficiency (Yang et al., 2012). Alternate wetting and drying can reduce methane (CH_4) gas emissions by an average of 48% compared to continuous flooding (Richards and Sander, 2014). The combination of AWD with nitrogen-use efficiency and management of organic inputs can further help to reduce greenhouse gas emissions, as Richards and Sander (2014) explain. In terms of the net return for farmers, safe AWD does not reduce yields compared to continuous flooding and may in fact increase yields by promoting more effective tillering and stronger root growth in rice plants. Farmers who use pump irrigation can save money on irrigation costs and see a higher net return from using AWD. Alternate wetting and drying may also reduce labor costs by improving field conditions (soil stability) at harvest.

2.3 N fertilization application as a key for sustainable rice production

Fertilizer is a key input and one of the most important factors in paddy rice production. Proper management strategies, such as the appropriate rate and timing of fertilizer application, can increase rice yield and optimize production costs. Nitrogen (N), phosphorus (P), and potassium (K) are applied as essential fertilizers in large quantities to rice fields, and a deficiency of either of the nutrients leads to yield losses. Nitrogen is the most limiting element in almost all soils. Thus, an adequate application of N fertilizers is vital to improving crop growth and grain yields, especially in intensive agricultural systems. Insufficient and/or inappropriate nitrogen management can be detrimental to crops and the environment. Optimal N management strategies aim at matching fertilizer N supply with actual crop demand, thus maximizing crop N uptake and reducing N losses to the environment.

Nitrogen Use efficiency mainly depends on many factors, such as cultivar, soil type, fertilization technology, and environmental factors. Nitrogen is an essential constituent of amino acids, nucleic acids, nucleotides, and chlorophyll (Zhang et al., 2009; Liu et al., 2013). Because N is a constituent of amino acids, which are required to synthesize proteins and other related compounds, it plays a role in almost all plant metabolic processes. In rice cultivation, nitrogen application in the soil helps to increase plant growth and yield as well. It improves root growth, which is especially important for the absorption of water and nutrients. In addition, N also improves panicle number and panicle length in upland rice.

2.4 Rice fields as major sources of GHG Emissions

Rice fields have been identified as important anthropogenic sources of methane (CH_4), nitrous oxide (N_2O), and carbon dioxide (CO_2) emissions (Yan et al., 2003; Arunrat and Pumijumnong, 2017). According to Linquist et al., (2012), flooded rice emits approximately four times as much greenhouse gas per tonne of the product as wheat or maize (IPCC, 2014). These GHGs are also referred to as "Kyoto gases" and are listed in Table 1 (IPCC, 2007). The "global warming potential" (GWP) of a GHG indicates the amount of warming a gas cause over a given period (normally 100 years). GWP is a unit value, with CO_2 having a baseline unit of 1, and the GWP for all other GHGs is the number of times more warming they cause compared to CO_2 (IPCC, 2007.

Table 1: Kyoto gases and their global warming potentials (GWPs) (adapted from IPCC, 2007)

Greenhouse gas	GWP
CO_2	1
CH_4	25
N_2O	298
Hydrofluorocarbons (HFCs)	124-14800
Perfluorocarbons (PFCs)	7390-12200
Nitrogen trifluoride (NF3)3	17200

2.4.1 CO_2 emissions

The exchange of carbon dioxide (CO_2) in paddy fields is referred to as net ecosystem exchange (NEE). It results from the balance between the CO_2 uptake via apparent plant photosynthesis (gross primary production; GPP) and the CO_2 emission (ecosystem respiration; Reco) through autotrophic (Ra) and heterotrophic (Rh) respiration (Wohlfahrt and Gu 2015). Some factors are related to the net carbon dioxide emissions from the rice paddy fields such as the anaerobic decomposition of organic matter in the soil, respiration by the rice root, and uptake or release of CO_2 by algae and aquatic weeds (Nishimura et al., 2014). CO_2 emissions from flooded rice fields are suppressed during flood irrigation, but some escape into the atmosphere through bubble ebullition (Komiya et al., 2015). When the soil is drained, creating an oxidized environment in the soil, aerobic decomposition occurs, resulting in the consequent release of carbon dioxide (Jain et al., 2004). The CO_2 transport is mainly driven by molecular diffusion across the soil-atmosphere and plant-atmosphere boundary layers, as well as by mass flow through stomatal or cuticular conductance and ebullition processes (Livingston and Hutchinson, 1995). In the context of gaseous C exchange in terrestrial ecosystems, GPP and Reco constitute the most important consumption and production processes, respectively (IPCC, 2013). A generalized schematic representation of the gaseous CO_2 exchange of terrestrial ecosystems is shown in Figure 3

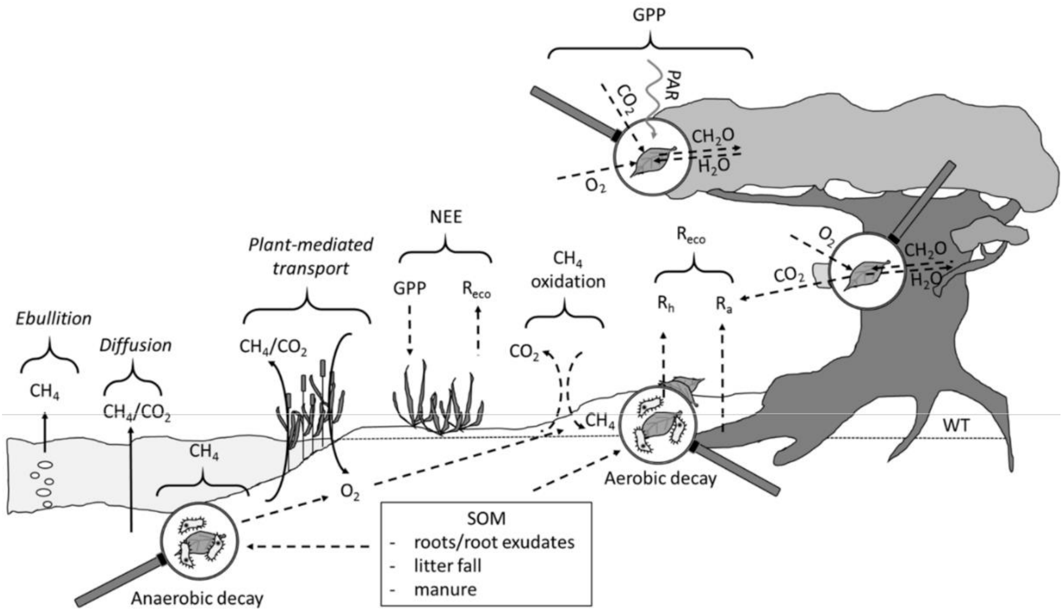

Figure 3: Generalized schematic representing production, consumption (dashed arrow lines) and transport processes (solid arrow lines), determining the CO_2 exchange of terrestrial ecosystems. Abbreviations WT and SOM denote water table and soil organic matter, respectively.
Source: Wohlfarth and Gu, 2015

2.4.2 CH_4 emissions

Irrigated rice production is the second largest source of anthropogenic methane after enteric fermentation from ruminants (Smith et al., 2007). Flooded rice paddy fields create anaerobic conditions in the saturated soils conducive to methanogenic archaea activities due to the temperate conditions, high moisture, and organic substrate (Khalil et al., 1998). Two microbial communities leading to methane production from the soil are attributed to methanogens and methanotrophs. The total methane emissions from flooded rice fields are the balance between methanogen and methanotroph activities (Fazli et al., 2013). Aerobic decomposition of soil organic matter (SOM) leads to the gradual depletion of oxygen present in most parts of the flooded soils by aerobic bacteria and chemical oxidation reactions creating anoxic conditions that lead to the usage of alternative electron acceptors (Horwath, 2011). Rice plant rhizosphere serves as the major carbon source and energy for CH_4 production in rice fields, especially at the later growth stages due to deposits of organic root exudates. (Ma et al., 2010). As a source of carbon and energy for CH_4 production, the rice plant also acts as an important site where CH_4 is oxidized by available oxygen from root secretion.

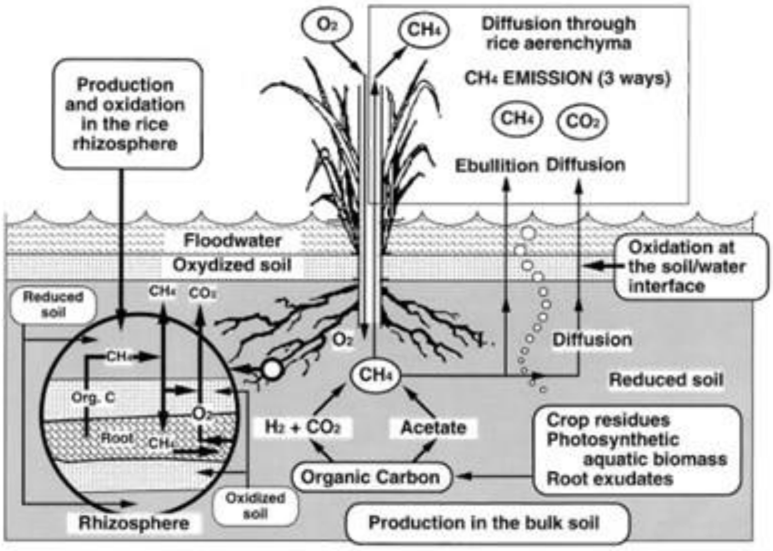

Figure 4: CH_4 production, oxidation and emission via rice plants, ebullition, and diffusion, from rice fields.

Source : Le Mer and Roger, 2001

2.4.3 N_2O emissions

Nitrous oxide (N_2O) is one of the important components of net GHG emissions from rice production. As part of the global nitrogen (N) cycle, it is naturally produced in the soils. N_2O emissions from agricultural soils are increased by the application of nitrogen (N) fertilizers that supply additional nitrogen to the global N cycle. Nitrous oxide production in the rice fields is a result of nitrification and denitrification processes mediated by microbial activities. N_2O emission from soil is correlated to many factors, such as soil moisture, that cause a difference in soil temperature, soil oxygen status, and soil redox potential (Eh) (Peng et al., 2011; Arunrat and Pumijumnong, 2017). Indeed, drainage of rice fields increases the N_2O emissions (Fazli et al., 2013) due to nitrification processes (oxidized layer), which require the presence of oxygen to produce N_2O (Fazli et al., 2013). Ammonium ($NH4^+$) is oxidized to nitrate (NO^{3-}) in nitrification processes, releasing part of the nitrogen produced as NO and N_2O to the atmosphere. Whereas, when fields are inundated during the growing season, denitrification processes occur in the reduced soil layer, and they are most important for producing N_2O. Therefore, nitrate (NO_3) or nitrite (NO_2) is reduced to nitric oxide, nitrous oxide, and nitrogen gas (NO, N_2O, or N_2, respectively).

2.5 Carbon cycling in rice paddy ecosystem

CO_2 exchange in paddy fields is driven by photosynthesis and autotrophic (plant) and heterotrophic (mainly microbial) respiration. During the photosynthesis activities, atmospheric carbon is converted from inorganic carbon (CO_2) to organic carbon by standing vegetation, such as algae. When the plants die, they become detritus, which then undergoes decomposition, and therefore the plants become the major source of carbon (C) in most wetlands (Figure 5). Many biological and physical processes regulate the exchange of CO_2 and CH_4 between paddy fields and the atmosphere. Previous studies indicated that a large amount of CO_2 is stored by the plants in paddy fields, and therefore a huge amount of GHGs is released from paddy fields (Liou et al., 2003; Zou et al., 2005; Tang et al., 2016). Plants utilize atmospheric CO_2 and respired CO_2 released by the soil and floodwater for the photosynthesis process (Wang et al., 2017).

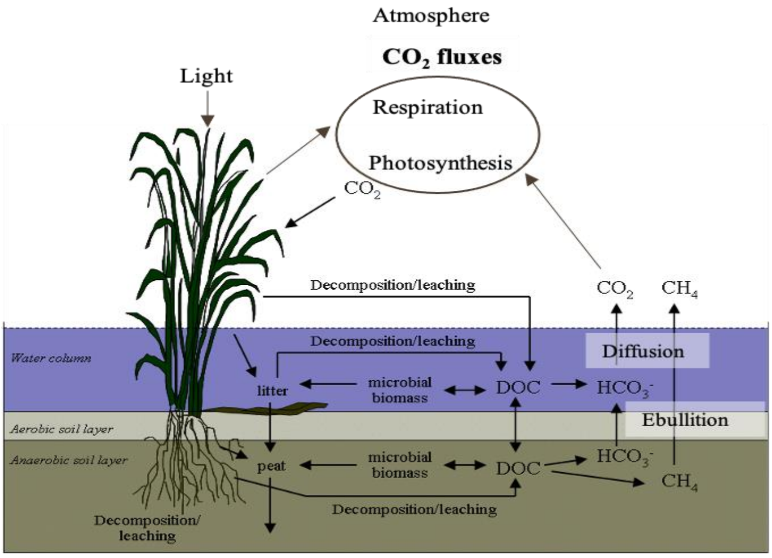

Figure 5: Carbon cycling in wetland rice ecosystem.

Source: Reddy and De Laune, 2008.

Rice is mostly cultivated under flooded conditions, and therefore, the decomposition of plant residues in rice field ecosystems goes on anaerobically. A large type of organic material from plant residues is incorporated into rice soils in line with field management. By decomposition, the final products of organic materials are CO_2 and CH_4 within the rice field ecosystem. Finally, they escape the system by water percolation into the subsoil layer and by flux into the atmosphere (Kimura et al., 2004).

Decomposition of plant residues is shown to be the active process in carbon cycling in rice fields. However, rice releases photosynthates into the rhizosphere (rhizodeposition), and then decomposition of plant residues occurs in the soil by different processes (Kimura et al., 2004). Both CO_2 and CH_4 are produced within the decomposition process of organic materials in flooded rice fields. CO_2, the final product of organic matter decomposition, is present in the form of the bicarbonate ion ($HCO3^-$) which occupies the biggest portion of anions in percolating water in rice fields. CO_2 in the floodwater is assimilated by algae and aquatic weeds through photosynthesis, which is then produced by their respiration. CO_2 fluxes exchanged in rice fields are specially controlled by the photosynthesis of aquatic plants and the respiration of both the plants and the soil microorganisms. Moreover, emissions due to soil respiration are suppressed by paddy water during flood irrigation (Nishimura et al., 2015). Komiya et al. (2015) investigated that the emission of CO_2 between flooded water and the atmosphere was mainly due to diffusion, whereas low CO_2 ebullition was due to CO_2 photosynthesis and respiration by aquatic plants throughout the day. Additionally, CO_2 produced in the upper layer of soil may diffuse upward into the floodwater.

2.6 Assessing the CO_2/ CH_4 exchange

Several different approaches are used to assess the gaseous C exchange between the pedosphere, biosphere, and atmosphere. These methods can be divided into instrument-based, direct C flux measurements and calculation-based balancing approaches (Table 2). Direct C flux measurements include non-intrusive microclimatological methods such as open- and closed-path eddy covariance (EC) systems (e.g., Haslwanter et al., 2009; Detto et al., 2011), as well as intrusive measurement methods such as gradient-based systems (e.g., Moldrop et al., 1999; Myklebust et al., 2008) and enclosure-based measurement methods, including open- and closed-chamber systems (e.g., Wik et al., 2013; Maeck et al., 2014) or bubble trap.

Among these multitude of methods, the closed chamber systems are widely used, and they are categorized into steady-state (SS) and non-steady-state (NSS) measurement systems, which are operated either in a flow-through (FT) or non-flow-through (NFT) measurement mode (Livingston and Hutchinson,1995). Steady state (SS) consists of the measurement of the required compensation for the enclosure-based target gas concentration increase or decrease within the chamber headspace during the time of chamber deployment, in contrast to only measuring the target gas concentration increase or decrease over time (NSS). During NFT measurements, the sampled air (e.g.: vials, syringes) is not replaced, whereas during FT measurements, the sampled air is either transferred directly back into the chamber headspace or compensated for by an open vent. In the past, NFT-NSS chamber measurements were extensively used for measuring soil CO_2 efflux and CH_4 emissions. However, especially FT-NSS measurements became more widely used when sufficiently accurate, portable, and affordable CO_2 and CH_4 analyzers became commercially available (Hutchinson and Rochette 2003).

By combining FT-NSS measurements with an extended chamber system (repeated deployment of opaque and transparent chambers throughout a measurement day or automatic chambers), separate measurements of Reco and NEE became possible. This provided a more adequate reflection of the spatial and temporal variability of CO_2 fluxes (Huth et al., 2017). Due to their operational simplicity as well as their low costs and power consumption, manual closed chamber systems are widely applied for obtaining ecosystem CH_4 emissions. This is the case for areas that are either difficult to access and lack power supply, or sites that are characterized by a distinct small-scale spatial heterogeneity and rather small vegetation. For the current study, the manual chamber will be used. This system is used to accurately measure direct CO_2 flux between the atmosphere and low canopies (Müller et al., 2009; Hoffmann et al., 2015) and it is classified as flow-through non-steady-state (FT-NSS) (Livingston and Hutchinson, 1995; Huth et al., 2017).

Table 2: Recapitulative of the main approaches used to assess gaseous C exchange.

Approach	Methods	Applicability	
		Advantage	Disadvantage
Direct (non-intrusive)	-Ground-based eddy covariance (EC)/ Aircraft-based EC • Open path • Closed path	-Continuous non-intrusive measurements (minimum disturbance); spatially integrated (large area) flux	-Not operating under calm wind conditions and at heterogeneous landscapes with a distinct topography; low spatial resolution; insufficient for small-scale treatment/biome comparisons
Direct (intrusive)	-Manual chambers/ Automatic chamber • Open chamber • Closed chamber (NFT-NSS, FT-NSS, NFT-SS, FT-SS)	-Allow for spatially explicit (AC and MC) measurements; applicable to ecosystems where EC is not working (e.g., hilly ground moraine landscapes). enable soil respiration, and daytime Reco measurements (opaque chambers	-Intrusive measurements, low temporal resolution (MC); point measurements (problem of up-scaling
	-Diffusion theory-based measurements.	-Less intrusive compared to chamber measurements regarding plant development	-Intrusive measurements of soil respiration only

2.7 The Evapotranspiration (ET)

Different measurement and estimation methods are used to assess the evapotranspiration. The measurement methods include use of lysimeter, water balance and eddy correlation method. The estimation methods include energy balance, mass transfer, combination of energy and heat, mass transfer and the use of crop coefficients.

2.7.1. Measuring Methods of the Evapotranspiration

Lysimeters: They are tanks filled with soil in which crops are grown under natural conditions to measure the amount of water lost by evaporation and transpiration. This method provides a direct measurement of the crop evapotranspiration (ET_c) and is frequently used to study climatic effects on ET_c and to evaluate estimating procedures. They can be grouped into three categories: (1) non-weighing, constant water-table type; (2) non-, percolating-type; and (3) weighing types.

Water Balance: This method has been used on large areas such as valleys in which the inflow and outflow are determined from streamflow and precipitation measurements, and where the basin is confined to eliminate other significant sources of inflow or outflow. This type of method generally provides only gross estimates of the average water evaporated and transpired from cropped and non-cropped areas.

Eddy Correlation: This method overcomes the need to determine each component in the water balance by using the energy balance approach. It also avoids soil surface heterogeneity issues by placing the sensors above the crop canopy and the evapotranspiration can be measured from various type of vegetation.

2.7.2. Estimating Methods of the evapotranspiration

Energy Balance: This method can be used for hourly or shorter values, especially during daylight hours. The Bowen ratio approach is the most used method. The Bowen ratio is the ratio of energy fluxes from one medium to another by sensible and latent heating, respectively.

Mass Transfer: Direct determination of ET can be accomplished for a specific field and crop by using eddy diffusion equations and meteorological data measured on site.

Crop Coefficients: This method estimates ET_c by multiplying reference evapotranspiration (ET_o) to a crop coefficient (K_c), like this: $ET_c = (ET_o)*(K_c)$

The ET_o can be calculated from weather data collected from a well-watered reference crop surface. Many methods have been developed to estimate the ET_o. It is important to note that the estimation of ET_c using crop coefficients requires crop coefficients developed using crop evapotranspiration measurements (ET_c) and ET_o estimates for a specific crop and location.

2.8 Trends and research features on greenhouse gas emissions from rice production

The full development of this subsection is published by Sossa et al. (2022) and could be found at ***https://doi.org/10.1007/s11356-022-22921-0***

Abstract

Greenhouse gas from rice production has become a great concern and the focus of a lot of research in recent years. The main aim of this section was to explore the research trend of GHG emissions from rice production by exploring the research hotspots and providing suggestions for future research directions over the period 1991 to 2020. A bibliometric analysis was conducted using the Scopus database, and the sample included 2535 articles. The methodology was based on descriptive analysis, co-occurrence analysis, factorial analysis, word dynamic over time, and the author’s keyword analysis over time. The results indicate a remarkable increase in the number of articles published on this topic, mainly in the journals of “Agriculture,” “Ecosystems,” and “Environment.” The main authors were Conrad R. and Wassmann R. Relating to the number of published articles, very few were contributed by African countries, whereas China, Japan, and India were the main contributors. The co-occurrence analysis showed that rice, methane, and nitrous oxide are the core keywords of the network. The multiple factorial analysis pointed out that greenhouse gas emissions from rice production depend on the farming practices, the environmental factors, and the plant growth as well. The evolutionary path showed that the current author’s keywords are more related to global warming potential, climate change, and biochar. The findings of this review can help researchers and scholars by providing a better overview of development trends that have emerged over the past 30 years and suggestions.

2.8.1. Methodology

The bibliometric analysis was carried out by selecting papers indexed by the Scopus database, using the advanced search to define the field of interest. Scopus, widely used to create datasets for systematic reviews of research, is also the largest abstract and citation database of peer-reviewed literature It is a typical online academic database that has a great impact on academic literature due to its access to a wide range of journals and sources in all kinds of knowledge areas (Baas et al., 2020).

Compared to other scientific databases such as the Web of Science, Scopus has a broader coverage and presents a better option for a research review and numerous reviews have also been used for the bibliometric analysis (Falagas et al., 2008; Vatananan-Thesenvitz et al., 2019). In this study, the retrieval strategy was TITLE (Rice) AND KEY (GHG OR GWP OR CO_2 OR CH_4 OR N_2O OR "Greenhouse gas*" OR "Global Warming Potential" OR "Carbon dioxide" OR " Methane " OR "Nitrous Oxide"). We selected "article" from the document types and "English" as a language option. Accordingly, the data span of this study is from 1991 to 2020. In addition, a preliminary screening was carefully done in terms of removing duplicate articles and articles without the names of the authors. In total, 3062 articles were initially found, and 2535 publications were finally selected on April 16, 2021. The dataset extracted from Scopus for the bibliometric analysis was downloaded as bib (BibTeX Bibliographical Database). These extracted data comprised much information such as the author's name, author affiliation, article title, keywords, abstracts, and multiple citations. The data. Bib file format is used with the statistical tool R using Bibliometrix. Biblioshiny, the shiny interface for the Bibliometrix package from R version 3.6.3, was used for this study. The inputs were the downloaded papers from Scopus datasets. This tool was used to characterize the descriptive analysis, the Visual analysis, and Evolutionary Path of Research Topics over the study period. More details about Biblioshiny for Bibliometrix can be found here: https://www.bibliometrix.org/Biblioshiny.html.

2.8.2. Some results

2.8.2.1. Principal countries

The publication of papers in different countries can generally reflect the influence and importance of a given topic. Regarding the average citation quantity of the articles, Italy and the Philippines have the highest multiple-country publication ratios (0.735 and 0.7121, respectively). Most of the top 15 countries are developed countries, and none of them is from Africa. Country scientific production is presented in Figure 6. The higher number of articles published in terms of frequency is materialized by the darker blue. The different clusters illustrate the differences in studies related to GHG emissions from rice production experienced by each country. Most of the articles are published in Asia, America, and Europe. Only 14 African countries were involved out of the 77 countries considered in this study. The most contributable African country is Egypt, with 31 papers. This result also shows the scarcity of research on GHG emissions from rice production in Africa's countries. A lot of work remains to be done in this perspective since rice is one of the major staple foods in Africa.

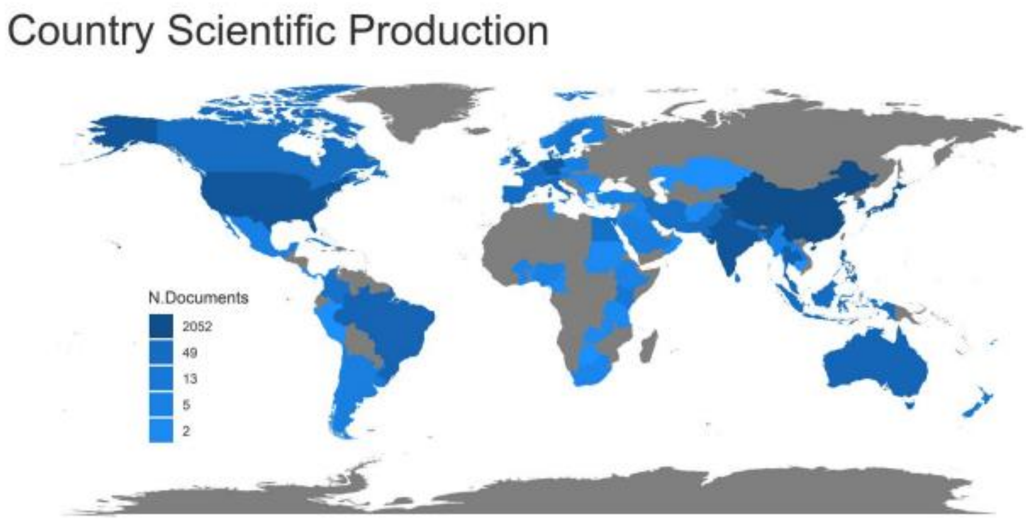

Figure 6: Country scientific production

2.8.2.2. Visual analysis

Keyword co-occurrence analysis of keywords used by authors in publications is an important tool for investigating trending topics and scholars focus on the field. It presents the correlation measures between words and reveals their appearance relationships (Abdallah et al., 2021). This study investigated the keyword co-occurrence network to gain further insight into the trends in the field of GHG emissions from rice production. Figure 7 identifies the keyword network related to rice production and greenhouse gas emissions. The color represents the cluster, and the thickness of the connecting line between nodes shows the strength level of the relationship between these keywords. In addition, the size of the node and the number of lines is proportional to the frequency of each keyword.

Three clusters were identified to represent different viewpoints on GHG emissions from rice production. The first cluster (red) indicated that the global warming potential of rice cultivation depends mainly on methane and nitrous oxide emissions. The second cluster (green) demonstrated that farming practices such as biochar and rice straw application can afect methane emissions from paddy soil. The third cluster (blue) highlighted the relationship between plant biomass and photosynthetic activities on CO_2 emissions from rice production.

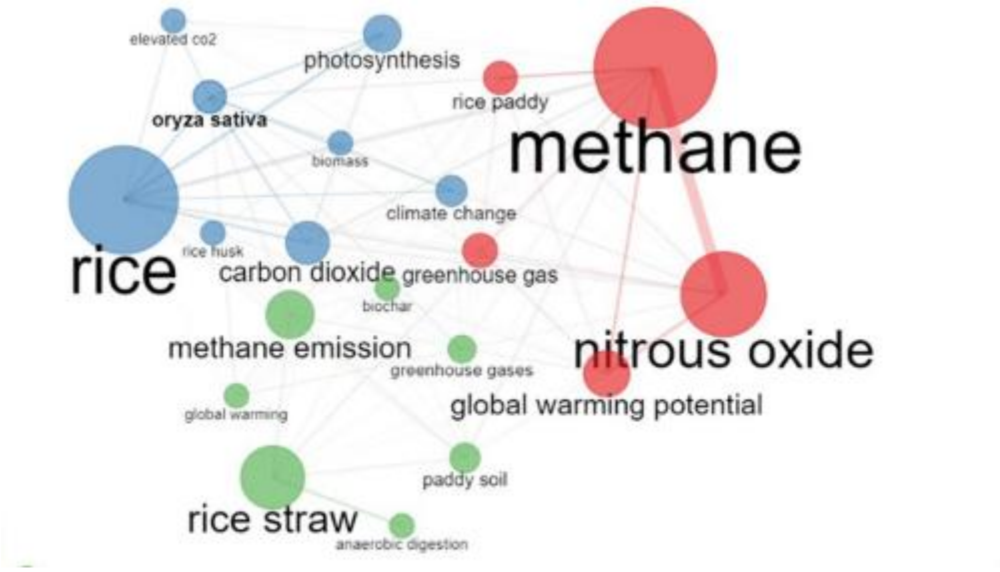

Figure 7: Keywords co-occurrence analysis

2.8.2.3. Factorial analysis

The Multiple-correspondence analysis (MCA) displays a large amount of data in two-dimensional (or three-dimensional) graphics to reflect the similarity between them. The keywords that have received more attention are those that are closer to the center of the graph and distributed in a more concentrated manner (Figure 8). However, those that are more evenly spread are related to less frequently discussed research topics or transitions to other topics. The multi-correspondence analysis of keywords confirms what was presented in the keyword co-occurrence. However, studies on GHG emissions from rice production can be summarized into the following two major categories (depending on the clusters' colors). The first category (the red group) mainly highlights the relationship between different management practices (rice straw incorporation, biochar, rice husk, etc.) and greenhouse gas emissions (mainly methane and nitrous oxide) from rice production, which leads to global warming. The second category (the blue group) mainly focuses on the interaction between carbon dioxide emissions and rice production. For rice production, significant carbon dioxide is emitted from the soil and the rice plants as well. The emission from the plant depends on the growth stage (biomass, physiology) and the natural conditions of production (photosynthesis). Concerning the emissions from the soil, it is more related to elevated temperatures.

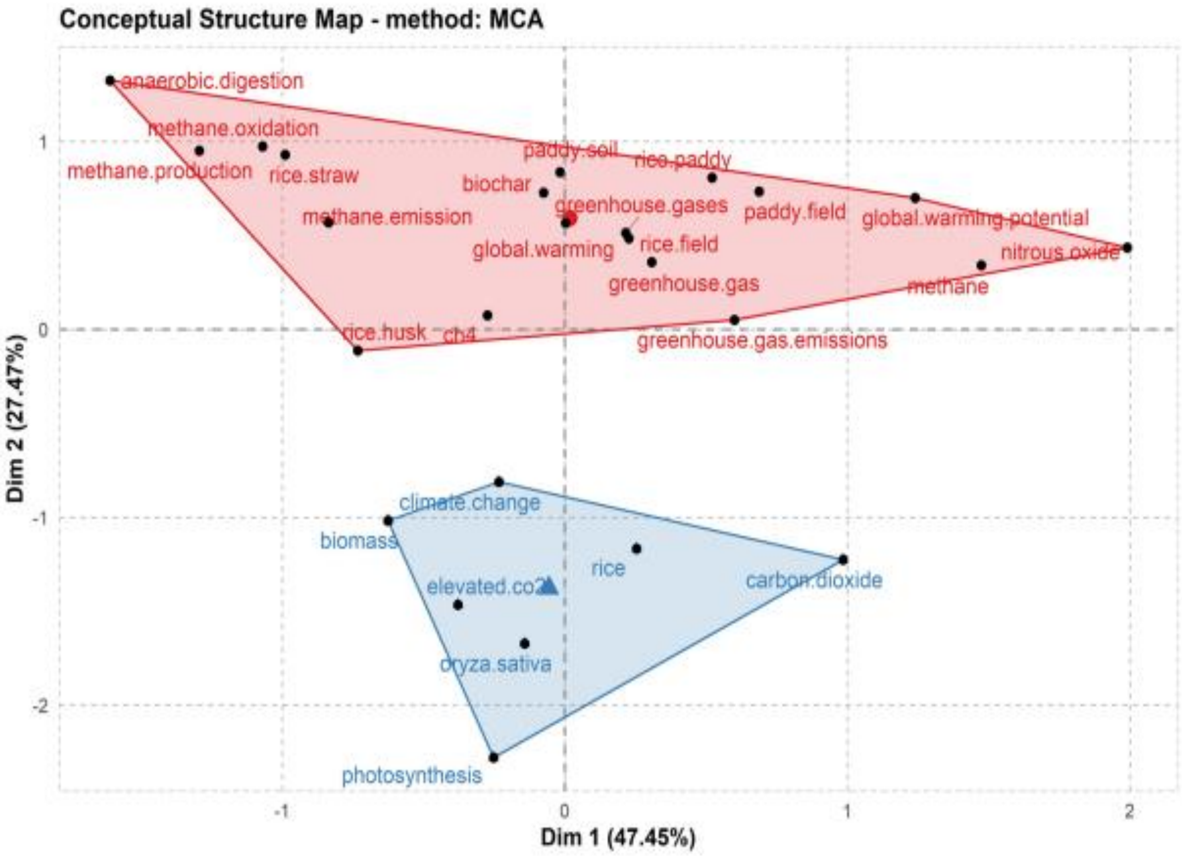

Figure 8: Multiple correspondence analysis of high-frequency keywords

2.8.2.4. Author's keyword analysis over time

The author's keyword analysis studies a theme's content and its evolutionary relations over time. In this paper, the evolution of the author's keyword over the three-decade study period is analyzed. Table 3 shows the 12 most frequently used keywords during each of the three decades, which can provide an overview of the evolution of the author's key words during the study period. In terms of the use frequency, except for "rice" and methane, which are the most cited over the whole period, the first period from 1991 to 2000 is more focused on soil CO_2 emission using the keywords "carbon dioxide" (18 times), "paddy soil" (18 times), and "temperature" (13 times). The second decade, starting from 2001 to 2010, is specifically related to the assessment of methane and nitrous oxide emissions from rice production and the introduction of rice straw as a soil management practice. It is focused on the following keywords: "photosynthesis" (27 times), "nitrous oxide" (25 times), "nitrous oxide (17 times), and rice straw (14 times). The last decade, from 2011 to 2020, used mostly the keywords global warming potential (95 times), "greenhouse gas" (74 times), and climate change (69 times), "biochar" (58 times), and "rice husk" (56 times). However, during this last decade, more scholars have begun to pay attention to climate change and global warming potential assessment from rice production as affected by different farming practices. Therefore, recent dynamic seems focus on climate change and different agricultural practices as the primary subject of GHG assessment from rice production.

Table 3: The 12 most frequently used Author’s keywords during the three decades of the study period

#	1991-2000		2001-2010		2011-2020	
1	*Methane Emission*	46	Rice	70	Methane	205
2	Methane	42	Methane	50	Rice	183
3	Rice	34	Methane Emission	39	Rice Straw	150
4	Oryza Sativa	21	*Photosynthesis*	27	Nitrous Oxide	143
5	Methane Production	19	*Nitrous Oxide*	25	*Global Warming Potential*	95
6	*Carbon Dioxide*	18	Carbon Dioxide	23	*Greenhouse Gas*	74
7	*Paddy Soil*	18	Oryza Sativa	19	*Climate Change*	69
8	Methane Oxidation	15	Free-Air CO_2 Enrichment	18	*Biochar*	58
9	Photosynthesis	15	*Rice Straw*	17	*Rice Husk*	56
10	Rice Straw	14	Rice Paddy	15	Rice Paddy	56
11	*Temperature*	13	Yield	15	Greenhouse Gases	54
12	Hydrogen	12	*Elevated* CO_2	14	Carbon Dioxide	51

2.9 Crop model for rice production

2.9.1. Different crop models to simulate rice production.

Crop modelling has become an important tool in modern agricultural research. So far, different models and methods have been employed by many researchers across the world in attempts to assess the impacts of climate change on rice production, such as crop production models, yield prediction, and quantities of water or fertilizer consumption. Crop simulation models are widely used in agricultural production and provide us with the opportunity to build scenarios of agricultural output in changing climates. Thus, they can help to compare experimental research findings across sites, extrapolate experimental field data to wider environments, develop management recommendations and decision support systems, and make predictions (Jones et al., 2003). Using crop models depends not only on the availability of models and application software but also on the availability of information to run models for a specific purpose. Some models act better than others in specific contexts, for instance, when they are applied to crops, climates, cropping patterns, soil quality indicators, and management practices. Different crop growth simulation models exist for rice, but thorough validation and evaluation reports are inadequate. Table 4 presents the key attributes of some crop simulation models for rice production.

Table 4: Some crop simulation models for rice production.

Model	Application	Advantages	Disadvantages
ORYZA 2000	-Simulation of growth and development of rice including water, C, and N balance in lowland, upland, and aerobic rice ecosystems.	-Improve and integrate all previous versions of the ORYZA series into one model.	-Any effect of either CO_2 or N on dry matter partitioning is not considered; overestimation of leaf biomass and LAI under elevated CO_2, and cannot be used for the modelling of upland rice
RICESYS	-Assessment of the dynamics of rice growth and development; represent the effect of delays in transplanting date and planting density on growth and yield of rice plant	-Assessment of the effect of climate change on the rice plant, its weeds, and herbivores	-The influence of CO_2 is not included.
CERES-Rice	-Simulation of crop growth and yield responses to scenarios of field management changes; assess regional climate change impacts.	-Simulation of more realistic responses to temperature and the long-term consequences of potential climate change on rice production	-Many input data are required
RICEMOD	-Simulation of leaf water stress and prediction of the growth and yield comp component of different rice varieties.	-Useful for predicting future production scenarios.	-The influence of CO_2 is not included

2.9.2. CERES Rice model to simulate rice prediction.

Crop Estimation through Resource and Environment Synthes is-Rice (CERES-Rice) is a generic and dynamic simulation model which was developed under the International Benchmark Sites for Agrotechnology Transfer (IBSNAT) project. It is part of the Decision Support System for Agrotechnology Transfer (DSSAT) system. It is a physiological-based and management-oriented model which can simulate the growth and development of rice under optimal, nitrogen-limited, and water-limited conditions (Timsina and Humphreys, 2003). Like other crop modules of CSM, the model uses a minimum of readily available daily weather data, soil profile characteristics, crop management, and variety-specific genetic inputs. To simulate rice growth, development, and yield the model considers the following processes:

- Rice development, especially as affected by genotype and weather. The model simulates the effects of photoperiod and temperature on the timing of panicle initiation and the duration of each major growth stage. A provision has been made within the model to calculate the effect of transplanting shock on phase duration.
- Biomass accumulation using a CERES-type radiation use efficiency approach that includes the effect of atmospheric CO_2 concentration.
- Biomass partitioning using phenology to drive the development and growth of vegetative and reproductive organs.
- Water balance that simulates the daily evaporation, runoff, percolation, and crop water uptake under fully irrigated conditions, rainfed conditions with intermittent flooding and drying, and fully upland conditions where the soil is never flooded. The latter code is shared with all CSM crop modules. (Ritchie, 1998)

As a process-based model, CERES-Rice can be applied to a wide range of research problems, including response to both irrigation and nitrogen management (Ahmad et al., 2012; Zhang et al., 2018), yield-gap analyses (Zhang et al., 2018), yield forecasting (Jha et al., 2019) and breeding and rice genetics (Gao et al., 2020; Buddhaboon et al., 2018). This also includes the potential impacts of climate change.

CHAPTER THREE

RESEARCH METHODOLOGY

3.1. Study areas

3.1.1. Location and climate of the fields experiment.

Prior to the fields implementation in Benin on rice cultivation, a laboratory and field validations were conducted in Germany on the new developed device. The laboratory tests were performed at the Leibniz Center for Agricultural Landscape Research (ZALF), working group for isotope biogeochemistry and Gas Fluxes, Eberswalder Str. 84, 15374 Müncheberg, Germany. The field validation was conducted at the experimental field “PatchCrop”. It is located near the village of Tempelberg, Northeast Germany (52°44’86.2” N, 14°14’05.1” E). The temperate climate is characterized by a mean annual air temperature of 9.7°C and a mean annual precipitation of 544 mm (ZALF weather station, 2010–2019). The soil is medium loamy, sand textured soil that can be classified as Luvisol (WRB). The "PatchCrop" experimental field is managed by the Leibniz-Centre for Agricultural Landscape Research (ZALF).

The field experiments were implemented at the Koussin-Lele irrigated scheme (7°15′N, 2°16′E), in the Cove district of southern Benin (Figure 9). This site was selected because: (1) it’s the second largest scheme for irrigated rice production in Benin; (2) it's crossed by the Zou River and its tributaries, which offer an excellent opportunity for rice production; and (3) several projects were conducted in this area, which might be an opportunity to carry out research dealing with the challenges of innovation (Saidou et al., 2014). The region is representative of a transitional climate between the sub-equatorial climate and the humid tropical climate of North Benin (Sintondji et al., 2017). It experiences a bimodal annual rainfall distribution characterized by two rainy and two dry seasons (Saidou et al., 2014). Over 1991–2020, the average of total annual rainfall amounted to 1099.5 ± 195.8 mm in the study area. For the same period, the annual means for minimum temperature, maximum temperature, and solar radiation were 21.4 ± 0.6 °C, 33.7 ± 0.7 °C, and 19.9 ± 0.5 MJ m^{-2}. d^{-1}, respectively. Irrigated rice farming is done twice every year. The first campaign typically runs from March to June, while the second runs from September to January (Sintondji et al., 2017). The distribution of rainfall and temperature during the two years of the field experiment is presented in Figure 10.

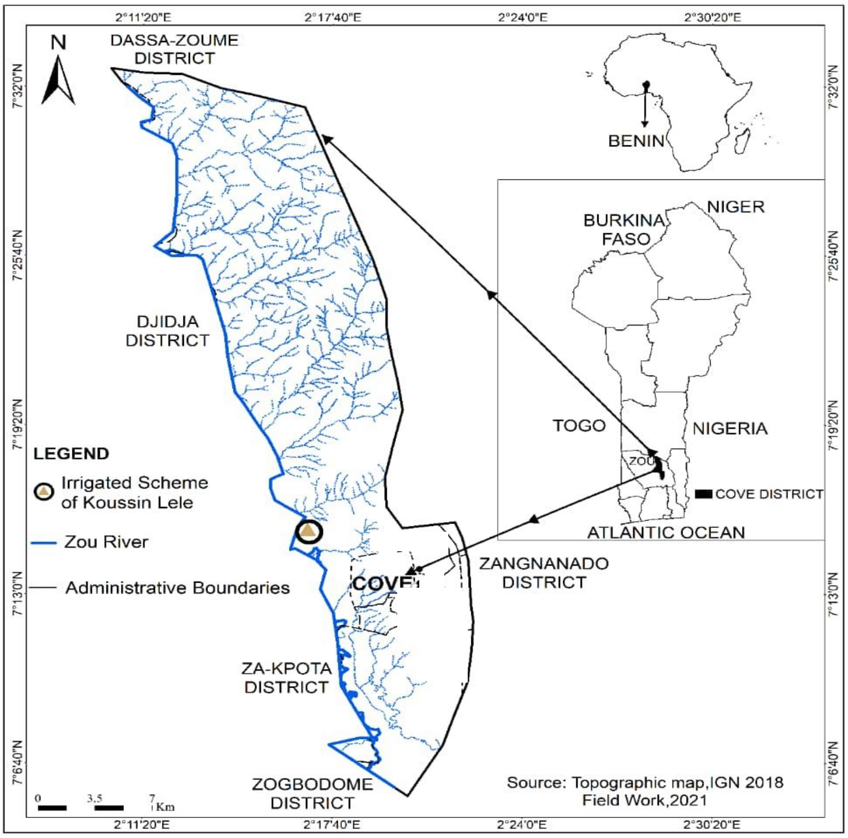

Figure 9: Map showing the location of the field experiment in COVE district, Benin.

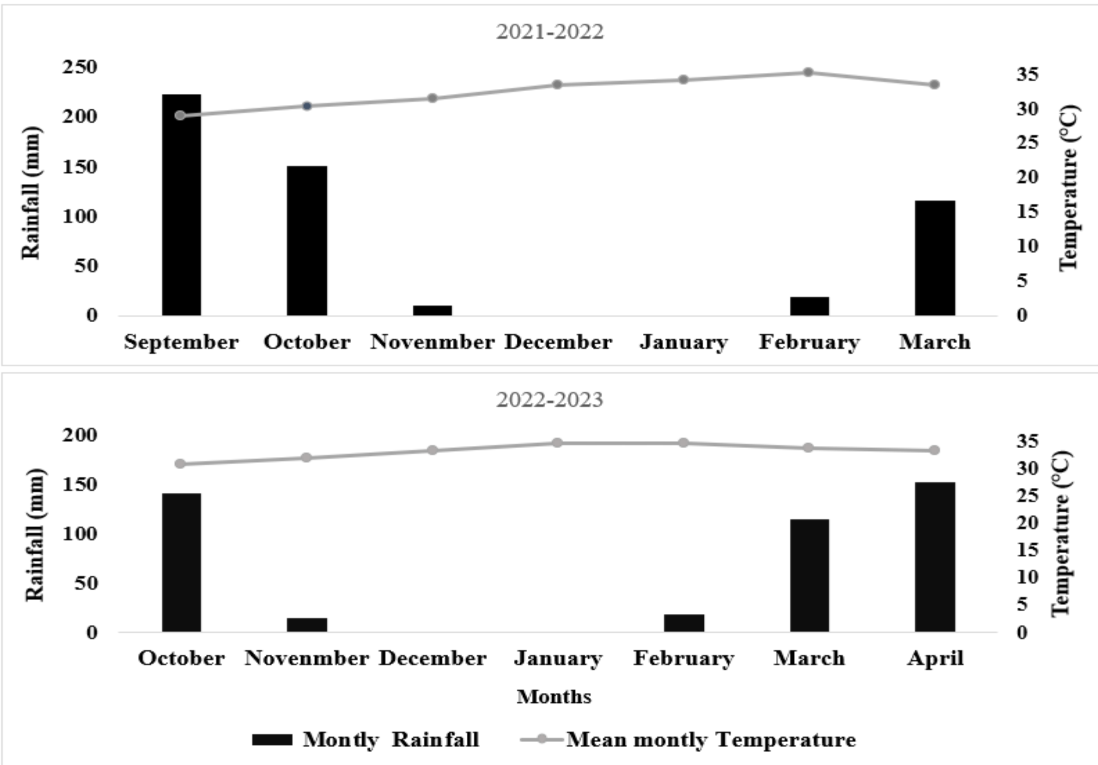

Figure 10: Distribution of rainfall and Temperature during the two years of the field experimental

3.1.2. Soils of the experimental site

According to FAO taxonomy, the upper soil of the Koussin-Lele irrigated scheme was classified as gleysols (Youssouf and Lawani, 2000) and it belongs to the group of “hydromorphic soil”. To identify both soil chemical and physical properties, soil samples were taken at four different depths (0-20 cm; 20-40 cm; 40-60cm; 60-80 cm) in August 2021, before the onset of the experiment. Nine composite samples were taken at each depth. Each sample, which weighed approximately 200g, was sealed in a plastic bag and transported to the laboratory of the National Institute of Agricultural Research of Benin. In the laboratory, the soil samples were air-dried, crushed using a mortar and pestle, and then sieved through a 2 mm sieve. The sieved sample was subdivided into two portions: one for physical analysis and the other for chemical analysis.

The particle size distribution was determined based on the hydrometer method (Bouyoucos, 1951). The soil pH was determined using a soil-to-water ratio of 1 to 2.5. The content of soil organic carbon was determined by chromic acid digestion, and the total nitrogen was determined by the Kjeldahl digestion method. The Bray-1 method (0.5 M HCl + 1 M NH_4F) was used to determine the available phosphorus content of the soil. The soil potassium was extracted with 1 M NH_4-acetate, and the content was determined by flame emission spectrophotometry.

The mean values of soil characteristics at the experimental site are presented in Table 5. The scheme used in this study for the interpretation of soil chemical characteristics is presented in OC is organic carbon content, N is nitrogen content, P is phosphorus content, K is potassium content, CEC is cation exchange capacity and OM is the Organic Matter content.
Table *6*. The texture of the soil varies slightly according to the different layers. For the different soil layers, the texture was sandy loam (0–20), sandy clay loam (20–40), sandy loam (40–60), and sandy clay loam (60–80). The topsoil presents a medium organic and nitrogen content compared to other layers with a low organic content (<0.5%), medium nitrogen content (0.045–0.08), very low available phosphorus (5 ppm) and medium potassium concentration.

Table 5: Mean values of soils characteristics at different depth of the experimental site.

Layer (cm)	Silt (%)	Sand (%)	Clay (%)	PH eau	OC (%)	N (%)	P_{ass} (ppm)	K_{mEq} 100 g	CEC	OM (%)
0-20	11.56	76.82	11.62	5.85	0.81	0.09	5.74	0.09	8.24	1.39
20-40	11.55	58.07	30.38	5.67	0.42	0.06	1.69	0.04	15.52	0.72
40-60	7.99	79.74	12.27	5.30	0.38	0.04	1.57	0.07	15.72	0.66
60-80	12.58	64.77	22.65	5.16	0.29	0.03	5.15	0.07	11.12	0.50

OC is organic carbon content, N is nitrogen content, P is phosphorus content, K is potassium content, CEC is cation exchange capacity and OM is the Organic Matter content.

Table 6: Interpretation scheme of soils chemical properties

Soil chemical	Interpretation scheme			
characteristics	Very low	Low	Medium	High
PH water	<6.10	6.10-6.50	6.60-7.30	>7.30
Organic carbon	<0.58	0.58-0.80	0.80-1.50	>1.50
Total Nitrogen	<0.03	0.03-0.045	0.045-0.08	>0.08
Phosphorus	<5.00	5.00-10.00	10.00-20.00	>20.00
Potassium	<0.40	0.40-0.80	0.80-1.60	>1.60

Source: Sys et al., 1993

3.2 Experimental design and treatments

3.2.1 Hard- and software implementation

The developed, highly portable CO_2 and H_2O flux measurement device consists of a logger and sensor unit, both assembled out of a combination of various low-cost, off-the-shelf components. A complete list of used components, distributors and prices is given in Table 7 . Figure 11shows the assembled logger and attachable sensor unit, together with a schematic representation of the wiring.

The logger unit consists of an Arduino Uno like microcontroller (Atmega328, AZ-Delivery Vertriebs GmbH, Germany) with attached Logger Shield module (AZ-Delivery Vertriebs GmbH, Germany) including a SD card reader and SD card (2GB) to store sensor readings and a real time clock (RTC) which helps to keep the time and date even when the system is switched off. A BME280 air temperature (±1˚C), air humidity (±3 %) and air pressure sensor (±1 hPa; reichelt elektronik GmbH & Co., Germany) as well as an LCD display (AZ-Delivery Vertriebs GmbH, Germany) and HC-05 Bluetooth module are part of the logger unit and connected to the microcontroller. The logger unit is fitted into a weather and shock resistant outdoor housing (B&W Outdoor Case Type 500, OVERHAUL MEDIA GmbH, Germany).

The external sensor unit consists of a nondispersive infrared (NDIR) based CO_2 (0-10,000 ppm, ±30 ppm ±3 % accuracy; K30FR, Senseair AB, Sweden) and an air humidity (RH) and air temperature sensor (SHT31, DHT22). Both sensors were connected through a seven-core cable to the logger unit using UART (K30FR) and I2C (SHT31) data communication, respectively.

The power supply of the microcontroller is ensured by 6 rechargeable AA NiMH batteries (1.2 V; 2600 mAh) in a 6xAA battery holder, which supply 7.2 V. Due to the power requirements of the external sensor unit (K30FR and SHT31), an additional 6xAA battery holder is attached to the housing to supply it directly. Software implementation was done using Arduino IDE 2.0.3 (program code given as supplement).

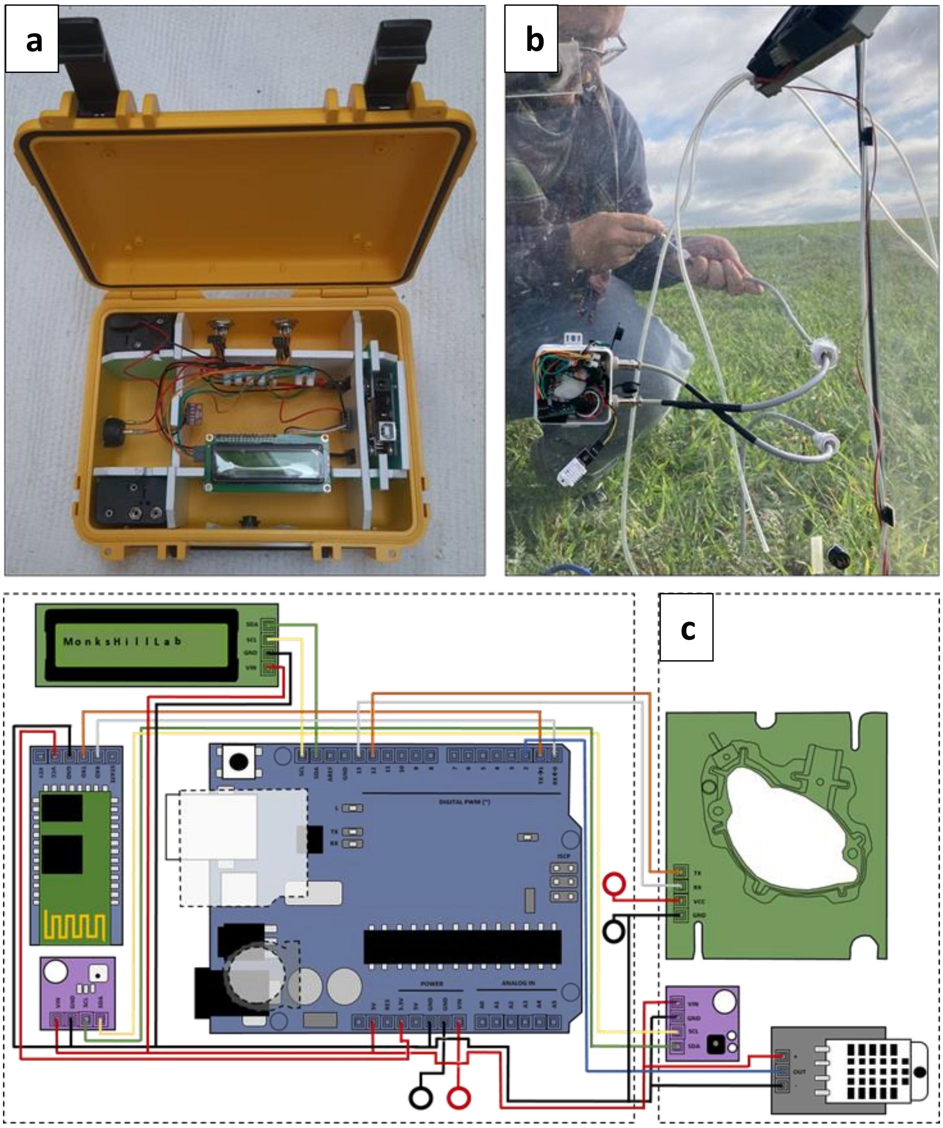

Figure 11: (a) Logger unit in weather and shock resistant housing, (b) external sensor unit attached to a transparent non-flow-through non-steady-state closed chamber and (c) schematic representation of the wiring.

Table 7:Sensor components and cost (in Euro) at time of writing, including weather and shock-proof housing, and energy supply (batteries). Components needed for optional semi-automatic mode are listed in addition.

Component	Amount	Description	Price	Distributor
B&W Outdoor Case Typ 500	1	Outdoor case for housing electrical components	28.75 Euro	www.profikoffer.de
PVC hard foam plate	1	PVC 5mm hard foam plate to create interior of housing for electronic components	1.5 Euro	www.amazon.de
Luster terminals	12	Luster terminals for wiring electrical components within housing	0.6 Euro	www.amazon.de
0.2mm² 24awg Electrical wire		Electrical wires for wiring electrical components within housing		www.amazon.de
7 Pin Aviation connector	2	Aviation connector to connect logger unit within weatherproof housing with passive NDIR sensor installed in the closed chamber to be attached	2.9 Euro	www.amazon.de
7 core rubber cable (1.5m)	1	Cable to connect logger unit within weatherproof housing with passive NDIR sensor installed in the closed chamber to be attached	3.75 Euro	www.conrad.de
WS R13-112 AAAA Rocker switch	1	Rocker switch for switching on and off	1 Euro	www.reichelt.de
Atmega 328	1	Arduino Uno like microcontroller	5 Euro	www.azdelievery.de
DataLogger Module	1	Loggershield for Arduino UNO like microcontroller with SD card reader and RTC unit	4.6 Euro	www.azdelievery.de
HAMA Class 4, SD memory card, 2 GB, 10 MB/s	1	SD memory card to save sensor readings	6 Euro	www.saturn.de
HC-05 Bluetooth Wireless RF-Transceiver-Module RS232	1	Bluetooth module for wireless communication	5.2 Euro	www.az-delievery.de
16x2 LCD or OLED Display	1	LCD or OLED display for data visualization	3.7 Euro	www.az-delievery.de

with I2C adapter				
BMP280	1	Air pressure, air humidity and air temperature sensor	1.7 Euro	www.reichelt.de
DHT22 or SHT31 modul	1	Air temperature and air humidity sensor	6.4 Euro	www.az-delievery.de
SenseAir K30 FR (fast response)	1	CO_2 measuring module with fast response time; Measuring range: 0 to 5000 ppm CO_2, operating range: 0 to 50 °C	85 Euro	www.driessen-kern.de
Goobay 11467 6x (4x) Mignon (AA) Battery holder	2 (1)	Battery holder for 6x NiMH rechargeable mignon (AA) batteries	4.6 Euro	www.conrad.de
Conrad energy HR06 Mignon (AA)-Akku NiMH 2600 mAh 1.2 V	12 (16)	NiMH rechargeable mignon (AA) batteries	38 Euro	www.conrad.de
4.5V metal brush air pump	2	Air pump for flushing headspace of small chambers	9.45 Euro	www.berrybase.de
IRLZ44N Mosfet	1	Mosfet to control power supply to pumps	0.75 Euro	www.reichelt.de
Total costs			**199.7 Euro**	

3.2.2 Laboratory validation

To identify the non-dispersive infrared (NDIR) sensor, most suitable for in-situ, dynamic closed chamber measurements, four different NDIR-based sensors, namely 1.) MHZ-19 (Winsen Electronics Technology CO., LTD, China), 2.) MHZ-14 (Winsen Electronics Technology CO., LTD, China), 3.) SCD30 (Sensirion AG, Switzerland) and 4.) K30 FR (Senseair AB, Sweden) were tested and validated regarding their precision and accuracy during a laboratory experiment. For this, sensors were placed separately into a sealed, ventilated, cylindrical vessel (

Figure *12*; V: 1425.5 cm2) and connected to the developed low-cost logger system. All sensors were calibrated in ambient air prior to use according to manufacturer instructions. Afterwards different distinct amounts (5 to 30 ml; in 5 ml steps) of a technical gas containing 10.000 ppm CO_2 (Linde, Germany) were repeatedly (n=30 per sensor) injected into the sealed vessel using a syringe and a closable valve. In between injections, the vessel was flushed with ambient air by two pumps (1.5l min^{-1}) connected to it (semi-automatic measurement mode of the developed system). Finally, CO_2 concentration increases inside the vessel, measured in a 5s interval by the NDIR-based sensors, from before to after injection (Δ CO_2 in ppm) were compared against mixing-induced CO_2 concentration increases. Sensors that performed best in terms of accuracy and precision were consequently validated in the field.

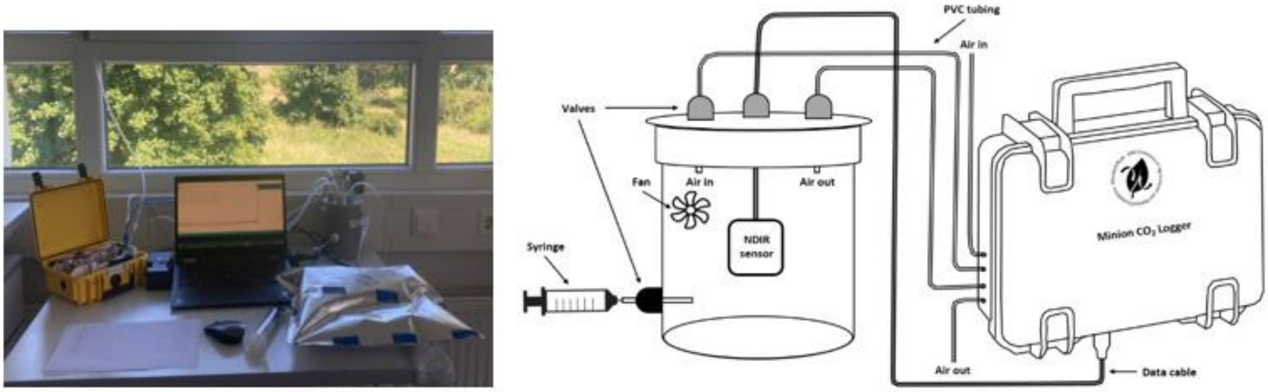

Figure 12: Experimental setup of the performed laboratory validation of four different NDIR *CO_2* sensors connected to the developed low-cost CO_2-flux measurement system (MHZ-14, MHZ-19, SCD30 and K30FR) through injecting distinct amounts of technical gas (Linde, Germany; 10,000 ppm CO_2) into an air-tight sealed cylindrical vessel.

3.2.3 Field validation

Field validation of the low-cost CO_2 and ET flux measurement system was performed through parallel manual closed chamber measurements using an infrared gas analyzer (IRGA; LI-850, LI-COR, USA) and NDIR/RH sensors passing previous laboratory validation. Measurements were conducted at the “PatchCrop” experimental field. “PatchCrop” features multiple smaller patches (72 x 72m), with diverse and site-specific crop rotations, aiming to create synergies and interactions between fields.

Figure 13:Parallel opaque (Reco) manual closed chamber measurements with a Li-COR 850 IRGA (LI-850, LI-COR, USA) and the developed, low-cost CO_2 and ET flux measurement system.

The developed system was equipped with a K30FR and SCD30 NDIR, as well as SHT31 and DHT22 sensor. Net ecosystem exchange (NEE), ecosystem respiration (Reco) and ET measurements were conducted for a mixture of *Phacelia* and *Guizotia abyssinica* at three repetitive plots, established at one of the patches through installing PVC collars (A: 0.5625 m2; 5 cm deep) in the beginning of October 2022. Measurements started shortly after sunrise and lasted to late afternoon during two consecutive days, using a dynamic, (non-)flow-through non-steady-state ((N)FT-NSS) manual closed chamber system. Used transparent (86 % light transmission; NEE flux measurements) and opaque (ecosystem respiration (Reco) flux measurements), cubic shaped PVC chambers had a total volume of 0.296 m^3 and were equipped with a fan for efficient headspace mixing. CO_2 and H_2O concentrations, as well as RH, during chamber deployment were recorded in parallel using a LI-850 IRGA and the developed, low-cost measurement system, equipped with a K30FR, SCD30, SHT31 and DHT22 sensor, respectively. NEE, Reco, and ET fluxes were measured by alternately deploying the opaque and transparent chambers on the three pre-installed PVC frames. During an individual 4 min measurements, CO_2, and H_2O concentration, as well as RH, changes in the chamber headspace, air temperature inside and outside the chamber, soil temperature and humidity (TMS-4, TOMST, Czech Republic) as well as PAR (outside the chamber, Skye, UK) were recorded at a 3s (Li-850) to 5s interval (NDIR and RH sensors). To validate the low-cost CO_2 and ET flux measurement system, measured Reco, NEE and ET fluxes, as well as derived temperature (Reco) and PAR dependency functions (GPP), were directly compared against results obtained in parallel with the IRGA.

3.2.4 Fields application and treatments

Two field experiments were established at the same site to study (i) the responses of rice production to water management and N fertilizer application and (ii) the effect of heat stress induced by different planting dates on rice yield.

3.2.4.1 Description of the field experiment 1

The goal of this experiment was to instigate the effect of water management and N fertilizer application on rice growth, water and Nitrogen use efficiency, yields, CO_2 emissions, the net ecosystem balance, and the evapotranspiration.

3.2.4.1.1 Experimental treatments and design

The first experiment was a factorial combination of three levels of water management and three levels of inorganic nitrogen (N) fertilizer application. The water management technologies included continuous flooding (CF) and two alternate wetting and drying (AWD) methods (AWD15 and AWD25) of irrigation. Nitrogen fertilizer levels were: 0 (N0), 90 (N90; which corresponds to all farmers' practices two years ago) and a high level of 120 kg N. ha^{-1} (N120). Most of the farmers on the irrigated scheme have started applying this high amount of nitrogen due to soil fertility decline.

The experimental design was a split-plot design with three replications of the nine treatment combinations. Water management was the main plot treatment, and N fertilizer levels were the subplot treatment. The size of each plot was 5 x 4 m (20 m^2). The distance between the main plots was 2 m, and the subplots' distance was 1 m. To mitigate the risk of nitrogen moving across the plots and reduce the risk of lateral flows, a 200-micron layer of plastic was laid down 0.40 m deep into the edges of the levees along the inner perimeter of all plots. Also, bunds were constructed on the perimeter of each plot to stop the runoff of the irrigation water.

3.2.4.1.2 Crop and soil management

In the continuous flooding treatment, the depth of water was kept at 3 cm just after transplanting and increased gradually (depending on plant height) to 4–7 cm at the active tillering stage and maintained until 10 days before harvest to minimize the water requirement at the vegetative stage of the crop. In the AWD treatments, a perforated PVC pipe, of about 20 cm in diameter was installed in each AWD plot to depths of 15 and 25 cm, which correspond to two levels of AWD (AWD15 and AWD25), respectively. Pipes were installed near the bund for easy water monitoring (Figure 14). After burying the pipes, the soil inside the tubes was removed so that the bottom level was visible. The water depth in the tube was monitored using a meter stick, and irrigation was applied when there was no visible water in the tube until the depth above the soil surface reached 5 cm (Lampayan et al., 2015). However, the frequency and timing of irrigation varied, sometimes slightly, across experiment replicates. At transplanting, the AWD plots were kept flooded to maintain uniform moisture content at saturation for the first 2 weeks to ensure the full establishment of the juvenile plants. At the start of flowering, when 5 % of the panicles had fully emerged from the boot, all AWD treatments were suspended, and the water level was maintained at 5 cm above the soil surface to reduce the risk of spikelet sterility due to water-deficit stress at this sensitive stage. One week after the completion of the flowering stage, AWD was applied again until 10 days before the expected time of harvest in all water treatments.

The nitrogen fertilizer (urea) was applied three times that was 50% at transplanting, 25% at the beginning of the tillering stage, and the last 25% at panicle initiation. Straight fertilizers of triple superphosphate (P_2O_5) and muriate of potash (K_2O) were applied at a rate of 40 kg ha^{-1} as the basal rate for all treatments on transplanting day.

Prior to transplanting, the field was cleared, flooded with irrigation water for about four (4) days, and puddled to a depth of 15-20 cm to reduce water percolation and soften the soil for transplanting. The rice (Oryza sativa L.) variety IR841 was used as the test crop. This variety was selected because it is the most improved by the Ministry of Agriculture and is widely grown by most of the farmers in Benin. It can be cultivated during both the rainy season and the dry season. Also, it is resistant to pest attacks and presents an attractive aroma (Totin et al., 2003). The certified seeds were used for the nursery. 14-day-old seedlings were transplanted in the puddled field on October 2nd ,2021 and November 4th, 2022, respectively, at the rate of 25 hills m^{-2} (20 cm between rows and 20 cm between plants within a row), with 2 seedlings per hill. During the transplanting, all plots were kept saturated with water to prevent transplant shock (Yakubu et al., 2018). Insecticides (Super gros and Emacot) were used at the vegetative stage to control stem borer infestations and at the flowering stage. The experimental field was covered with nylon nets from the flowering stage until harvesting to prevent bird and rat attacks during the grain filling period. Pre-emergence herbicide was applied once during land preparation, and thereafter, the field was kept free of weeds every 10 days till the flowering stage by handpicking to avoid yield loss. Rice plants were harvested on January 14–15 and February 17 of the year 2022, and 2023, respectively.

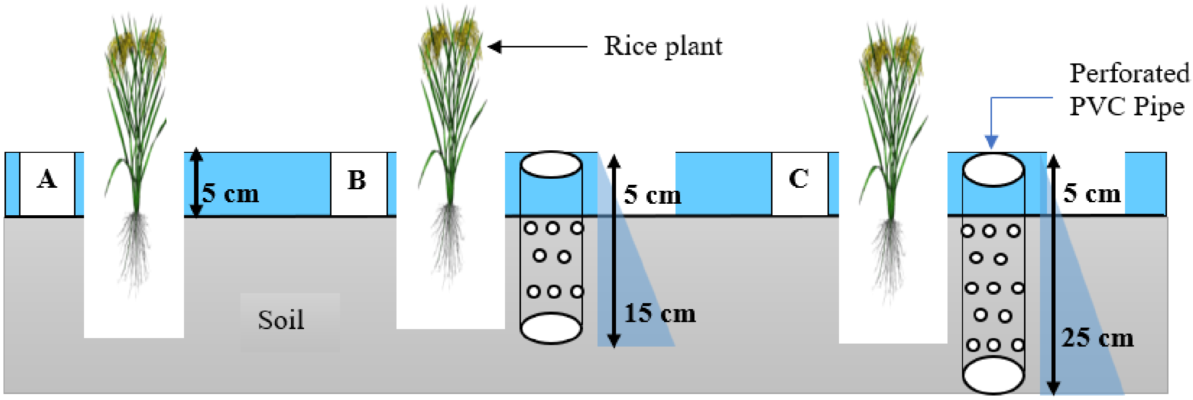

Figure 14: Schematic representation of (A) CF, (B) AWD15, (C) AWD25

3.2.4.2 Description of the field experiment 2

The goal of this experiment was to collect critical data for calibrating and validating the CERES-Rice crop growth model.

3.2.4.2.1 Experimental treatments and layout or design

The second experiment consisted of three levels of transplanting date (D1, D2, and D3) of the same variety of rice transplanted in experiment 1. D1 is the transplanting date of experiment 1; D2 and D3 correspond to two and four weeks after D1, respectively. The size of each plot was 5 m x 4 m, and all the experimental plots were arranged in a Randomized Complete Block Design with three replications. The distance between blocks was 1 m, and the plot-to-plot distance was 0.5 m.

3.2.4.2.2 Crop and soil management

The experiment was set up under non-water-limiting conditions (continuous flooding) and non-nutrient-limiting conditions (120 kg N/ha). These conditions were chosen to avoid nutrient and water stress. Field preparation, transplanting conditions, continuous flooding water management, fertilizer application, weed and pest management remained the same as described in experiment 1.

3.3. Measurements and field data collection

3.3.1 Net CO_2 Ecosystem Exchange and Ecosystem Respiration measurements

The developed, low-cost measurement system has been tested for applicability and reliability under challenging environmental conditions at an experimental field at Koussin-Lele. Case study measurements of CO_2 exchange were conducted from November 2022 until March 2023 using a closed chamber system in experiment 1. This system is used to accurately measure direct CO_2 flux between the atmosphere and low canopies (Müller et al., 2009; Hoffmann et al., 2015). Classified as flow-through non-steady-state (FT-NSS) (Huth et al., 2017, Livingston and Hutchinson, 1995), two chambers (height of 1 m, a surface area of 0.16 m^2 and a thickness of 4 mm) made with acrylic sheet were used to collect CO_2 fluxes from all fertilized plots of the experiment. The acrylic sheet was used because it is non-reactive with the CO_2 trapped inside the chambers. During the measurement campaigns, Net CO_2 Ecosystem Exchange (NEE) and Ecosystem Respiration (Reco) were measured. NEE was measured by using an acrylic transparent chamber, and Reco was measured by covering the transparent chamber with opaque sheet to exclude light and thus, photosynthesis activities.

The stainless-steel bases of the chambers (frames) were inserted permanently into the ground before rice transplanting with a sealing groove. They remained in their position for the entire measurement period to ensure reproducible placement of the chamber as well as airtight closure during successive CO_2 flux measurements during the rice growing period. The frames covered 4 rice hills, and for each measurement campaign, the chambers were placed on pre-installed frames (Hoffmann et al., 2015; Hoffmann et al., 2017).

A vent tube made of plastic material (length 50 cm and inner diameter 0.5 cm) was placed on top of the chamber to allow pressure equilibrium between the chamber's headspace and the ambient atmosphere (Dossou-Yovo et al.,2016). A rubber belt was sealed at the bottom of each chamber to ensure airtight closure during measurements. To ensure efficient headspace and avoid mixing errors due to air stratification during the measurement, chambers are equipped with an adjustable fan (12 VDC, 0.1 A), which is operated by a power bank device of 2600 mAh. The concentration of CO_2 development inside the chamber over chamber deployment time (7 min; 3 sec record interval) was recorded using our new powerful low-cost logger that was connected to the K30FR CO_2 sensors and DHT22 temperature-humidity sensors. During each measurement campaign, NEE, Reco, and ET fluxes were measured by alternately deploying the opaque and transparent chambers on pre-installed frames (A: 0.16 m^2) at each of the measured plots. The CO_2 campaign was performed biweekly during the whole growing season, from two weeks after transplanting to one day before the harvest. It generally starts before the sunrise and ends in the late afternoon in order to cover the entire temperature and photosynthesis activity range (Hoffmann et al., 2015). Before each campaign, the weeds were carefully removed from each frame.

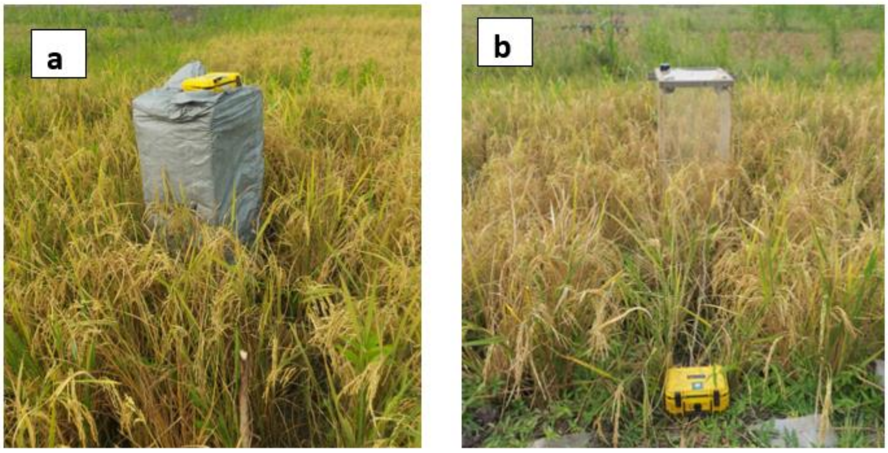

Figure 15: (a) Ecosystem respiration measurement and (b) the Net ecosystem exchange measurement

3.3.2 Below Autotrophic and heterotrophic soil CO_2 respiration

A small cylindrical chamber (25 cm in height and 16 cm in inner diameter) was custom-made of PVC to measure below autotrophic and heterotrophic soil CO_2 respiration. A long PVC pipe (50 cm in length) was used as a frame for heterotrophic respiration, whereas a short PVC pipe (13 cm in length) was used as a frame for soil respiration. These frames were inserted permanently in the ground (only 5 cm is visible above the soil surface) before the rice transplanting, and they remained in their position for the entire measurement period. By adding 6V pumps to flush air out for 5 minutes after 7 minutes of measurement (7-second record interval), the manual system used for ecosystem respiration measurement was improved into a semi-automatic system for soil CO_2 respiration measurement. This semi-automatic system was connected to the SCD30 CO_2 sensor. In each frame, rice was not cultivated, and weeds were entirely removed before each campaign. CO_2 flux measurement campaigns were performed monthly during the growing season. Below autotrophic respiration (Ra) was determined as the difference between soil respiration (Rs) and heterotrophic respiration (Rh).

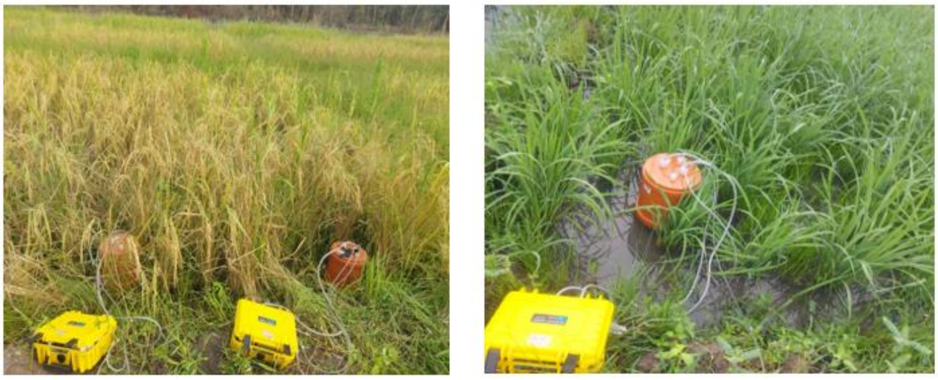

Figure 16: Soil CO_2 measurement

3.3.3 Meteorological parameters measurements

Meteorological parameters such as soil moisture, soil and air temperatures, and photosynthetically active radiation (PAR) were measured at a 30-min frequency during the entire experimental period. The Tomst-TMS-4 dataloggers were used to measure temperature and soil moisture at three different levels using three temperature sensors and one soil moisture sensor. It is mainly used to record soil moisture and temperature at a depth of -6, +2, and +15 cm (Wild et al., 2019). The devices were installed into the ground prior to the transplanting. There was one device per plot (close to the frame) and another one as a central station for the experimental site. More information regarding the device can be found at https://tomst.com/web/en/systems/tms/tms-4/. Different values of PAR were recorded using the Apogee SQ-420X USB smart quantum sensor. The device is designed, built, and calibrated in Logan, Utah, USA. More details regarding the device can be found at https://www.apogeeinstruments.com/sq-420x-smart-quantum-sensor-usb-output/. In addition, during each measurement, outside air temperature and air pressure were also logged from the BMP280 sensor installed in the minion (the developed low-cost logger).

Figure 17: Device for (a)PAR measurement and (b) soils and air temperature measurements

3.3.4 CO_2 and ET Data Processing

3.3.4.1 Flux calculation and separation of NEE into GPP and Reco.

For laboratory validation, the changes in CO_2 concentrations in the vessel, expressed as ΔCO_2 in ppm, were calculated as the mixing-ratio of measured ambient air and injected technical gas CO_2 concentration (10,000 ppm). These were compared with the ΔCO_2 obtained for the different NDIR sensors as the difference in mean CO_2 concentrations measured for one minute right before and two minutes after injection.

For the field validation and the field experiment 1, measured CO_2 and ET fluxes were calculated using a modular R script, described in detail by Hoffmann et al. (2015; CO_2) and Dahlmann et al. (2022; ET), respectively. Prior to CO_2 and ET flux calculation a death-band of 10 % was applied to the data of each chamber measurement. CO_2 concentrations measured using the IRGA were additionally corrected for changes in water vapor during chamber measurements (Webb et al., 1980).

Unlike the IRGA which provided H_2O as mole fraction, used low-cost RH sensors (DHT22 and SHT31) required additional post processing. RH measurements were converted into a mass concentration following Hamel et al (2015; Eqn. 1):

$$\mathbf{H_2O = \frac{RH \cdot e^s}{100 \cdot P}} \qquad \text{[Eqn. 1]}$$

where RH is the relative humidity and e^s is the saturated vapor pressure (Pa), calculated according to Allen et al., (1998). Thereafter, CO_2 and ET fluxes were calculated based on the ideal gas law using a linear regression approach (Eqn. 2):

$$\boldsymbol{f = \frac{MpV}{RTA} \cdot \frac{\Delta c}{\Delta t}} \qquad \text{[Eqn. 2]}$$

where M denotes the molar mass of the gas (g mol^{-1}), p denotes the ambient air pressure (Pa) and V denotes the chamber volume (m^3). Since plants accounted for < 0.1 % of the total chamber volume, a static chamber volume was assumed. R denote the gas constant (8.314 m^3 Pa K^{-1} mol^{-1}), T denote temperature inside the chamber (K), A denotes the basal area (m^{-2}) and $\Delta c/\Delta t$ denotes the linear CO_2 (e.g., Leiber-Sauheitl et al., 2014) and H_2O concentration change over time (e.g., Dahlmann et al., 2022). The variables T as well as more importantly dc/dt, were obtained by applying a variable moving window (0.5 to 3 min.) to each chamber measurement. Thus, resulting multiple ET and CO_2 fluxes per measurement (based on generated variable moving window data subsets) were further evaluated according to the following criteria: 1.) fulfilled prerequisites for applying a linear regression (normality

(Lillifor´s adaption of the Kolmogorov-Smirnov test), homoscedasticity (Breusch-Pagan test) and linearity); 2.) significant regression slope ($p \leq 0.1$, t-test); 3.) range of within-chamber air temperature not larger than ± 1.5 K and a PAR deviation (only transparent chamber measurements) not larger than ± 20 % of the average to ensure stable environmental conditions within the chamber throughout the respective measurement; 4.) no outliers present (±6xIQR). Calculated CO_2 and ET fluxes that did not meet all criteria were discarded. In cases where more than one flux per measurement met all criteria, the CO_2 and ET flux with steepest slope and closest to chamber deployment were chosen. The remaining set of flux rates is further reduced by selecting the 25% with the steepest absolute slope, as suggested in the literature (Drewitt et al., 2002; Kutzbach et al.,2007). The final flux per measurement is finally selected, based on the minimum Akaike Information Criterion (AIC). Paired-sample Wilcoxon signed-rank, t- and Z-tests were also performed to screen the final obtained fluxes of NEE plots, which evidenced significantly different flux patterns throughout consecutive campaigns, a plot wise modelling exercise was also performed.

3.3.4.2 Gaps filling

Empirical models based on nighttime Reco and daytime NEE measurements, as described by Hoffmann et al., (2015), were used to account for gap filling and obtain cumulative NEE values. Reco flux was calculated using a temperature-dependent Arrhenius-type model that considered both recorded air and soil temperatures at different depths (Lloyd and Taylor, 1994; Eqn. 3).

$$\mathbf{R_{eco} = R_{ref}\ x\ e^{E_0\,(1/(T_{ref}-T_0)-1/(T-T_0))}} \qquad \text{[Eqn. 3]}$$

where Reco is the measured ecosystem respiration rate (μmol−1C m−2 s−1), Rref is the respiration rate at the reference temperature (273.15 K, Tref), E_0 is an activation energy-like parameter, T_0 is the starting temperature constant (227.13 K) and T is the mean air or soil temperature during the flux measurement. A separate Reco model is parametrized for each temperature collected from the Tomst sensor. Out of the four obtained Reco models (one model for air temperature; soil temperature at 2, 5 and 10 cm depth), the model with the lowest Akaike information criterion (AIC) was finally used.

For GPP fluxes, a PAR-dependent, rectangular, hyperbolic light-response function based on the Michaelis–Menten kinetic was used (Wang et al., 2013; Hoffmann et al., 2015; Eqn. 4). Since GPP cannot be measured directly, GPP fluxes were calculated as the difference between measured NEE and modelled Reco fluxes, using campaign specific, previously derived parameters Rref and T_0.

$$GPP = \frac{GP_{max} . a.PAR}{a.PAR + GP_{max}}$$ [Eqn. 4]

where GPP is the calculated gross primary productivity (μmol^{-1} CO_2 m^{-2} s^{-1}), GP_{max} is the maximum rate of C fixation at infinite PAR (μmol CO_2 m^{-2} s^{-1}), α is the light use efficiency (mol CO_2 mol^{-1} photons) and PAR is the photon flux density (inside the chamber) of the photosynthetically active radiation (μmol^{-1} photons m^{-2} s^{-1}).

In cases of unsuccessful fitness using the rectangular hyperbolic light-response function, a non-rectangular hyperbolic light-response function was finally used (Eqn. 5), Gilmanov et al., 2007, 2013), which usually results in significant parameter estimates.

$$GPP = a.PAR + GP_{max} - \sqrt{(a.PAR + GP_{max})^2 - 4.a.PAR.GP_{max}.\theta}$$ [Eqn. 5]

where θ is the convexity coefficient of the light-response equation.

Reco and GPP model sets were considered in cases of negative (GPP), positive (Reco) or significant parameter estimates, and therefore, the model set with the lowest AIC (Reco) was used. Averaged flux rates were applied for Reco and GPP if no fit or a non-significant fit was achieved. Based on the lowest standard deviation (SD) of measured fluxes, the length of the averaging period was thereby selected, and this procedure was repeated until the whole study period was parameterized for each treatment.

Reco, GPP and NEE were modelled in half-hour steps for the entire study period using the continuously recorded temperature and PAR. GPP was parameterized using PAR records from inside the chamber with 86 % light transmission, but it was modelled using PAR records from outside the chamber. The uncertainty of CO_2 exchange was evaluated using a comprehensive error prediction algorithm described by Hoffmann et al., (2015).

For ET, campaign-wise average daily ET fluxes (for nighttime ET fluxes measured before, for daytime ET fluxes measured after 7:00) were determined and linearly interpolated between campaigns for the entire crop growth period.

3.3.4.3 Error calculation and CO_2 statistical analysis

To test for normal distribution ($p<0.05$) of the data obtained from laboratory and field validation measurements, Kolmogorov-Smirnov test was performed. In case of normal distribution, significant differences between ΔCO_2 in ppm or Reco, NEE, and ET fluxes measured from low-cost sensors and mixing ratio ΔCO_2 or IRGA-based Reco, NEE, and ET fluxes ($p<0.05$) were determined using one-sample t-test. Error calculation for CO_2 and ET fluxes, as well as crop season CO_2 exchange and ET, were quantified using a comprehensive error prediction algorithm described in detail by Hoffmann et al., (2015).

3.3.5 Calculation of Net Ecosystem Carbon Balance (NECB) and the Water Use Efficiency (WUE)

The NECB, based on mass balance approach, was calculated as the difference between C inputs and outputs to estimate the rate of C accumulation (or loss) from each plot (Smith et al., 2010). NECB was calculated using the following equations based on previous studies (Ma et al., 2013; Wang et al., 2013, Hoffmann et al.,2015), with negative values indicating net C loss from ecosystem and positive values net sink of atmospheric CO_2.

$$\boldsymbol{NECB} = \mathbf{NEE} + \mathbf{C\ trans} - \boldsymbol{C\ grain\ yield} \qquad \text{[Eqn. 6]}$$

where, NEE is the net ecosystem exchange, C trans is the C from the juvenile transplanted plant using the biomass and C grain yield is the C removed from grain yield. Soil C losses through runoff, and leaching were negligible (Smith et al., 2007), and therefore not accounted in the present study.

For The water use efficiency, it was computed by dividing the dry weight by the evapotranspiration.

3.3.6. Phenology and growth parameters

3.3.6.1 Phenology

From each plot of both field experiments, the dates of panicle initiation, 50% anthesis and physiological maturity were recorded. Days to 50% anthesis was reached when about 50% of the plants within a plot had flowered. The physiological maturity was reached when 2/3 of the leaves turned yellow in each plot.

3.3.6.2 NDVI measurement and Leaf Chlorophyll Content

In experiment 1, non-destructive spectral vegetation indices such as the normalized difference vegetation index (NDVI) was used as a good indicator of canopy greenness, photosynthetic size, and plant health. The handheld NDVI measurement device used in this study consisted of a combination of two-faced up and two faced down visible (AS7262) and IR (AS7263) sensors, as well as Adafruit CCS811 and BME280 sensors for parallel measurements of relevant environmental parameters (e.g., ambient temperature and relative humidity). Sensor control, data visualization, and storage are implemented using a Bluetooth enabled, battery powered, compact microcontroller-based logger unit. Comparatively to the CR1000 data logger (Campbell Scientific Ltd., USA), this new low-cost device performed very well and has been tested in the field with many crops for its validation (Figure 18). Measurements were generally conducted between 11 a.m. and 13 p.m. and performed weekly during the whole growing period, starting from transplanting to harvest. During the fallow period, measurements were performed monthly. For each campaign, at least 3 replicates of a 60 s measurement with a 3-second frequency were performed per plot.

$$\boldsymbol{NDVI} = \frac{\mathbf{NIR-R}}{\mathbf{NIR+R}} \qquad \text{[Eqn. 7]}$$

Where NIR is the Near Infra-Red (NIR), and R is the red bands.

The Chlorophyll content (CC) of leaves was recorded using the atLEAF CHL PLUS meter (Wilmington, DE 19801, USA, www.atleaf.com). In each plot, 10 leaves were randomly selected, and the average value was considered for each treatment. To capture the optimal period of the day for crop photosynthetic activity, field measurements were generally conducted between 10:00 a.m. and 2:00 p.m. Both NDVI and chlorophyll content measurements were performed biweekly starting from the transplanting date to the harvest

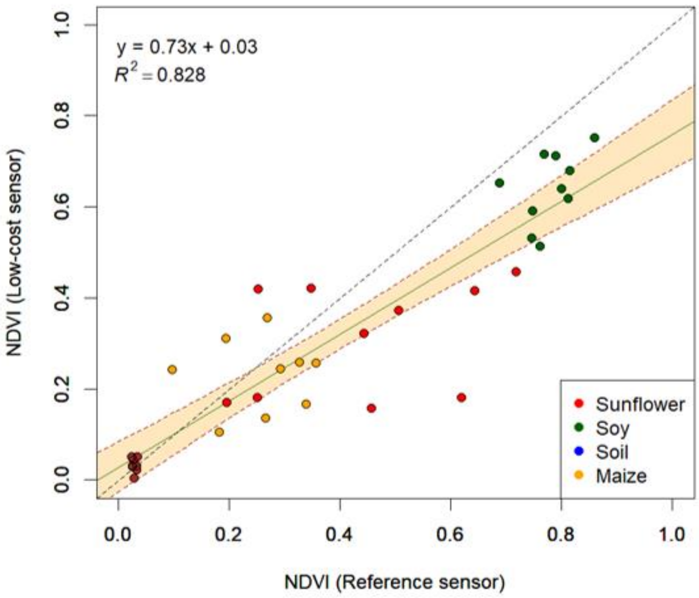

Figure 18: 1:1 correlation plot from measured NDVI using reference sensor vs. low-cost sensor.

Figure 19: NDVI and chlorophyll content measurement

3.3.6.3 The Leaf Area Index (LAI) and the dry matter weight

The leaf area of each plot in both experiments was determined by measuring the length and average width of a sample of leaves taken from four randomly selected hills. It was computed following the methods of (; Yoshida, 1981; Tadesse et al., 2013).

$$Leaf\ area\ (cm^2) = L \times W \times K. \qquad \text{[Eqn. 8]}$$

Where L is leaf length, W is maximum width of the leaf and K is a correction factor of 0.75. The leaf area index is computed as the ratio of the sum of the total leaf area of all leaves to the ground area of field where the leaves have been collected.

From each plot of both experiments, plant samples were taken on the same day of LAI measurement. Plant samples were taken from two bordered rows to avoid the border effect. At each sampling time, plant samples from 4 hills of rice were randomly selected for LAI measurement and were cut at the ground level. The fresh weight or a sample (depending on the growth stage) was weighed, placed in brown paper envelopes, and oven-dried in the laboratory at 70 ^{0}C for 72 hours to determine the dry matter weight. Both LAI and dry matter weight were taken at five occasions such the beginning (two weeks after transplanting), mid-tillering, panicle initiation, flowering, and physiological maturity.

3.3.7 Straw and Grain Yield

In both experiments, a harvest area of 4m2 (2m x 2m) was considered at the center of each plot to determine the yield. Rice plants were harvested manually using sickle, sun dried and threshed manually. Grains were obtained by winnowing and weighed at 14% moisture content using a 8988N grain moisture meter (Xiamen Hyhoo Imp. & Exp. Co., Ltd, Fujian, China). The straw obtained from the harvest area was also weighed to record the straw yield. Both grain yield and straw yield were finally converted to Mg. ha^{-1}. The harvest index was determined based on the ratio of grain yield to total biomass produced.

3.3.8 Water use measurement and water productivity.

Through a network of pipes installed on the experimental site, the amount of water consumed per plot for both experiments were measured using a flow meter (GRK, GMETERS, Goners-Udine, Italy). It was placed at the entrance of each main plot. The amount of water use was calculated as the sum of daily measurements. The depth of irrigation water was then computed by dividing the total volume of water applied by the area. The seasonal water supplied per treatment from transplanting to harvesting was the sum of all irrigation water used and the total rainfall observed over the growth period. This total amount of water did not include water used for land preparation. Water productivity (WP) was calculated as grain yield divided by the total amount of seasonal water supplied.

$$\mathbf{WP} = \frac{\mathbf{Y_i}}{\mathbf{I + R}} \qquad \text{[Eqn. 9]}$$

Where Y_i is the potential grain yield, I is the total amount of irrigation water and R is the total amount of rainfall

3.3.9 Plant analysis

3.3.8.1 Nitrogen uptake and Nitrogen Use Efficiency (NUE)

In experiment 1, after harvest, the N content from aboveground biomass was determined using micro Kjeldahl digestion, distillation, and titration to calculate aboveground total N uptake (Yoshida et al., 1976; Bremmer and Mulvane, 1982). Different parameters of Nitrogen Use Efficiency were assessed (Xue et al., 2013) such as the Agronomic N use efficiency, the Fertilizer N recovery efficiency, the Partial factor productivity of N and the Physiological N use efficiency.

Agronomic N use efficiency (ANUE, kg grain kg $^{-1}$) was calculated using the increased yield due to N application at a given rate. Fertilizer N recovery efficiency (NRE, %) was calculated based on the difference in total aboveground plant N uptake in fertilized and unfertilized plots divided by the N application rate. Physiological N use efficiency (PNUE, Kg grain Kg^{-1}) was estimated as grain yield divided by the total N Uptake. The partial factor productivity of N (PFPN, Kg grain Kg^{-1}) was calculated as the ratio of grain yield to the N rate applied.

3.3.8.2 Carbon content analysis

The rice grain from each treatment was used for total C content using a CHNS analyzer (Leco, CHNS-932 Analyzer, USA). The C content value was multiplied by the rice yield to determine the potential carbon from the grains.

3.3.8.3 Statistical analysis

Analysis of variance was performed using R software, version 4.2.2 for a split-plot design with water as the main factor and nitrogen as the sub-factor. The statistical model used included sources of variation due to replication, year, irrigation regime, N rate and the interaction of year × irrigation regime, year × N rate and irrigation regime × N rate. Mean comparison among treatments was based on the least significant difference (LSD) test at the 5% probability level.

3.3.10. The CERES-Rice model

3.3.10.1. Brief description and justification of the CERES-Rice model

The CERES-Rice model selected in this study was included in the Decision Support System for Agro-technology Transfer (DSSAT) version 4.7 (Jones et al., 2003; Hoogenboom et al., 2017). Many researchers around the world have used it for gene-based modeling, on-farm management, and precision management. The CERES-Rice model is a software application program that simulates growth, development, photosynthesis, respiration, dry matter distribution, and yield under different environments and management strategies. The model simulates rice crop growth based on the physiological processes that describe the response of rice to local soil and weather conditions. Potential growth is mainly dependent upon photosynthetically active radiation (PAR), light interception, and the light conversion efficiency through different crop management, soil, and weather interactions (Hoogenboom et al., 2010). It estimates the yield of irrigated and rainfed rice, determines the duration of growth stages, dry matter production and partitioning, the effect of soil water and N on photosynthesis and photosynthate partitioning, carbon balance, and water balance under different climate scenarios. Further descriptions regarding the CERES-Rice model can be found at the website: http://dssat.net/.

3.3.10.2. CERES-Rice model inputs

Technical reports of the DSSAT software were used as a guide for data collection. Over the two-growing seasons, data sets were collected from sample analysis, observations, and the data collected from the two experiments. Daily weather data such as maximum and minimum air temperatures, precipitation, and solar radiation from the transplanting date to the harvesting date were collected from different sources. Maximum and minimum air temperatures were collected from a Tomst sensor installed in the research field. The precipitation was collected from the rain gauge installed by the National Institute of Agricultural Research of Benin on the irrigated scheme. The data of solar radiation were obtained from the Bohicon weather station (~ 25 km from the research site). Laboratory results and FAO soil classification were used to obtain soil data such as soil class, texture, bulk density, organic carbon percentage, sand percentage, silt percentage, clay percentage, P^H, and cation exchange capacity. The crop management data, such as the planting method, planting date, plant density, row spacing, amount of fertilizer application, irrigation data, panicle initiation date, panicle maturity date, harvesting date, harvesting method, grain yield/m2, aboveground biomass, and leaf area index, were also collected from the fields.

To run the CERES Rice Model in the DSSAT software, the soil input files were created by inputting measured soil properties into the soil file creation utility program (SBuild). The weather files for the two years' experiment were created with the Weatherman utility program. All the data on crop management, growth, and yield collected for the two seasons were created using the program Xbuild.

3.3.10.3 Calibration and validation of CERES-Rice model

The calibration of the CERES rice model was based on the 2021–2022 data set from field experiment 2. The genetic coefficients of the rice that affect the occurrence of phenological stages in the CERES-Rice models were derived using the GLUE (Generalized Likelihood Uncertainty Estimation) program of DSSAT v 4.7 (Jones et al., 2010). This program was developed using the R statistical programming language and is used to estimate the coefficients for a genotype (P1, P2O, P2R, P5, G1, G2, G3, and G4) by iteratively running the crop model with an approximate value of the coefficients concerned. Likelihood values are then calculated for each set of coefficients using the differences between model predictions and measurements. Weights and probabilities are calculated with the Bayesian equation, and the posterior coefficients are estimated.

The validation of the model used the collected data from field experiment 2 of the year 2022–2023. This was done to ensure that applications of the models to assess different seasonal conditions in the study region are reliable. For that, the same genetic coefficients recently calibrated were considered to assess the performance of the model based on the different genetic parameters described below. For both calibration and validation of the model was done using date regarding the phenology, growth, grain, straw yields, and N uptake from both in grain and straw.

Table 8: Genetic coefficients of the rice variety IR841 as derived by GLUE of DSSAT model.

Genetic parameters	Description	Range of values	Default values IR36	Calibrated IR841
Development aspects				
P1(Juvenile Phase)	Time period or basic vegetative phase of the plant (expressed as growing degree days [GDD] in ˚C from seedling emergence during which the rice plant is not responsive to changes in photoperiod	150-800 ^{o}C-d	556.8	462.166
P2O (Critical Photoperiod)	Critical photoperiod or the longest day length (in hours) at which the development occurs at a maximum rate.	11-13 h	12.87	11.17
P2R (Photoperiodism Coefficients)	Extent to which phasic development leading to panicle initiation is delayed (expressed as GDD) for each hour increase in photoperiod above P2O.	5-300 ^{o}C-d	53.88	162.961
P5 (Grain filling duration coefficient)	Time period in GDD) from beginning of grain filling (3 to 4 days after flowering) to physiological maturity with a base temperature of 9˚C.	150-850 ^{o}C-d	373.4	340.615
Growth aspects				
G1 (Spikelet number coefficient)	Potential spikelet number coefficient as estimated from the number of spikelets per gm of main culm dry weight (less lead blades and sheaths plus spikes) at anthesis.	50-75 #/g	68.00	63.538
G2 (Single grain weight)	Under ideal growing conditions, i.e., non-limiting light, water,	0.015-0.030 g	0.023	0.027

	nutrients, and absence of pests and diseases.			
G3 (Tillering coefficient)	A higher tillering cultivar would have coefficient greater than 1.0	0.7-1.3	0.95	0.977
G4 (Temperature tolerance coefficient)	Usually, 1.0 for genotypes grown in normal environments. G4 for rice growing in a warmer environment would be 1.0 or greater.			1

The calibration for our rice cultivar was based on an existing rice cultivar included in DSSAT, namely IR36. The default coefficients for the thermal time from emergence to the end of juvenile phase (P1), the Critical Photoperiod (P2O) and the Spikelet number coefficient (G1) were reduced to match the observed phenology values. The Photoperiodism Coefficients (P2R) and the Tillering coefficient (G3) were decreased to match the observed physiological maturity, while the Single grain weight (G2) and Tillering coefficient (G3) were adjusted to match the observed grain yield and biomass (Table 8).

3.3.10.4. Evaluation of model performance

Given that none of the model parameters were calibrated and validated using the 2 years of experiment 1, an evaluation of the model performance can be considered for a true validation using the data from experiment 1 (Kadiyala et al., 2014). Therefore, to evaluate the accuracy of the model, the different parameters recently calibrated and validated for the model were used to run the model using the data collected during the two years of experiment 1.

Summary measures used in the present study were the mean and the standard deviation of observed and simulated values. We computed the statistical assessments to judge the accuracy of model outputs, including the coefficient of determination (R2), the root-mean-square error (RMSE), the normalized-RMSE (nRMSE), and the index of agreements (d) (Willmott, 1981). These indicators were computed as follows:

$$\mathbf{RMSE}\left[\mathbf{N}^{-1}\sum_{\mathbf{i=1}}^{\mathbf{N}}(\mathbf{Y_i}-\mathbf{X_i})^{\mathbf{2}}\right]^{\mathbf{1/2}} \quad \text{[Eqn. 10]}$$

$$\mathbf{nRMSE}=\frac{\boldsymbol{RMSE}}{\bar{\mathbf{x}}} \quad \text{[Eqn. 11]}$$

$$\boldsymbol{d}=\mathbf{1}-\frac{\sum_{\boldsymbol{i=1}}^{\boldsymbol{N}}(\boldsymbol{Y_i}-\boldsymbol{X_i})^{\mathbf{2}}}{\sum_{\boldsymbol{i=1}}^{\boldsymbol{N}}(|(\boldsymbol{Y_i}-\bar{\boldsymbol{x}})|+|(\boldsymbol{X_i}-\bar{\boldsymbol{Y}})|)^{\mathbf{2}}} \quad \text{[Eqn. 12]}$$

where N is number of observations, Y_i and X_i are the simulated and observed values for the i^{th} measurement, respectively; $\overline{Y}$ is the mean of the predicted values, and $\bar{x}$ is the mean of the observed values.

The model performed well when predicted values exactly fitted the observed values, RMSE and nRMSE are 0 and the corresponding d-value is 1. The criteria of agreement between observed and simulated values were defined according to Yang et al. (2014). The minimum criterion $d \geq 0.60$ was set as threshold for the acceptance of the accuracy of simulations. The models were considered accurate when evidenced by the lowest RMSE and nRMSE and with $d \geq 0.75$. These different indicators were used to evaluate the different outputs from both calibration and validation, such as the panicle initiation date, the antithesis date, the maturity date, the leaf area index, the grain yield, the aboveground biomass, and the top N at maturity. The evaluation of the performance of the model was done using the parameters such as the grain yield, the biomass at maturity, and the aboveground N uptake.

CHAPTER FOUR

RESULTS AND DISCUSSIONS

4.1 Laboratory and field validation for the adaptive, low-cost, open-source data logger

4.1.1 Laboratory validation

Differences in accuracy and precision among the tested, four different low-cost NDIR sensors are shown in Figure 20 as 1:1-agreement plots between mixing-ratio derived (calculated) and measured ΔCO_2. While accuracy can be assessed as deviation from the 1:1-agreement line, precision is determined by the residual SD and the coefficient of determination (r^2) of the linear regression fitted on calculated and measured ΔCO_2.

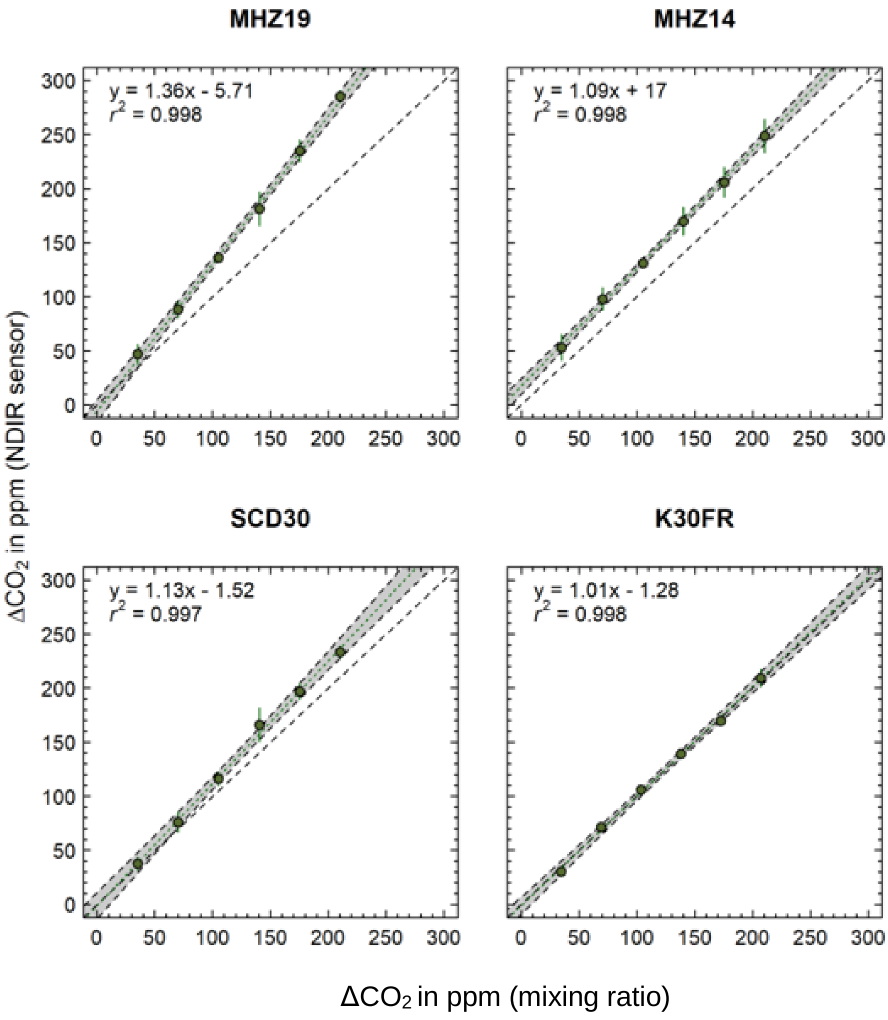

Figure 20: 1:1-agreement between measured ΔCO_2 in ppm from the four low-cost sensors tested (K30FR, SCD30, MHZ-14 and MHZ-19) and ΔCO_2 in ppm of mixing ratio. The dashed black line indicates the 1:1-agreement. The dotted green line shows the linear

regression through the measurement dots. The grey shaded area represents the respective confidence interval of the regression line. Error bars indicate ±1.96 SD.

The K30FR sensor showed the highest accuracy among all tested sensors, reflecting well the increase in CO_2 concentration (ΔCO_2) derived through mixing-ratio. Correspondingly, no significant difference (one sample t-test, $p=0.80$) was found between calculated and measured ΔCO_2. The SCD30 sensor, even though fairly accurate at lower, failed to reflect higher calculated ΔCO_2 values and generally tends to overestimate actual ΔCO_2. Neither the MHZ-14 sensor nor the MHZ-19 sensor, were sufficiently accurate and able to reflect calculated ΔCO_2. While the MHZ-14 showed a rather constant offset from the 1:1-agreement by 28 ppm, the MHZ-19 tends to increasingly overestimate higher ΔCO_2 values derived through mixing ratio. Hence, unlike the K30FR, all other NDIR sensors measured significantly higher ΔCO_2 when compared to calculated ΔCO_2 (One sample t-test, $p<0.01$). Unlike the accuracy, overall precision, and measurement repeatability among all four NDIR sensors was generally high and comparable, showing a residual SD of 2.78 ppm, 4.23 ppm, 2.52 ppm and 3.58 ppm, respectively. Regarding the response time (defined as mean time from injection to measured initial CO_2 concentration increase) all four NDIR sensors differed substantially, with only 44 seconds for the K30FR and more than 280 seconds for the MHZ-14. The same was true for the response strength (defined as the mean time from beginning to end or steepness of measured CO_2 concentration increase), with 61, 160 and 265 seconds for the K30FR, SCD30 and MHZ-19 respectively. In case of the MHZ-14, response strength could not be evaluated, since no clear saturation after injection induced CO_2 concentration increase could be observed. While accuracy and precision are of course highly relevant, response time and response strength in particular play a key role in determining the extent to which the tested NDIR sensors can be used for in-situ NFT-NSS closed chamber measurements. With a response time of almost 2 min and 5 min, respectively, as well as low response strength, MHZ-19 and MHZ-14 will likely fail to correctly reflect CO_2 concentration changes during short-time (<4min) closed chamber measurements, regardless of their low accuracy, which makes them additionally unsuitable.

Laboratory validation performed by Brändle and Kunert (2019) using similar MHZ-14 sensor from the same manufacturer against reference gas exchange fluorescence system (GFS-3000) also observed sensor delay before matching reference sensor concentrations and found an overall measurement offset of ~ 40 ppm. Their field validation implied a similar limitation that it is unsuitable for very short measurements (<5 mins). On the other hands, the SCD30 sensor showed acceptable accuracy and response time. This is consistent with the findings of

Rivero et al., (2023) where the sensor measurements were highly accurate in measuring reference calibration gas concentration in a closed box experiment. Multiple studies (Ali et al., 2016; Blackstock et al.,2019; Mendes et al., 2015) that have tested and determined the accuracy of the K30 sensor for CO_2 measurement also support our results. Laboratory testing by Blackstock et al., (2019) validated the accuracy of SenseAir K30 sensor against known CO_2 concentrations using span gas measurements and found that it falls within the accuracy stated by manufacturer. Their experiment also verified the sensor accuracy since it was capable to measure the reference gas mixture within the analytical error. Similarly, performance test performed by Mendes et al. (2015) found that the K30 sensor has nearly perfect linear response against calibration gas CO_2 concentration. Lastly, the study by Ali et al., (2016) also determined that the sensor K30 can measure CO_2 concentration in an indoor environment setting with high accuracy based on the strong correlation found when compared against reference commercial CO_2 sensors. They also highlighted the advantage of its self-calibration capabilities that contributes to its stable performance and high repeatability with minimal maintenance. Therefore, only the K30FR (and to a much lower extent the SCD30) with its fast response time and high response strength passed laboratory validation and met all necessary requirements for accurate and precise in-situ measurements of CO_2 exchange.

4.1.2 Field validation

A total of 41 closed chamber measurements (Reco: 21; NEE: 20) has been conducted during the two days of field validation using the LI-850 as reference for both NDIR sensors passing the laboratory validation (CO_2) and the two tested RH sensors (ET). While 41 valid CO_2 exchange fluxes (Reco: 21; NEE: 20) could be calculated for the LI-850, 35 (Reco: 21; NEE: 14) and 36 (Reco: 21; NEE: 15) valid fluxes were obtained for K30FR and SCD30, respectively. For ET, 13 valid fluxes could be calculated for the LI-850 as well as the SHT31 and DHT22. Only transparent chamber measurements were considered to avoid systematic impact of opaque chambers on plant transpiration via stomatal closure upon darkening (Larcher, 2003). The 1:1-agreement plots in Figure 21 (a-d) show the differences in accuracy and precision for CO_2 and ET fluxes calculated based on NDIR (a-b) and RH measurements (c-d) compared to CO_2 and ET fluxes calculated based on LI-850 measurements. While the comparison between Reco and NEE fluxes calculated from LI-850 and K30FR CO_2 concentration measurements (Figure 21a), was in accordance with the laboratory validation and showed again the overall accuracy and precision of this NDIR sensor, a small positive offset was found. This resulted in significantly higher Reco (mean diff. 1.12 µmol m^{-2} s^{-1}; one sample t-test, $p<0.05$) and less negative NEE (mean diff. 1.41 µmol m^{-2} s-1; one sample t-test,

$p<0.05$) fluxes for the K30FR when compared to LI-850. No such offset was found in case of the SCD30 (Figure 21b), which showed significantly lower Reco (mean diff. -1.33 µmol m^{-2} s^{-1}; one sample t-test, $p<0.05$) and much less negative NEE fluxes (mean diff. -4.18 µmol m^{-2} s^{-1}; one sample t-test, $p<0.05$) compared to LI-850. Since neither of the NDIR sensors showed a similar effect, nor an overestimation was found for the K30FR during the laboratory validation, it can be assumed that the detected offset in case of the K30FR is not a direct result of microclimatic effects (e.g., increasing humidity) or incorrect sensor readings. Instead, inter-alia differences within the chamber headspace and the position of the NDIR sensor right below the chamber top, approx. 10 cm above the LI-850 inlet and outlet, might help to explain it.

Figure 22 shows Reco and GPP parameter estimates for flux measurements performed with the LI-850 compared to K30FR and SCD30 respectively. Since the Reco and GPP parameters are based on the fluxes presented in Figure 21, similar differences between LI-850, K30FR and SCD30 could be obtained. With an Rref and E_0 of 4.60 and 212.71, the K30FR had similar, but slightly higher Reco parameters when compared to the LI-850 (Rref: 4.14; E0: 195.01). This indicates not only in general higher Reco fluxes but more importantly also a stronger increase of Reco fluxes with rising temperature. In the case of the SCD30 (Rref: 2.54; E_0: 270.07), differences in Reco parameters were, however, much more pronounced. The same tends to be true for obtained GPP parameters, which were highly comparable for LI-850 (α: -0.048; GPmax: -39.83) and K30FR (α: -0.042; GPmax: -38.42), but distinctly different for SCD30 (α: -0.029; GPmax: -31.83). As a result, the fitted K30FR PAR dependency function was fully within the confidence band of the LI-850 PAR dependency function.

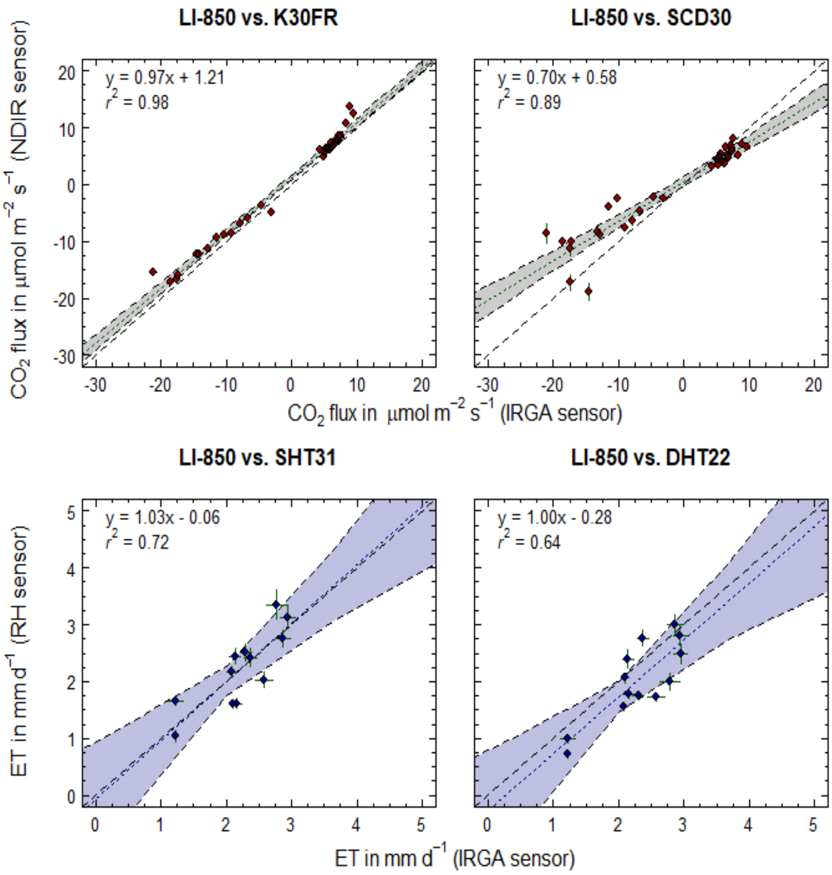

Figure 21: 1:1-agreement between (a-b) CO_2 and (c-d) ET fluxes measured with infrared gas analyzer (IRGA; LI-850, LI-COR, USA) and low-cost NDIR sensors (K30FR and SCD30). The dashed black line indicates the 1:1-agreement. The dotted red/blue line shows the linear regression through the measured CO_2/ET fluxes. The grey/blue shaded area represents the respective confidence interval of the regression line. Error bars indicate calculated flux error (α=0.9).

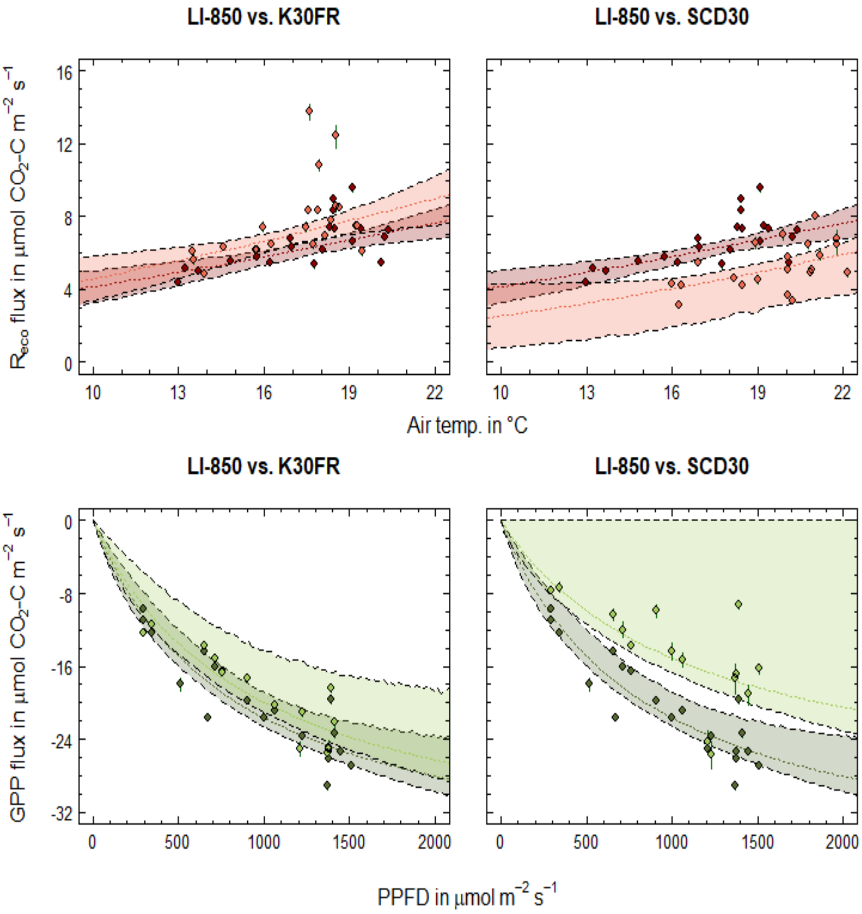

Figure 22: Comparison of Reco temperature dependency (dotted red lines) and GPP PAR dependency functions (dotted green lines) between LI-850 (dark red/green) and K30FR and SCD30 (light red/green), respectively. Shaded red/green areas indicate confidence band around functions. Dots represent measured Reco and derived GPP fluxes. Error bars indicate calculated flux error (α=0.9).

The lowest NEE flux obtained from the K30FR sensor (-3.8 µmol m-^{2} s^{-1}) also falls within the range of daily average NEE values (between 0 to -10 µmol m^{-2} s^{-1}) obtained from field site with Phacelia cover crop measured in the study by Emmel et al. (2018) in the same month period. Compared to the K30FR, especially NEE fluxes obtained by the SCD30, were characterized by a very low precision. The reason for this is certainly the lower CO_2 concentrations (<400 ppm) in the NEE measurements, which are far outside the measurement range specified by the manufacturer (400 to 10000 ppm). This also explains the decreasing precision with increased negative NEE fluxes obtained by SCD30, since these are likely related to CO_2 concentration measurements well below 400 ppm. The general underestimation of Reco and NEE fluxes derived from SCD30, however, is probably a result of its rather long response time and lower response strength when compared to the K30FR. No significant difference (mean diff. -0.01 mm d^{-1}; one sample t-test, p=0.89) was found between ET fluxes calculated from H_2O concentration and RH measurements, using the LI-850 and SHT31, respectively (Fig. 20). Together with an r^2 of 0.72, this indicates a reasonable accuracy of SHT31 derived ET flux estimates. Compared to that, ET fluxes, determined through RH measurements using the DHT22 (Fig. 20), were significantly smaller (mean diff. 0.28 mm d^{-1}; one sample t-test, $p<0.05$) than LI-850 based ET fluxes and with a r^2 of 0.64 less accurate. This is consistent with sensor accuracy for measuring relative humidity specified by corresponding manufacturers, which are ±2% accuracy for SHT31 and ±2-5% for DHT22. The overall precision of SHT31 and DHT22 derived ET fluxes was similar, but with a residual SD of 0.36- and 0.39-mm d^{-1} rather high.

The K30FR sensor well represented Reco and GPP fluxes measured with the LI-850 and theron based parameter estimates for Reco and GPP, while the SCD30 was only conditionally able to reflect the measured Reco and GPP fluxes and to make accurate parameter estimates. Instrument validation by Brown et al. (2020) of the K30 sensor shows consistent results that the sensor has comparable accuracy against reference commercial sensors such as the PP-Systems EGM-4 Infrared Gas Analyzer (IRGA) and the Los Gatos Ultraportable Greenhouse Gas Analyzer (UGGA). Our results also concur with the findings of Curcoll et al. (2022) where the K30 sensor integrated in a NSS-NTF measurement system was able to accurately measure CO_2 flux measurements for a grassland ecosystem.

4.2 CO_2 seasonal dynamics and soil CO_2 respiration

The developed low-cost measurement system was reliable and capable to differentiate Reco, GPP, NEE, and ET fluxes among the different treatments, which was required to obtain valid NECB and WUE estimates.

4.2.1 Seasonal dynamics of Gross primary production (GPP), ecosystem respiration (Reco) the Net ecosystem exchange (NEE) over the growing season

The Figure 23 shows the seasonal dynamics of GPP, Reco and NEE over the growing period.

The average GPP, Reco and NEE of paddy fields under different treatments displayed a certain seasonal dynamic across the rice growth stages. An U-shape was observed in the seasonal dynamics of Reco and GPP, whereas an inverted U-shape was observed in the seasonal dynamics of NEE. The daily GPP of all treatment rice was very low during the early vegetative stage. It started to increase during active tillering and reached its maximum during the heading stage. The highest value was obtained with N120 in CF (17.82 g C m^{-2} d^{-1}) and the lowest with N90 in AWD15 (-10.78 g C m^{-2} d^{-1}). After that, it all declined until harvest.

At the beginning of the growth stage, the Reco was higher than the GPP and it started to increase at panicle initiation and reached its maximum at flowering. It was highest under AWD15 with N120 (9.79 g C m^{-2} d^{-1}) and the lowest value was (8.05 g C m^{-2} d^{-1}) under AWD25 with N90. For all treatments, the rice field was allowed to dry for 10 days before harvest, so Reco was increased again. Across all treatments, the net ecosystem exchange varied with different water management and N applications. It ranged from 156.22 g C m^{-2} to 329 g C m^{-2} for the entire measuring period. The highest value was recorded under CF treatments, and the lowest value was recorded under AWD25 treatment. Considering each water management, NEE increased with the increase in N application except for the AWD15 treatment.

The GPP values were consistently larger than the Reco values, and thus, the NEE values were negative during the entire rice growth period, demonstrating that the paddy field ecosystem acted as a sink for CO_2. From the regreening stage to the initial tillering stage (2–17 days after transplanting, (DAT)), GPP, Reco, and NEE fluctuated smoothly because of the weak respiration and assimilation capabilities of the recently transplanted rice plants. Both GPP and Reco increased until the initial jointing and stage (56–64 DAT), and GPP increased to a higher degree than Reco. In all treatments, rice field started to become a sink for CO_2 at active tillering and reached its maximum uptake during the heading stage Therefore, NEE decreased substantially, and the maximum net CO_2 absorption rate occurred at 55 DAT. GPP and Reco decreased starting at the flowering stage (72 DAT), and the degree of the decrease in GPP was higher than that in Reco, which accounted for the decrease in NEE. In addition, during the early and late rice growth periods, the GPP and Reco values were low and similar, and the paddy field became a net source for CO_2 emissions after harvest. Moreover, GPP is an important variable used in studies of climate change and the carbon cycle (Wang et al., 2013) and functions as an indicator of the photosynthesis rate of terrestrial ecosystems (Arunrat et al., 2022). Our results showed that the GPP varied with different plant growth period, which is in line with many previous findings focusing on various terrestrial ecosystems, such as grasslands and forests (Liu et al., 2009; Liang et al., 2016). This could be explained by the fact that the most powerful photosynthesis in paddy fields occurred at the heading stage (Min et al.,2020; Nyambo et al., 2020). The increase in rice plant growth is mainly due to the increase in soil nutrient contents and the enhancement of the soil environment due to nitrogen application (Zhang et al., 2016).

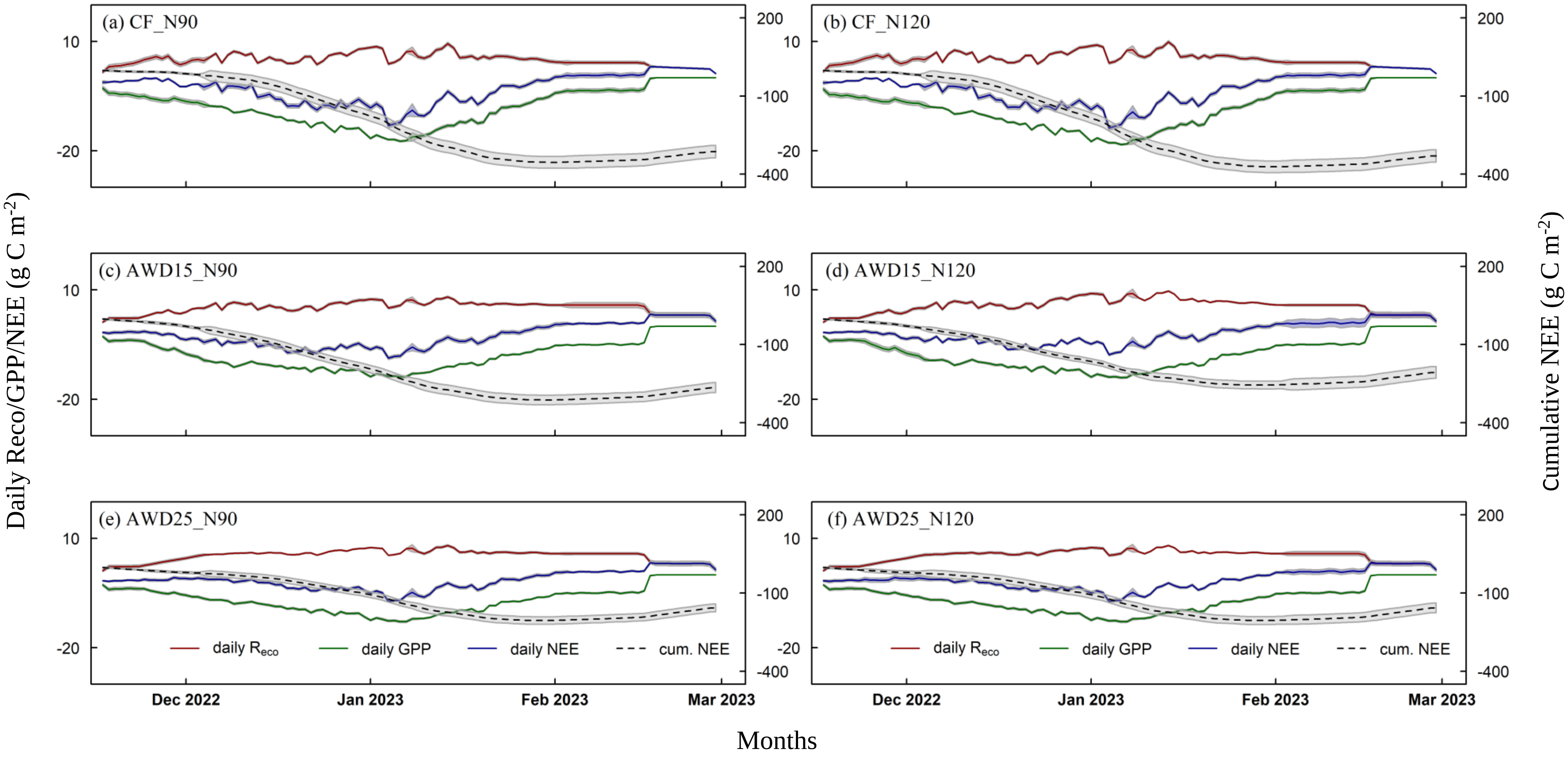

Figure 23: Seasonal dynamic of Gross primary production (GPP), ecosystem respiration (Reco), the Net ecosystem exchange (NEE) during the growing season. CF, AWD15 and AWD25 represent continuous flooding, alternate wetting and drying at 15 cm and 25 cm threshold, respectively.

4.2.2 Cumulative heterotrophic respiration (Rh), sol respiration (Rs), below autotrophic respiration (BG_Ra) and the net primary productivity (NPP)

Figure 24 presents the cumulative heterotrophic respiration (Rh), sol respiration (Rs), below autotrophic respiration (BG_Ra) and the net primary productivity (NPP) for the different water regime combined two level of N fertilizers. It shows that both cumulated heterotrophic respiration and below autotrophic respiration varied with the interaction of different water management and N application levels.

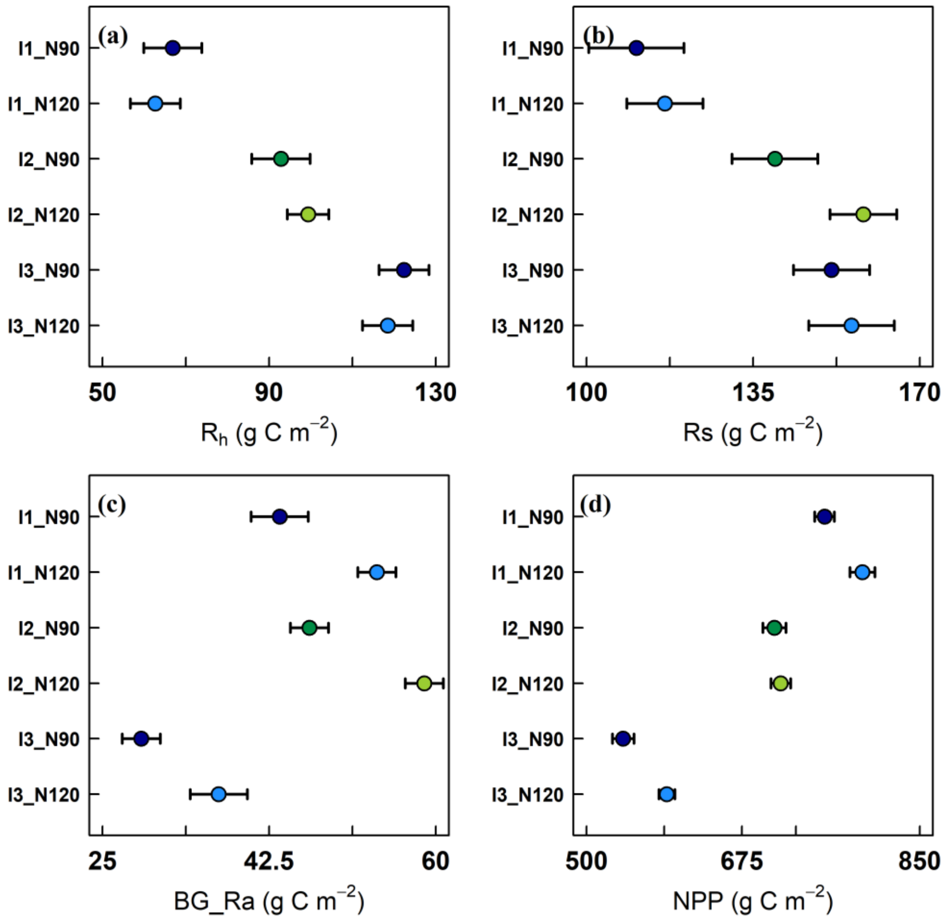

Figure 24: cumulative (a-b-c-d) Rh, Rs, BG_Ra and NPP (g C m^{-2})

I1_N90 is continuous flooding irrigation (CF) with N90 kg. ha^{-1}

I1_N120 is continuous flooding irrigation (CF) with N120 kg. ha^{-1}

I2_N90 is alternate wetting and drying irrigation at 15 cm threshold (AWD15) with N90 kg. ha^{-1}

I2_N120 is alternate wetting and drying irrigation at 15 cm threshold (AWD15) with N120 kg. ha^{-1}

I3_N90 is alternate wetting and drying irrigation at 25 cm threshold (AWD25) with N90 kg. ha^{-1}

I3_N120 is alternate wetting and drying irrigation at 25 cm threshold (AWD25) with N120 kg. ha^{-1}

The cumulative heterotrophic respiration was highly affected by the soil's moisture condition and nitrogen application as well. However, treatments under CF recorded a lower Rh whereas treatments under AWD25 presented the highest Rh. In terms of nitrogen application, there was not much difference between the two levels of nitrogen application, even though the highest Rh was recorded with N120. All combined treatments showed that treatment CF with N90 recorded the lowest Rh (58.34 g C m^{-2}) and treatment AWD25 with N120 recorded the highest Rh (93.18 g C m^{-2}). By contrast to the Rh, below autotrophic reparation (BG_Ra) was highest under CF followed by treatment under AWD15 and AWD25. It also increased with the increase of Nitrogen application. All combined treatments showed a lower below autotrophic (BG_Ra) respiration, which was recorded under AWD25 with N90 (45.22 g C m^{-2}) and the highest value was recorded under CF with N120 (68.78 g C m^{-2}). Soil respiration (Rs) was highest in AWD25 with N120 (158.15 g C m^{-2}) whereas the lowest respiration was recorded under CF with N90 (110.45 g C m^{-2}). In general, it also increased with the increase of nitrogen application. The net primary production (NPP) ranged from 541.11 g C m^{-2} to 810.37 g C m^{-2}. The highest NPP was recorded under CF treatments, and the lowest NPP was recorded under AWD15 treatments when the same N fertilization level was applied. As with other components, it also increased with the increase application of nitrogen.

Our results showed that heterotrophic respiration was affected by the different soil conditions and nitrogen application. The increase of Nitrogen application increased the Rh. This finding is not in line with those found by Bowden et al. (2004) who reported that Rh was significantly reduced by high N addition. Enrique et al. (2008) found that low N addition could cause an increase in soil microbial respiration (Rh); on the contrary, high N resulted in a decrease in Rh. At the same time, some results demonstrated that N could react with organic substances to form more chemically recalcitrant compounds, which is also likely responsible for the increase in Rh under high N supply (Wang et al., 2019). One of the important variables which affect Rh is the soil moisture (Hoffmann et al., 2015). Indeed, our results showed that treatment under CF recorded less Rh compared to the others. This could be explained by the variation in soil temperature across all these treatments (Moyano et al., 2018).

Regarding the soil below autotrophic respiration (BG_Ra), it varied across the different water regimes and the application of nitrogen. Our results showed a BG_Ra increase in CF treatment with a high level of nitrogen as well. This could be correlated with the plant's growth. However, it has been demonstrated that BG_Ra is tightly coupled with aboveground photosynthesis and increases with increasing root biomass (Ren et al., 2017). The meta-analysis studies generally find that high applications of nitrogen can promote plant photosynthesis rate and, therefore, increase net primary productivity (NPP), resulting in higher root biomass (Greaver et al., 2016; Oliver et al., 2019). In terms of water management, Oliver et al., (2019) reported that BG_Ra is similar in CF and AWD15 treatments since the root biomass was not significantly different, and then, high-potential relationships could be established between growth stage, soil temperature, and C fluxes during the different growth stages. Although the optimum N supply under different soil moisture conditions for root growth was larger for microorganism activity, as indicated by the different response patterns of BG_Ra and Rh to soil mineral N. It could be expected that excessive N in different water regimes could also inhibit BG_Ra, which necessitates further studies with a large gradient of N addition level. In addition, our findings are also broadly in agreement with other paddy studies that have sought to partition soil respiration (Rs) and Rh by measuring soil CO_2 flux between unvegetated plant rows (i.e., Rh ranging from 0.02 to 3.91 g C m^{-2} d^{-1}) (Nishimura et al., 2008; Iqbal et al., 2009; Li et al., 2010), emphasizing the important role of plant metabolism in modulating both Rs and Rh in rice systems. Furthermore, our results are also surprising because other intermittent drainage studies suggested that aerobic soil conditions can enhance soil respiration (Nishimura et al., 2008; Liu et al., 2013; Qi et al., 2018), with some paddy systems changing from a net sink to a source of CO_2 with increased soil drainage (Miyata et al., 2005). Morever, the soil aerobic conditions strengthen microbial activities and soil respiration and thus promote CO_2 production, which is emitted from the soil through the roots and soil respiration (Miyata et al., 2000, Zhou et al., 2016). The same authors reported that irrigation mode, irrigation volume, and irrigation frequency influence CO_2 emissions. Our results are also in agreement with those of Yang et al., (2017), who reported that intermittent irrigation strongly increased soil respiration, which resulted in a decrease in NEE in paddy fields. Akter et al., (2018) also demonstrated that proper water-saving irrigation regimes enhanced root activity, which thereby benefited other physiological processes and resulted in rice growth. The net primary productivity (NPP) under CF was higher than AWD15 and AWD25 by 10% and 29%, respectively, when the same N fertilization level was applied. Our finding is in agreement with Li et al., (2022), who reported that the net NPP under CF was higher than controlled irrigation by 18–38% and 11–33%, respectively, when the same N fertilization level was applied in Northeast China. In this study, no additional C inputs were detected, and the C inputs only contained NPP. This may be because CF increased the rice dried matter weight and C contents. These results agreed that an increase in rice dried matter weight and C contents resulted in increased C inputs. Kim et al. (2017) reported that the higher-level N fertilization significantly increased NPP, mainly through the increase in rice dried matter weight. These findings were consistent with the results of this study.

4.3 Cumulative GPP, Reco, NEE, ET, NECB and the WUE

The cumulative (a-d) Reco, GPP, NEE (g C m^{-2}) and ET fluxes (mm) as well as thereon based estimates of (e-f) NECB (g C m^{-2}) and WUE (g mm^{-1}) for the different treatment are presented in Figure 25. It shows that these different parameters varied with the interaction of different water management and N application levels.

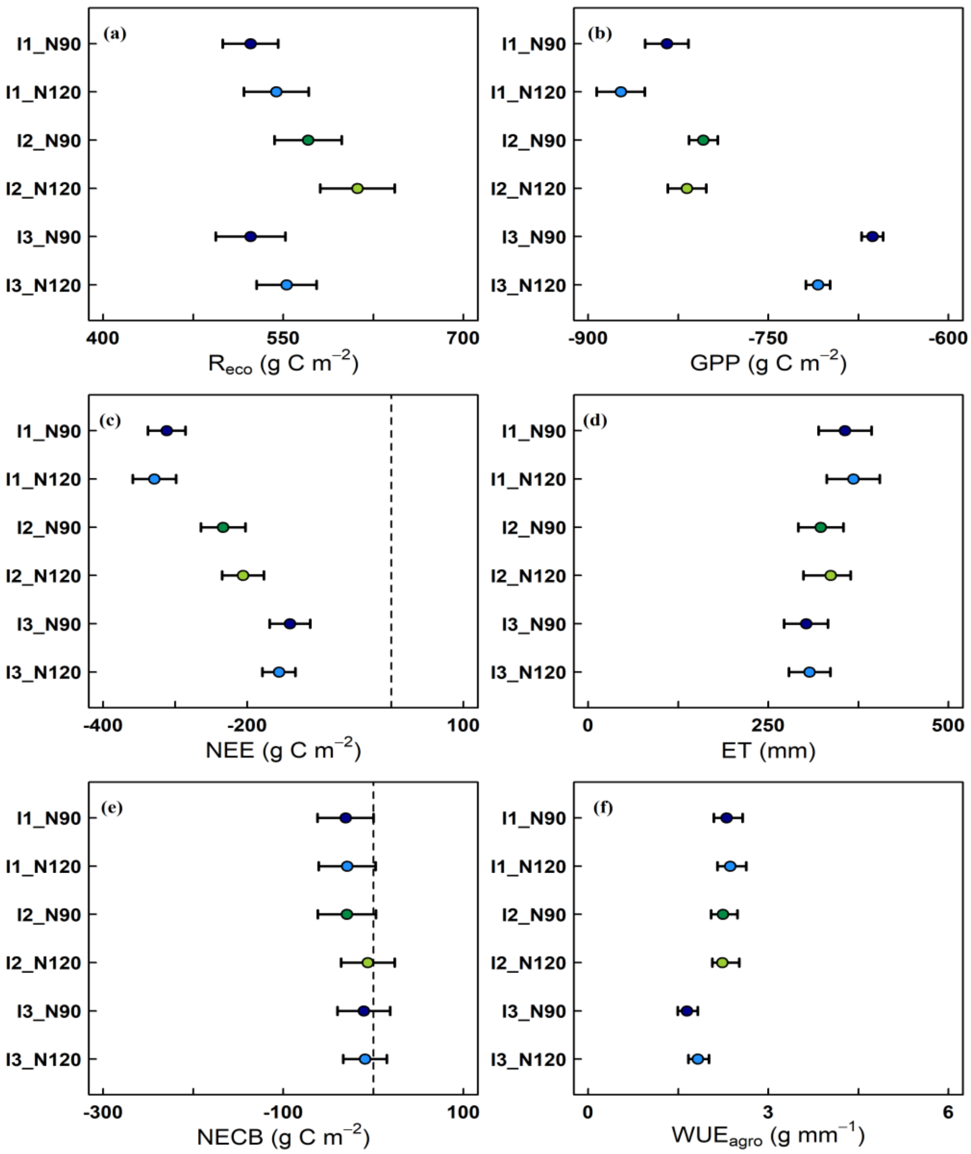

Figure 25: Panels (a-b-c-d) refer to the cumulative values of Reco, GPP, NEE (g C m^{-2}) and ET fluxes (mm) and panel (e-f) indicate the cumulative of NECB (g C m^{-2}) and WUE (g mm^{-1}).

I1_N90 is continuous flooding irrigation (CF) with N90 kg. ha^{-1}

I1_N120 is continuous flooding irrigation (CF) with N120 kg. ha^{-1}

I2_N90 is alternate wetting and drying irrigation at 15 cm threshold (AWD15) with N90 kg. ha^{-1}

I2_N120 is alternate wetting and drying irrigation at 15 cm threshold (AWD15) with N120 kg. ha^{-1}

I3_N90 is alternate wetting and drying irrigation at 25 cm threshold (AWD25) with N90 kg. ha^{-1}

I3_N120 is alternate wetting and drying irrigation at 25 cm threshold (AWD25) with N120 kg. ha^{-1}

Reco and GPP flux ranged from 522 to 611 g C m^{-2} and from -873 to-663 g C m^{-2} respectively. The highest GPP and Reco were recorded under CF with N120 and AWD15 with N120, respectively. The lowest fluxes were recorded under AWD15 with N90 and CF with N90, respectively. In terms of nitrogen application, both parameters increased with the increase in nitrogen application. The treatments under CF recorded the highest GPP, followed by the treatment under AWD15 and the treatment under AWD25. The opposite trend was observed for the Reco, and the highest value was found under AWD15, whereas the lowest value was recorded under CF. The GPP and Reco under CF were 1.5 and 1.2 times higher than treatment under AWD15 and AWD25, respectively. The ratio of Re/GPP in flooded fields was approximately 0.6, while it was approximately 0.7 for rice fields under the alternate wetting and drying fields.

The net ecosystem exchange (NEE) also varied significantly with different water management. It ranged from -140 to -329 g C m^{-2}. The highest value was recorded under CF with N120, and the lowest value was recorded under AWD25 with N90. For all the treatments, the increase of nitrogen application increased the NEE except for the treatments under AWD15. The NECB, which is a good indicator of C balance in each treatment, ranged from 9.2 g C m^{-2} to 30.9 g C m^{-2}. This indicated that all the treatments were sinks of carbon. The highest value was recorded under CF with N90, followed by the treatment under AWD15 with N90 (29.53 g C m^{-2}) and the lowest value was recorded under AWD15 with N120. In all water management treatments, the NECB decreased with the increase in N application. Furthermore, the ET fluxes obtained ranged from 302 mm to 367 mm. It significantly varied with different water management, and the treatment under CF recorded more ET than the two other treatments. The lowest value was recorded under AWD25. It also increased with the increase nitrogen application. A similar trend was found for the water use efficiency (WUE) in the treatment under AWD15, where the WUE was higher with N90 than with N120. Considering the different water management, treatment under CF presented the highest WUE, and the lowest value was recorded with AWD25, even though the WUE under CF and AWD15 are almost similar.

The ratio of Re/GPP in continuous flooding fields was about 0.6, while it was about 0.7–0.8 for treatment in alternate wetting and drying rice fields. A similar Reco/GPP ratio (0.65) was also obtained by Saito et al. (2005) for a rice paddy field in Mase, central Japan. Different values from GPP and Reco from continuous flooding are higher than those reported by Oliver et al. (2019), who found the values of -778 g C m^{-2} and 521 g C m^{-2} for GPP ad Reco, respectively. This difference could be explained by the fact that the climate conditions are not the same as well as the rice variety (Oliver et al., 2019). At the same time, this difference of Reco across the different treatments could also be attributed to the difference of soil temperature and plant growth. However, under CF, soil temperature was relatively lower than the other treatments.

Rates of GPP, Reco, and NEE were more affected by the specific stage of plant development, soil temperature, and water management. There was a clear seasonal trend in CO_2 fluxes, with more negative NEE values observed when plants reached the flowering growth stage. These results are consistent with other rice studies and are explained by an increase in plant biomass and leaf area index (LAI) when the plants reach the heading tages (Saito et al., 2005; Alberto et al., 2009). This stage is followed by a decline in NEE towards the maturity stage due to leaf senescence or a reduction in leaf greenness (Pakoktom et al., 2009; Swain et al., 2016). Factors such as temperature and light play an important role in regulating rates of Reco, NEE, and GPP, with peaks in temperature and light availability facilitating high rates of C uptake during heading and flowering (Wohlfarth and Gu, 2015; Xin et al., 2017). The findings of this study are also in line with some prior results of rice paddy studies using eddy covariance techniques in East Asia, India, and the USA, where the NEE was estimated between 5 and 39 g C m^{-2} day^{-1} and the GPP was between 5 and 50 g C m^{-2} day^{-1} (Alberto et al., 2009; Bhattacharyya et al., 2013; Swain et al., 2016). Some studies also reported a high NEE in intermittently flooded systems compared to the CF system (Liu et al., 2013, Alberto et al., 2014), which is not consistent with our finding even though a small difference was observed between the GPP values.

The study revealed that the C balance in each treatment ranged from -9.2 g C m^{-2} to -30.9 g C m^{-2}. This is in line with Li et al. (2022), who found that the NECB ranged from 1151 to 2663 kg C ha^{-1} after implementing water-saving irrigation in northeast China, indicating that all treatments acted as net C sinks. Whether paddy field ecosystems function as C sinks or sources is related to the balance of organic C inputs and outputs. It is well known that appropriate agricultural practices can enhance the ability of C sequestration and mitigate CO_2 emissions to combat climate change (Soussana et al., 2010). In Tanzania, Alavaisha et al.,

(2022) also reported that water management practice that involves AWD with for one cropping season is a plausible approach to maintaining high Soil carbon with the potential for increasing crop production. Li et al. (2022), in Northeast China, reported that Water-Saving Irrigation increased the NECB through increasing NPP, which exceeded increased removal of harvest and C mineralized losses. The same authors also demonstrated that, the NECB was significantly higher than conventional irrigation and controlled irrigation when the same N fertilization level was applied.

The evapotranspiration (ET) is correlated with the water use efficiency (WUE), and it describes the total amount of water that evaporates from a given area (Fohrer et al., 2016; Rothfuss et al., 2021). Evapotranspiration (ET) is one of the most important components in field water cycles. The accurate measurement or estimation of ET in fields is of great importance for quantifying soil hydrological processes and, thus, making appropriate decisions regarding irrigation measures to improve water use efficiency levels in agricultural areas. Our findings showed that ET varied with the different treatments and ranged from 302 mm to 367 mm for the entire growing season, which means 2.85 mm d^{-1} to 3.5 mm d^{-1}. This is a close estimate when compared to the FAO (2020) database for ET (with crop factor for rice) in the study area, which is an average of 343 mm during the measurement period. However, this result is lower than those found by some scholars in other parts of the world. However, seasonal rice evapotranspiration (ET) varied between 400 and 700 mm in the Philippines (Tabbal et al., 2002) and 540 and 730 mm in India (Chahal et al., 2007). A range of ET between 750 and 850 mm was reported by Moratiel et al. (2011) under sprinkler irrigation in Spain. This diversity in ET could be explained by the fact that irrigated lowland rice water use differs with agroecosystems, climate, and management practices.

4.4. Effects of water management and N fertilizer levels on growth, water productivity, N uptake, and grain yield of irrigated rice

4.4.1. Crop growth and development

4.4.1.1 Shoot dry weight and Leaf Area Index

Table 9:Shoot dry weight and Leaf Area Index (LAI) of irrigated rice as affected by different water and N fertilizer managements and their interaction in 2022 and 2023.

Year/ irrigation regime	N rate (Kg. ha^{-1})	Shoot dry weight (Mg. ha^{-1})			Leaf Area Index (LAI)		
		MT	PI	MAT	MT	PI	HD
2021-2022							
CF	N0	0.20f	3.01e	8.19e	0.51d	1.72cd	2.91f
	N90	0.63a	5.72b	13.62b	0.63ab	2.40b	4.65b
	N120	0.65a	6.51a	14.53a	0.64a	2.57a	4.83a
AWD15	N0	0.19f	2.17f	7.90e	0.50de	1.63d	2.74g
	N90	0.50c	5.33c	13.04c	0.61b	2.26b	4.38c
	N120	0.57b	5.96b	13.86b	0.63ab	2.39b	4.61b
AWD25	N0	0.18f	1.58g	5.71f	0.49e	1.29e	2.04h
	N90	0.32e	3.62d	10.42d	0.52d	1.65d	3.62e
	N120	0.40d	3.77d	10.89d	0.55c	1.82c	3.82d
2022-2023							
CF	N0	0.22f	3.21e	8.30e	0.56de	1.92f	2.96f
	N90	0.60b	5.93bc	13.74b	0.68ab	2.67b	4.70b
	N120	0.66a	6.73a	14.64a	0.69a	2.84a	4.87a
AWD15	N0	0.21f	2.38f	8.01e	0.55e	1.90f	2.84f
	N90	0.52c	5.66c	13.16c	0.66b	2.47c	4.42c
	N120	0.60b	6.17b	13.97b	0.68ab	2.66b	4.65b
AWD25	N0	0.20f	1.79g	5.83f	0.52f	1.46g	2.09g
	N90	0.34e	3.83d	10.54d	0.59dc	1.96ef	3.67e
	N120	0.41d	3.98d	11.00d	0.60c	2.15d	3.87d
Analysis of Variance							
Year (Y)		ns	ns	ns	ns	ns	ns
Irrigation regime (I)		**	**	**	*	**	**
N rates (N)		**	**	**	**	**	**
Y x I		ns	ns	ns	ns	ns	ns
Y x N		ns	ns	ns	ns	ns	ns
I x N		**	**	ns	**	*	ns

*, **means F values is significant at p=0.05 and p=0.01 levels, respectively.
ns means no significant at p=0.05 level. Different letters indicate statistical significance at the p=0.05 level within the same column and the same year. MT means mid-tillering, PI is panicle initiation, MAT is maturity and HD is heading.
CF, AWD_{15} and AWD_{25} represent continuous flooding, alternate wetting and drying at 15 cm threshold and alternate wetting and drying at 25 cm threshold.

Table 9 showed that the shoot dry weight and Leaf Area Index (LAI) of irrigated rice as affected by different water and N fertilizer managements and their interaction in 2022 and 2023. It showed that shoot dry weight increased from the mid-tillering stage to the maturity stage, and across both years, results exhibited the same tendency. Indeed, it varied with irrigation regimes and nitrogen rates. During the three-growing stages, the total shoot dry weight was the highest in the CF, followed by the AWD15, and the lowest in the AWD25 regime when the N rate was the same. It also in general increased with the increase of nitrogen application over the growing stages. Moreover, shoot dry weight at maturity showed no significant difference between N90 and N120 for the treatment under AWD25, but it was significantly increased with the increase of N rates in both the CF and AWD15 regimes. It ranged from 5.71 Mg. ha $^{-1}$ to 14.53 Mg. ha $^{-1}$ and from 5.83 Mg ha $^{-1}$ to 14.64 Mg. ha $^{-1}$ in 2022 and 2023, respectively. The highest value was recorded in CF with N120, followed by the treatment under CF with N90. In contrast to tillering and panicle initiation stages, there is no significant difference in the interaction effect of water regime and nitrogen application at maturity stage.

Similarly, to the shoot dry weight, LAI increased from the mid-tillering to heading stage. Except for the maturity stage, there was a significant difference in the interaction effect of water regime and nitrogen application at both the tillering and panicle initiation stages. Across N treatments in both years, LAI tended to increase with nitrogen application, and N120 was highest among the treatments at MT, PI, and HD, although N90 and N120 were not significantly different in AWD15 at MT in 2022. Regarding the different water regimes, LAI was largest in CF and the smallest in the AWD25 regime when N rates were the same. At heading, the average LAI ranged from 2.04 to 4.83 and from 2.09 to 4.87 in 2022 and 2023, respectively. The highest value was recorded under CF combined with N120, followed by the treatment under CF with N90, and the lowest value was recorded under AWD25 with N_0.

With regard to shoot dry matter, many reports showed that plants under continuous flooding performed better in terms of shoot dry matter production and leaf area index (Sun et al., 2012; Yakubu et al., 2016; Mboyerwa et al., 2022). Indeed, our results showed that over the three different growing stages, the total shoot dry weight was the highest in the CF, followed by the AWD15, and the lowest in the AWD25 regime when the N rate was the same. This confirms a report by Akram et al. (2013), who found out that the dry matter weight decreased when water stress was imposed during the panicle initiation stage of rice. This difference in plant growth could also be attributed to the development of root growth, the variation in plant height, and the reduced absorption of nutrients due to insufficient moisture (Sun et al., 2012). This finding is in line with Sabbour et al., (2007), who showed that the cumulative effect of water stress on plants led to a reduction of both leaf area index and dry matter accumulation. Many reports also showed that both shoot dry matter and LAI increased with the increased application of nitrogen. The results obtained in this study are in agreement with those reported by El-Wahab et al., (2007) and Khairi et al., (2015), who observed that applications of nitrogen fertilizer usually produce more vegetative growth than plants treated with no N fertilizer. However, a strong relationship should be established between shoot dry matter and LAI according to the soil moisture level.

4.4.1.2 Chlorophyll content and NDVI

Table 10:Chlorophyll content (CC) and Normalized Difference Vegetation Index (NDVI) of irrigated rice as affected by different water and N fertilizer managements and their interaction in 2022 and 2023.

Year/ irrigation regime	N rate (Kg. ha^{-1})	Chlorophyll content			NDVI		
		MT	PI	MAT	MT	PI	HD
2021-2022							
CF	N0	37.43e	40.40f	45.40e	0.16d	0.42e	0.58e
	N90	40.20c	44.03b	48.86b	0.21ab	0.55ab	0.76ab
	N120	40.93b	45.30a	50.30a	0.22a	0.57a	0.78a
AWD15	N0	37.76e	41.06e	46.06de	0.15d	0.43de	0.56e
	N90	40.93b	45.00a	49.10b	0.20bc	0.52c	0.73bc
	N120	42.20a	45.26a	50.50a	0.21ab	0.54abc	0.75 ab
AWD25	N0	35.96f	39.00g	43.63f	0.15d	0.36f	0.46f
	N90	38.70d	42.13d	46.56d	0.18c	0.45d	0.67d
	N120	39.13d	43.00c	47.63c	0.18c	0.52bc	0.69cd
2022-2023							
CF	N0	37.80e	40.86f	40.86f	0.17d	0.42e	0.55e
	N90	40.46c	44.20c	44.20c	0.22ab	0.56ab	0.70b
	N120	40.96b	45.46a	45.46a	0.23a	0.57a	0.74ab
AWD15	N0	37.70e	41.23f	41.33e	0.16d	0.43de	0.57e
	N90	40.96b	44.76b	45.26b	0.21bc	0.53c	0.75ab
	N120	42.23a	45.43a	45.53a	0.22ab	0.56a	0.77a
AWD25	N0	36.00e	39.16g	39.26g	0.16d	0.37f	0.45f
	N90	38.73d	42.30e	42.40d	0.19c	0.45d	0.66cd
	N120	39.16d	43.16d	43.26c	0.19c	0.53bc	0.69c
Analysis of Variance							
Year (Y)		ns	ns	ns	ns	ns	ns
Irrigation regime (I)		**	**	**	**	**	**

N rates (N)	**	**	**	**	**	**
Y x I	ns	ns	ns	ns	ns	ns
Y x N	ns	ns	ns	ns	ns	ns
I x N	ns	ns	ns	ns	*	ns

*, **means F values is significant at p=0.05 and p=0.01 levels, respectively.
Ns means no significant at p=0.05 level. Different letters indicate statistical significance at the p=0.05 level within the same column and the same year.
MT means mid-tillering, PI is panicle initiation, MAT is maturity and HD is heading.
CF, AWD_{15} and AWD_{25} represent continuous flooding, alternate wetting and drying at 15 cm threshold and alternate wetting and drying at 25 cm threshold.

Across the two years and over the three growing stages, chlorophyll content (CC) and NDVI were significantly affected by both water and nitrogen inputs (Table 10). Indeed, they all increased with the increase of nitrogen application and the highest CC was recorded with N120 for all water regimes, although NDVI under N90 and N120 were statistically the same. At maturity, in average, CC increased by 10.20 % and 7.77 % respectively, with N120 and N90 compared to control (N0). For the same nitrogen inputs and for the three growing stages, CC was significantly ($p<0.05$) higher in AWD15, and the lowest was recorded with AWD25. In average, at maturity, CC content from AWD15 and AWD25 in both years was increased by 1% and decreased by 4.6% compared to CF, respectively. The NDVI presented the highest values in CF, followed by AWD15 at the MT and PI stages, and the highest values at maturity were recorded in AWD15. Statistically, plants under AWD15 and CF present similar NDVI contents at maturity. However, NDVI content from AWD15 and AWD25 was decreased by 3.9 % and 10.7 % compared to CF, respectively. In all, the interaction effect of N0 with AWD25 showed the lowest chlorophyll and NDVI compared to all the other treatment combinations.

The chlorophyll content (CC) and Normalized Difference Vegetation Index (NDVI) are good indicators of canopy greenness and a key pigment involved in photosynthesis, which is the global biological process that supplies energy for plants and other living things (Shpilyov et al., 2013). Many reports showed that both NDVI and CC increased with the increased nitrogen application and water regime, (Mafakheri et al., 2010). This study is in line with that report and demonstrated that the chlorophyll content of rice increased with nitrogen application and decreased continuously under drought stress. This could be attributed to the influence of the interaction between water and fertilizer application, which is essential for biomass production by the plants. In addition, Sun et al. (2012) pointed out that drought stress can significantly reduce the chlorophyll content of plants, and the higher the degree of stress, the greater the decrease. Surprisingly, plants under AWD15 presented similar NDVI to those under the CF regime. This could be attributed to the high root-oxidizing activity of the widely spaced rice plants, which improved N uptake. Regarding NDVI responses, our results showed that NDVI increased with both the increase in nitrogen application and soil moisture. Indeed, the higher values were recorded under CF, and the lowest values were recorded with AWD25 . These findings are in agreement with many reports that revealed that NDVI responded reciprocally to increasing water contents (Jahan et al., 2014), showing that water is an important substrate for this process. Still, the addition of nitrogen has augmentative effects by means of nutrient provision to the plants. Interestingly, our results for NDVI showed a similar NDVI for both plants under CF and AWD15. This could be attributed to the fact that only severe water stress could negatively impact the photosynthetic rate and reduce the NDVI through CO_2 assimilation (Jahan et al., 2014).

4.4.2 Yield components

The grain yield, straw yield, and the harvest index of irrigated rice as affected by different water management (W) and nitrogen fertilizer (N) and their interaction in 2021-2022 and 2022-2023 is represented in Figure 26. In both years, grain yield increased with the increase in nitrogen application. In all treatments, the average grain yield ranged from 1.17 to 6.01 Mg. ha^{-1} and from 1.54 to 6.07 Mg. ha^{-1} in 2021-2022 and 2022-2023, respectively. For both years, the maximum grain yield was recorded under CF regime with N120 whereas the lowest grain yield was recorded under AWD25 with N0. When N rates were the same, grain yield was higher in AWD15 regime although there was no significant difference between treatments under CF regime and AWD15 regime whereas the lowest grain yield was recorded with the AWD25 regime. In AWD15 regime, the higher grain yield is achieved with N120, although it is not statistically different from the treatment under N90.

Straw yield increased consistently with the increase of nitrogen application in both years. In all treatments, the average straw yield ranged from 3.69 to 9.43 $Mg.ha^{-1}$ and from 3.75 to 9.45 $Mg.ha^{-1}$ in 2021-2022 and 2022-2023, respectively. In both years, all combined treatments showed that the highest straw yield was recorded under CF regime with N120 and the lowest was recorded under AWD25 with N0. Regarding the water regime, treatments under CF presented a higher straw yield, followed by treatments under AWD15 and the lowest straw yield was recorded under AWD25. Straw yield under AWD15 regime with N120 was not statistically different from treatment under CF regime and N90. Also, the two rates of nitrogen inputs under AWD25 presented a similar straw yield.

Harvest index (HI) was significantly affected by the different N rates during both experiment years. Considering the different rates of nitrogen, HI increased with N90, although there is no significant difference with N120. The lowest HI was recorded with N0. Regarding all water regimes, the highest HI was recorded under AWD15 followed by CF whereas the lowest HI was recorded under AWD25. The interaction between water regime and nitrogen application showed that the highest HI was recorded under AWD15 with N90 (0.42 and 0.43, respectively in 2021-2022 and 2022-2023) followed by AWD15 with 120 (0.41 and 0.40, respectively in 2021-2022 and 2022-2023), even though both are not statistically different.

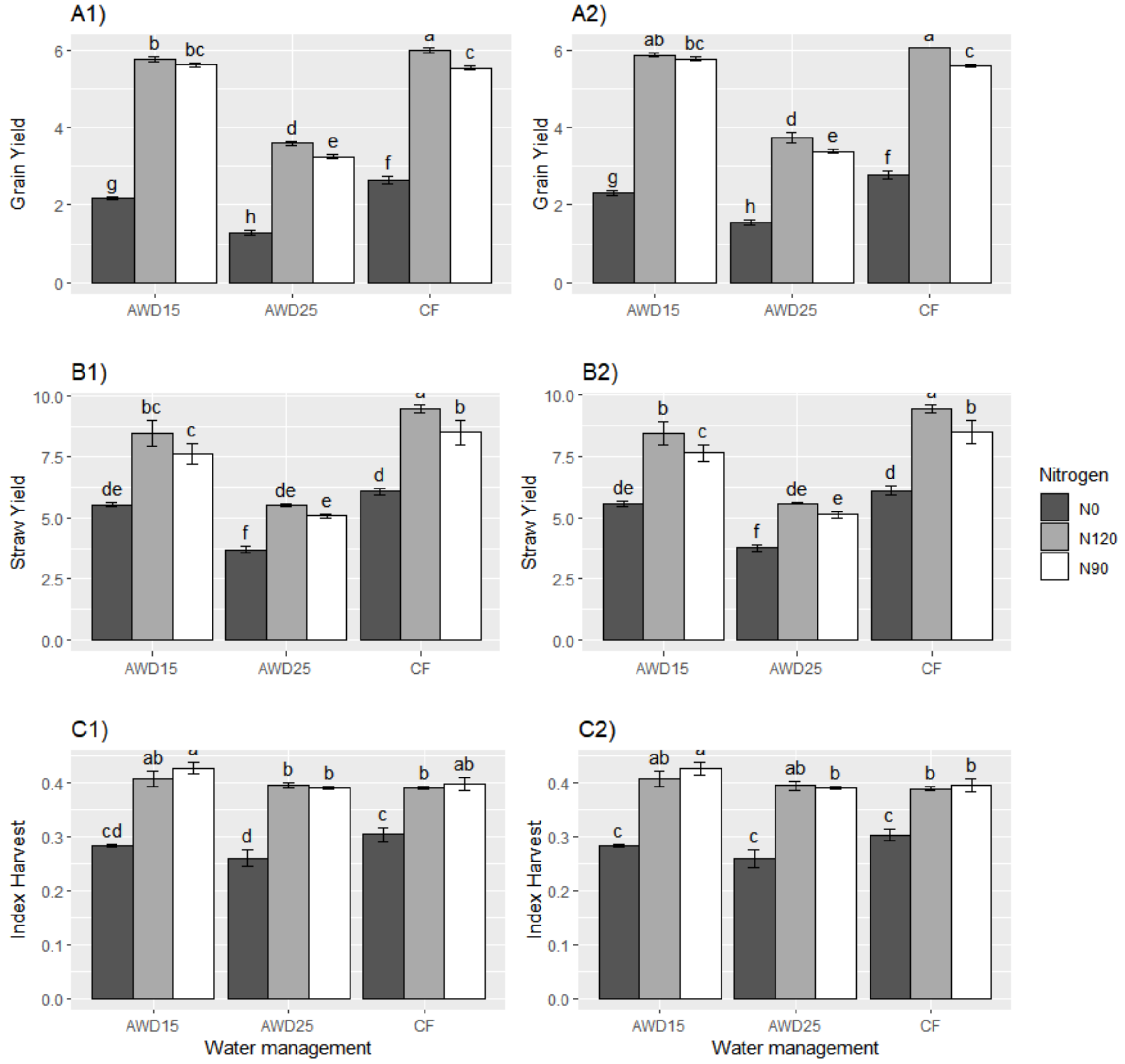

Figure 26: grain yield, straw yield, and Harvest Index of irrigated rice as affected by different water and N fertilizer managements and their interaction in 2021-2022 (A1, B1 and C1) and 2022-2023 (A2, B2, C2).

CF, AWD_{15} and AWD_{25} represent continuous flooding, alternate wetting and drying at 15 cm threshold and alternate wetting and drying at 25 cm threshold, respectively.

Different letters indicate statistical significance at the p=0.05 level within the same column and the same year

Across the two years, grain yield in 2022–2023 was a bit higher than in 2021–2022, probably due to the longer sunshine and more water inputs in the second year. Rice grows better under longer sunshine duration and thus more solar radiation (Zhao et al.,1993; Lampayan et al., 2015). Our results showed that the grain yield under AWD15 and CF are comparable for irrigated production in southern Benin, whereas the yield under AWD25 is significantly lower. It is noteworthy that some previous studies are in agreement with these results and reported that the soil water potential (−20 kPa) during the rice-growing season was usually not a limitation factor for plant growth and yield formation when AWD15 was practiced (Yao et al., 2012; Khairi et al., 2015; Liang et al., 2016). Carrijo et al., (2017) found that AWD25 is considered a severe drying period, which usually leads to yield penalties. Consequently, at the limit of the threshold of 15 cm of water depth below the soil surface, the lower parts of the rice roots could still be able to take up enough water from the saturated soil (Bouman et al., 2007b; Lampayan et al., 2015a; Carrijo et al., 2017). Plus, reduced yields under AWD25 soil conditions might be due to inhibition of photosynthesis and less translocation of assimilates due to low soil moisture availability (Tabbal et al., 2002). Nonetheless, another study revealed that AWD irrigation reduced the rice yield. A meta-analysis by Carrijo et al. (2007) found that AWD irrigation led to yield reduction compared to flood irrigation, with yield losses ranging between 3% and 23%. Previous studies revealed that the grain yield of rice decreased but weeds increased under AWD if paddy fields were not timely irrigated. Meanwhile, AWD irrigation requires steady water sources with complex drying and irrigation treatment, which is relatively difficult (Zhang et al., 2009; Yao et al., 2012; Yakubu et al., 2018). The differences in rice yield under different water regimes can be attributed to both external (rainfall, air temperature, solar radiation, etc.) and internal factors (soil type and properties, irrigation duration, rice variety, etc.) (Yao et al., 2012; Liu et al., 2013).

Furthermore, with regard to the effect of N nutrition on rice yield under different soil moisture conditions, many studies have reported that with the increase of N application, the yield would increase, and excessive N application resulted in a decrease in yield (Fageria et al., 2011; Zhou et al., 2015; Deng et al., 2018). Our findings are consistent with these reports and showed that grain and straw yields increased with the increase of nitrogen. In the AWD15 regime, the interaction effects of both N90 and N120 had similar yields. Mannan et al., (2012) and Azarpour et al., (2014) reported the same observation and demonstrated that the application of 90 N kg. ha^{-1} increased rice yield significantly under AWD15 regime. However, the findings are not in line with the report by Rezaei et al., (2009), in which application of nitrogen fertilizer above 60 kg N ha^{-1} did not improve yield significantly. This observation might also be attributed to an adequate amount of nitrogen being transported to the plant when plants were treated with higher doses of nitrogen.

Moreover, our results showed that the harvest index was higher with AWD15 regimes, and it remained similar under N90 and N120. This could be explained by the fact that the AWD15 regime promoted carbon remobilization from stems during the maturity period and increased the harvest index comparatively to both CF and AWD25 (Pan et al., 2017). Strict regulations, such as maintaining the threshold of water depth at 15 cm below the soil surface, must be carried out to guarantee its safe use. In the present study, the threshold of soil water potential for rewatering in the AWD15 regime under N90 could be used as the index for a safe way to achieve a higher yield and a high harvest index in a sub-Saharan country such as Benin.

4.4.3. Water consumption and water productivity

Table 11: Irrigation water input, Total water input, and Total water productivity (WP) of irrigated rice as affected by different water and N fertilizer managements and their interaction in 2022 and 2023.

Year/ irrigation regime	N rate (Kg. ha^{-1})	Irrigation water input (mm)	Total water input (mm)	Total Water productivity (Kg.m^{-3})
2021-2022				
CF	N0	695.0b	775.1ab	0.34g
	N90	698.0a	778.6a	0.71e
	N120	705.3a	785.4a	0.76d
AWD 15	N0	445.0d	525.1cd	0.41f
	N90	450.8c	530.9c	1.06a
	N120	457.0c	537.1c	1.07a
AWD25	N0	285.3f	369.4e	0.35g
	N90	291.5e	371.6e	0.87c
	N120	294.6e	374.7e	0.96b
2022-2023				
CF	N0	761.0b	781.4b	0.35g
	N90	764.0b	784.4ab	0.72e
	N120	770.3 a	790.7a	0.77d
AWD 15	N0	510.0d	538.4c	0.43f
	N90	518.6c	539.0c	1.08a
	N120	522.0c	542.4c	1.09a
AWD25	N0	350.3f	370.7ef	0.41f
	N90	356.6e	377.0e	0.89c
	N120	359.6e	380.0e	0.98b

Analysis of Variance			
Year (Y)	ns	ns	ns
Irrigation regime (I)	**	**	**
N rates (N)	**	**	**
Y x 1	ns	ns	ns
Y x N	ns	ns	ns
I x N	ns	ns	**

*, **means F values is significant at p=0.05 and p=0.01 levels, respectively.
Ns means no significant at p=0.05 level. Different letters indicate statistical significance at the p=0.05 level within the same column and the same year.
CF, AWD_{15} and AWD_{25} represent continuous flooding, alternate wetting and drying at 15 cm depth and alternate wetting and drying at 25 cm depth.

Table 11 showed that total irrigation water and total water inputs across the two-year experiment, followed the same tendency and increased with the increase of nitrogen inputs, even though there is no significant difference between N90 and N120 for all water regimes. The highest values for both parameters were recorded under CF regimes and the lowest values were recorded under AWD25 regime. The total water input was higher in 2022–2023 than in 2021–2022. Indeed, the total water input across water treatments ranged from 369.4 to 785.4 mm in 2021-2022 and from 370.7 to 790.7 mm in 2022-2023. In both years, there were neither significant of the interaction between water management (W) and nitrogen rate (N), nor significant effects of N, with respect to irrigation water input and the total water input. In average over the two-year experiment, the AWD15 and AWD25 regimes saved respectively 31.75% and 52.30 % of total water inputs compared to CF regime. The highest irrigation and water inputs were recorded under CF with N120, and the lowest irrigation and water inputs were recorded under AWD15 with N0.

The total water productivity (WP) was significantly affected by different water regimes (W), nitrogen rate (N) and the interaction W x N. Indeed, WP in all water regime increased with the increase of N application. In addition, the application of N90 and N120 was not significantly affected the WP in AWD15. For the same N inputs, AWD15 regime recorded the highest WP whereas CF regime recorded the lowest WP. However, on average, WP under the AWD15 and AWD25 regimes is, respectively, 41.32% and 23% higher compared to the CF regime. Among all the treatments, the highest WP was recorded under the AWD15 regime with N120 although there is no significant difference with AWD15 regime with N90. The lowest WP was recorded under CF with No.

The total water input was significantly ($p < 0.05$) influenced by water management, N fertilizer levels, and their interactions. Previous studies have reported a reduction of the total water input by 18–54% compared to CF less water use under AWD15 (Liang et al., 2016, Carrijo et al., 2017; Djaman et al., 2018). Our results were in accordance with these studies and showed that, when compared with the CF regime, both the AWD15 and AWD25 regimes significantly decreased irrigation up to 31.75% and 52.30 % respectively. Sun et al., (2011) also reported the reduction of irrigation water requirements for non-flooded rice by 20–50% compared to flooded rice. Many studies have reported that a water regime with large depths of standing water in paddy fields would lead to high water losses by evaporation, percolation, seepage, and surface runoff. Therefore, greater water productivity was consistently observed in both AWD15 and AWD25 than CF (Bouman et al., 2007; Tan et al., 2013; Wang et al., 2016). Our findings are in line with this regard and showed that WP under AWD15 plots is 41.32 % higher than in CF, and the WP under AWD25 plots is 23% higher than in CF. These results are in agreement with Carrijo et al., (2017), who reported water savings of 23–33% under AWD15. Yakubu et al., (2016) and Mboyerwa et al., (2022) also obtained similar results in Ghana and Tanzania, respectively, and they showed that AWD15 could increase the WP in rice production. This difference between water input and water productivity could be strongly attributed to the soil type and climate conditions such as evapotranspiration and rainfall (Carrijo et al., 2017, and Djaman et al., 2018). In addition, our study revealed that, under AWD15 regimes, WP was similar with both N90 and N120. This demonstrated that a moderate rate of nitrogen with a moderate wetting and drying regime (AWD15) could not only save water, but also increase the water productivity in west African climate conditions such as Benin.

With regards to nitrogen application, previous studies reported that the application of N significantly increased both irrigation water input and water productivity in comparison with N_0 (Yao et al., 2012; Liu et al., 2013; Yakubu et al., 2016; Mboyerwa et al., 2022). Our results are in line with these reports and showed that both water inputs and water productivity increased with the increase of nitrogen. The increased irrigation water input under the higher N rate was caused by increased water absorption due to its higher transpiration, and the increased water productivity was due to the much higher grain yield under the higher N application condition in rice (Ren et al., 2015). In addition, Mannan et al. (2012) observed that higher photosynthesis and metabolism during the growth stages led to a higher water requirement by plants in order to carry out their physiological functions.

4.4.4. The total Nitrogen uptake and Nitrogen Use Efficiency

Table 12: The Total N uptake, Total water input, the Nitrogen Use Efficiency of irrigated rice as affected by different water and N fertilizer managements and their interaction in 2022 and 2023.

Year/ irrigation regime	N rate (Kg. ha^{-1})	Total N Uptake (Kg. ha^{-1})	ANUE (Kg. Kg^{-1})	NRE (%)	PFPN (Kg. Kg^{-1})	PNUE (Kg. Kg^{-1})
2021-2022						
CF	0	78.21f				33.81cd
	90	151.61bc	32.31b	81.54ab	61.70b	36.70abc
	120	173.60a	28.10d	79.49ab	50.14c	34.66bcd
AWD 15	0	66.00g				33.10d
	90	143.62c	38.32a	86.24a	62.60a	39.29a
	120	154.81b	29.89c	74.00b	48.10d	37.37ab
AWD25	0	39.21h				32.93d
	90	89.51e	21.87e	55.88c	36.21e	36.40abc
	120	98.27d	19.28f	49.22c	30.03f	36.67abc
2022-2023						
CF	0	79.9f				34.37c
	90	155.91b	31.64b	81.01ab	62.49b	36.82bc
	120	174.85a	27.52d	79.04ab	50.66c	34.77bc
AWD 15	0	67.87g				34.35c
	90	145.83c	38.36a	86.62a	64.26a	39.69a
	120	156.64b	29.66c	73.97b	49.09d	37.65ab
AWD25	0	41.93h				34.32c
	90	91.74e	20.50e	55.34c	37.71e	37.01abc
	120	100.66d	18.40f	48.93c	31.30f	37.29abc
Analysis of Variance						
Year (Y)		ns	ns	ns	ns	ns
Irrigation regime (I)		**	**	**	**	ns
N rates (N)		**	**	*	**	*
Y x 1		ns	ns	ns	ns	ns
Y x N		ns	ns	ns	ns	ns
I x N		**	**	ns	**	ns

*, **means F values is significant at p=0.05 and p=0.01 levels, respectively.
Ns means no significant at p=0.05 level. Different letters indicate statistical significance at the p=0.05 level within the same column and the same year.
CF, AWD_{15} and AWD_{25} represent continuous flooding, alternate wetting and drying at 15 cm depth and alternate wetting and drying at 25 cm depth.
ANUE is the Agronomic N use efficiency, NRE is the Fertilizer N recovery efficiency, PFPN is the Partial factor productivity of N and PNUE the Physiological N use efficiency

For both years, total N uptake increased significantly as a result of the interaction between water management (W) and Nitrogen rate (N). Indeed, N uptake increased with the increase in nitrogen application. In addition, it is also affected by different water regimes. It was highest under CF regime whereas it was lowest under AWD25 regime. The N Uptake ranged from 39.21 to 173.60 and from 41.93 to 174.85 in 2021-2022 and 2022-2023 respectively. The highest value was recorded under CF regime with N120 whereas the lowest value was recorded under AWD25 regime with N0.

The higher PNUE was recorded under AWD15 regime followed respectively by AWD25 and CF although the three water regimes were not statistically different from each other for the same nitrogen application ($p \geq 0.05$). It is also increased with nitrogen application compared to the control (N0) although there is no significant difference between N90 and N120 plots. In general, for all treatment, the PNUE ranged from 32.93 to 39.29 and from 34.32 to 39.69 in 2021-2022 and 2022-2023 respectively. The highest value was recorded under AWD15 regime with N90 whereas the lowest value was recorded under AWD25 regime with N0. The ANUE was significantly affected by the different rates of nitrogen input and decreased with the increase of nitrogen. Considering the different water regimes and the same level of nitrogen application, the highest ANUE was recorded under AWD15 regime, and the lowest value was recorded under AWD25 regime. In general, for all treatment, the ANUE ranged from 21.87 to 38.32 and from 20.50 to 38.36 in 2021-2022 and 2022-2023 respectively. The highest value was recorded under AWD15 regime with N90 whereas the lowest value was recorded under AWD25 regime with N120. Furthermore, across the two-year experiments, the NRE and PFPN were not only affected by different rates of nitrogen application but also by the interaction WxN. In general, both parameters decreased with the increase in nitrogen application, even though both treatments under N90 and N120 are statistically similar for the NRE. At the same rate of nitrogen, the NRE for the different water regimes was not significantly different, although the lowest NRE was recorded under AWD25 regime. The PFPN under AWD15 and CF regimes are statistically the same, and the lowest was recorded with AWD25.

There are also different conclusions about the effect of different water regimes on N uptake and nitrogen use efficiency. Many studies reported that N-uptake in both grain and straw increased with increased nitrogen rates and biomass production (Yao et al., 2012; Liu et al., 2013; Yakubu et al., 2016; Mboyerwa et al., 2022). Our results showed that plants under N120 presented the highest N uptake. This could be due to the higher above ground biomass accumulation and larger leaf area index. Indeed, the large leaf area index results in a higher rate of transpiration and consequently increases nitrogen uptake by plant roots. In addition, some previous studies also showed that N uptake is higher under submerged conditions than alternate wetting and drying irrigation conditions (Dong et al., 2008; Ye et al., 2015; Xu et al.,2019). Our findings are in line with these reports and revealed that N uptake increased when plants were grown under CF. Some scholars have proposed that the adoption of alternate wetting and drying as an irrigation regime may reduce the total N uptake in plants due to increases in N losses through ammonia volatilization, nitrification, and denitrification (Dong et al., 2008; Xu et al., 2019).

In the present study, we did not determine N dynamics in soil. However, we observed that all the parameters of nitrogen use efficiency (NUE) were statistically the same or increased in AWD15 regimes compared to CF regimes and AWD25. This could be explained by the fact that AWD15 could increase the total cumulative plant N and NUE. The results of the study, however, are in agreement with Zare et al., (2014), who found that the NRE and ANUE are significantly higher in AWD15 water management than submergence conditions. Furthermore, the significantly higher ANUE, PNUE, and NRE in AWD15 than CF in this study (Table 12) suggested that the consequent nitrification–denitrification process under AWD15 was not severe enough to cause a greater loss of N compared with CF (Cabangon et al., 2011). In addition, the finding is consistent with Dong et al. (2008), who reported that the CF generally possessed a higher floodwater pH than the AWD15 and caused higher N output through ammonia volatilization. Our results showed that lower values of different parameters of NUE were recorded under AWD25 regimes. This could be explained by the fact that below a certain level of water stress (15 cm below the soil surface in our case), alternate wetting and drying creates severe aerobic conditions that don't enhance root growth and, therefore, don't provide a better surface area for the uptake of nutrients. Furthermore, this reduction in total accumulative plant N in the AWD25 may result from either the inhibition of plant N uptake or the increase of N losses from the soil (Tizon-Salazar et al., 2015; Cao et al., 2020). In all water regimes, NUE decreased with the increase in nitrogen application, even though both plants under N90 and N120 are statistically similar. We speculate that a moderate nitrogen application could achieve a high NUE, and the high nitrogen application could lead to N loss and then to environmental pollution.

In addition, moderate alternate wetting and drying irrigation could lead to lower runoff and thus reduce N losses compared to CF regimes (Zhao et al., 2021). Therefore, AWD15 could be an effective means for reducing N losses from leaching (percolation and seepage) and runoff, which might enhance NUE usefully. Further research is needed to understand the mechanism by which an alternate wetting and drying regime has a higher nitrogen use efficiency under moderate nitrogen application, considering the different pedoclimatic conditions and different types of rice cultivar.

4.5 DSSAT CERES-Rice crop growth model to simulate rice growth and rice yield.

4.5.1 Model calibration

Dataset from first year of experiment 2 was used for the calibration of our model. Table 13 presents the descriptive statistics showing the performance of CERES-Rice for calibration.

Table 13: Descriptive statistics showing the performance of CERES-Rice for calibration.

Variable	Obs	Sim	RMSE	NRMSE	d	R^2
PI date (DAP)	66	66	0.58	0.99	0.95	0.94
Anthesis date (DAP)	82	83	0.82	0.97	0.89	0.92
Maturity date (DAP)	105	106	0.56	0.55	0.92	0.98
LAI (cm2 cm2)	4.8	4.6	0.081	1.76	0.89	0.92
Grain yield ($T.ha^{-1}$)	5.8	5.7	0.081	1.41	0.88	0.99
AGB ($T. ha^{-1}$)	9.3	9.5	0.082	0.90	0.95	0.97
Tops N at maturity ($T Kg^{-1}$)	170	168	0.81	0.48	0.70	0.86

Obs: mean of observed value; Sim: mean of simulated value; RMSE: Root Mean Square Error, RMSEn: Normalized Root Mean Square Error (%), d: index of agreements; R^2: adjusted linear correlation coefficient between simulated and measured values.
LAI: Leaf Area Index, AGB: Above ground Biomass

A close agreement was observed between the simulated and observed values for anthesis, maturity, LAI, grain yield, biomass yield and N uptake. The model accurately predicted the days to anthesis and maturity, grain yield, topweight, and N uptake with an RMSE between 0.0081 and 0.82. the NRMSE was ranged from0.48% to 1.76 5%. All the d-values were ≥ 0.75 and the R^2 values were also all ≥ 0.80 indicating great performance of the model. However, the lowest value of R2 and other indexes of agreement was observed for the tops N at maturity.

4.5.2 Model Validation

Table 14:Descriptive statistics showing the performance of CERES-Rice for validation.

variable	Obs	Sim	RMSE	NRMSE	d	R^2
PI date (DAP)	67	67	0.59	0.99	0.97	0.96
Anthesis date (DAP)	84	85	0.84	0.98	0.90	0.94
Maturity date (DAP)	107	106	0.58	0.54	0.93	0.99
LAI (cm2 cm2)	4.9	4.6	0.074	1.87	0.81	0.89
Grain yield (T ha^{-1})	5.9	5.6	0.08	1.54	0.87	0.98
AGB (T ha^{-1})	9.2	9.6	0.079	0.87	0.94	0.96
Tops N at maturity (T Kg^{-1})	172	167	0.79	0.41	0.67	0.82

Obs: mean of observed value; Sim: mean of simulated value; RMSE: Root Mean Square Error, RMSEn: Normalized Root Mean Square Error (%), d: index of agreements; R^2: adjusted linear correlation coefficient between simulated and measured values.
LAI: Leaf Area Index, AGB: Above ground Biomass

Similar to the descriptive statistics for the calibration, a close agreement was also observed between the simulated and observed values for anthesis, maturity, LAI grain yield, biomass yield and N uptake for the validation (Table 14). The model accurately predicted the days to anthesis and maturity, grain yield, topweight, and N uptake with RMSE between 0.0074 and 0.84. the NRMSE was ranged from 0.41% to 1.87 %. All the d-values were ≥ 0.75 and the R2 values were also all ≥ 0.80 indicating great performance of the model for the validation according to Jamieson et al. (1991). However, the lowest values of R^2 and the index of agreement (d) were still observed for the tops N at maturity.

4.5.3 Evaluation of the model

The CERES-Rice weas evaluated using both dataset from experiment 1 on grain, straw yields, and total N uptake. This was done to ensure that applications of the models to assess different seasonal conditions in the study region are reliable. The graphical comparison between simulated and measured grain yield, biomass at maturity and aboveground N uptake is presented in Figure 27.

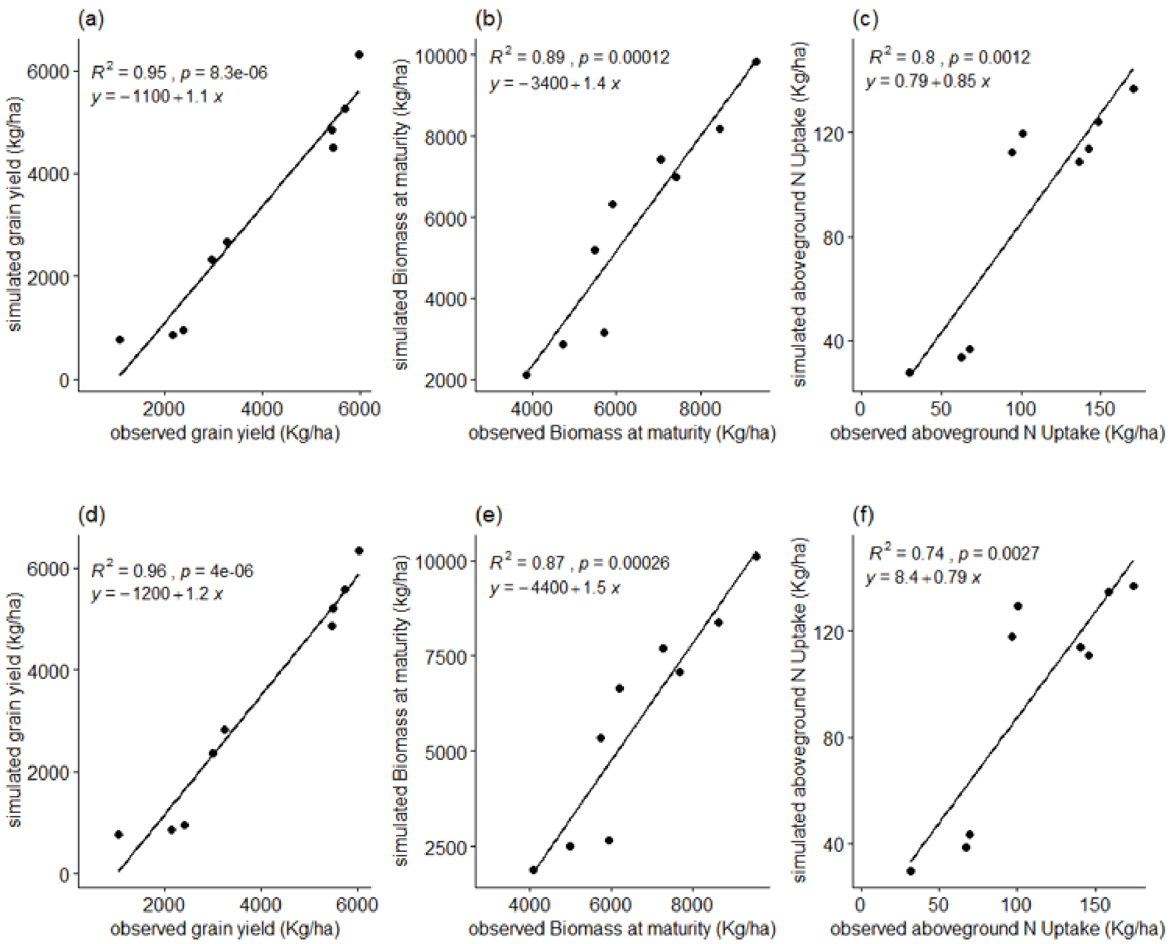

Figure 27: Graphical comparison between simulated and measured grain yield, biomass at maturity and aboveground N uptake using datasets (2021-2023).

For both years of experiments, the CERES-Rice model accurately predicted grain yield, biomass at maturity, and above-ground N uptake. The grain yield was predicted more accurately than other variables (R^2 = 0.95 and 0.96 for the two years, respectively). Aboveground N uptake presented the lowest R^2 for the two years of experiments, with R^2 values of 0.80 and 0.74, respectively.

In general, similar to the simulation results, the model performs well in simulating total crop biomass as well as grain yield. In this study, the crop parameters of the CERES-rice model were calibrated by way of the GLUE method, and the calibrated model successfully simulated LAI, AGB, and total N uptake at maturity under different water management and N application levels. Islam et al. (2021) and Kadiyala et al. (2013) used the GLUE method to accurately estimate the genotype coefficients and soil parameters of the DSSAT-CERES-rice model for rice production in northern India and Bangladesh under different management practices. The parameters were estimated simultaneously using several rounds of the GLUE method. The genotype coefficients were divided into five categories according to the model module, and the calibration of each of the genotype coefficients was done sequentially using the GLUE method. Whether the accuracy of sequentially calibrated genotype coefficients is superior to that of simultaneously calibrated genotype coefficients requires further exploration. In general, it has been demonstrated that DSSAT-GLUE software offers an effective method for estimating crop parameters (Hoogenboom et al., 2010). This study combined the systematic approach to model calibration with the GLUE method, which analyzes the performance of each module of the model.

This result from the model evaluation suggests that the grain yield was better than the other two output variables, which is consistent with the results of previous studies by Gérardeaux et al. (2021) in Senegal and Lu et al. (2022) in China. Explanations may include: (1) the CERES-rice model is a classical radiation use efficiency model, and (2) the measured accuracy of grain yield is superior to that of AGB and N uptake from the perspective of the process of measurement. In this study, model applications for the optimization of water and nitrogen fertilizer were evaluated. As we know, the DSSAT model was initially developed to help make better decisions by integrating knowledge of climate, soil, crops, and management (Jones et al., 2003). The results of this study indicate that it was a useful tool for optimizing water and nitrogen fertilizer management of rice in southern Benin. The study only tests the potential application of water and nitrogen fertilizer, and more field management practices such as optimal seeding rates, various types of fertilizers, and tillage should be validated in future studies so that more intelligent precision farming decision-management systems can be developed based on the DSSAT model. In addition, CO_2 concentration might have a significant effect on growth, the grain yield as well as on the nutrient use efficiency. Niang et al. (2014) reported that a positive effect of CO_2 on rice growth and yield. CO_2 affects the rice plant by enhancing the rate of photosynthesis and reducing stomatal conductance.

CHAPTER FIVE

CONCLUSION AND RECOMMENDATIONS

5.1. CONCLUSION

Laboratory and field validation showed that CO_2 and ET fluxes can be reliably measured over time using inexpensive NDIR and RH sensors in conjunction with a manual closed chamber system. The developed measurement system can be a valuable tool in evaluating and assessing global carbon and water flux models, which are both critical for climate change mitigation. As a result, this powerful, low-cost system was successfully used to assess soil respiration, the NECB, and ET from a rice field in southern Benin. Therefore, hypothesis H1 is confirmed. In addition, the field application demonstrated that alternate wetting and drying irrigation at a 15-cm threshold with N90 kg ha^{-1} could be a workable solution for sustainable and environmentally friendly rice cultivation in southern Benin. However, this treatment achieved a similar net ecosystem C balance compared to the continuously flooded rice with both N90 kg ha^{-1} and N120 kg ha^{-1}, even though it recorded a bit higher soil respiration (hypothesis H2 is confirmed and hypothesis H3 is rejected). Further, this combination demonstrated throughout the study its advantages over continuous flooded rice production in terms of rice yield, nitrogen use efficiency, and water productivity (hypothesis H4 is confirmed). The tool used in AWD15 is the perforated field water tube. It is simple and practical, and it can be fabricated with cheap materials such as polyvinyl chloride (PVC) pipe. In the irrigated rice production in West Africa, especially Benin, continuous flooding irrigation (CF) is still widely used by the farmers. By using the AWD15 technology, irrigation water input and labor costs can be reduced. This study highlights a new generation of watering technology after CF and the System of Rice Intensification (SRI) that is expected to be widely promoted and applied for sustainable rice production in Africa to save water and protect the environment. Furthermore, the calibration of the DSSAT CERES rice model was successfully done in simulating growth and yield using the GLUE estimator (hypothesis H5 is then confirmed). However, for the model evaluation, the grain yield was the most accurately predicted (R^2 = 0.95 and 0.96 for the two seasons, respectively) whereas the aboveground N uptake was less accurately predicted (R^2 values of 0.80 and 0.74, more accurately). The results illustrated that the model is a useful tool for evaluating alternative management options to maintain yields while saving water under Benin’s weather condition.

5.2. RECOMMANDATIONS

From the limitation of this study, the following recommendations are provided for further research.

- Only chemical fertilizer was used in this study. It would also be great to associate the organic manure to examine the combined effect on the soil's carbon metabolism.
- In this study, we did not measure CH_4 emissions from different rice ecosystems. It would be better to add this type of measurement in order to assess the full net ecosystem C balance and the global warming potential from each treatment.
- CERES Rice model was capable of well simulating the growth and grain yield under different water and N management strategies, especially in southern Benin. Therefore, for further study, the predicted model could be used to assess the impact of climate change for sustainable production using different climate model under different scenarios based on Shared Socioeconomic Pathways (SSPs): SSP1-2.6, SSP2-4.5, and SSP5-8.5 will be considered.

REFERENCES

Abdallah MB, Fekete-Farkas M, & Lakner Z. (2021). Exploring the link between food security and food price dynamics: a bibliometric analysis. Agriculture (switzerland) 11(3):1–19. https://doi. org/ 10.3390/ agriculture1103 0263

Ahmad, S., Ahmad, A., Manuela, C., & Soler, T. (2012). Application of the CSM-CERES-Rice model for evaluation of plant density and nitrogen management environment. 200–218. https://doi.org/10.1007/s11119-011-9238-1

Akram, H. M., Ali, A., Sattar, A., & Saeed-ur-rehman, H. (2013). Impact of water deficit stress on various physiological and agronomic traits of three Basmati rice (Oryza sativa L.) cultivars. January.

Akter, M., Deroo, H., Mostafa, A., Abdul, M., Verhoeven, E., Decock, C., Boeckx, P., & Sleutel, S. (2018). Agriculture, Ecosystems and Environment Impact of irrigation management on paddy soil N supply and depth distribution of abiotic drivers. Agriculture, Ecosystems and Environment, 261(October 2017), 12–24. https://doi.org/10.1016/j.agee.2018.03.015

Alberto, Ma.C.R., Wassmann, R., Hirano, T., Miyata, A., Kumar, A., Padre, A. & Amante, M. (2009). CO_2/heat fluxes in rice fields: comparative assessment of flooded and nonflooded fields in the Philippines. Agric. For. Meteorol. 149,2009,1737–1750. https://doi. org/10.1016/j.agrformet.2009.06.003.

Alberto, M.C.R., Hirano, T., Miyata, A., Wassmann, R., Kumar, A., Padre, A. & Amante, M, (2012). Influence of climate variability on seasonal and interannual variations of ecosystem CO_2 exchange in flooded and non-flooded rice fields in the Philippines. Field Crop. Res. 2012, 134, 80–94

Alberto, Ma.C.R., Wassmann, R., Buresh, R.J., Quilty, J.R., Correa, T.Q., Sandro, J.M. & Centeno,C.A.R. (2014).Measuring methane flux from irrigated rice fields by eddy covariance method using open-path gas analyzer. Field Crop Res. 160,12–21. https://doi.org/10.1016/j.fcr.2014.02.008.

Allen, R.G., Pereira, L.S., Raes, D., & Smith, M. (1998). Crop evapotranspiration guidelines for computing crop water requirements, FAO Irrigation, and drainage paper 56, Food and Agriculture Organization, Rome.

Arif, C., Setiawan, B. I., Fauzi, S., Saputra, D., & Mizoguchi, M. (2019). Water balance analysis on water management of organic System of Rice Intensification in West Java, Indonesia water balance analysis on water management of organic system of rice intensification in west java, indonesia. May 2020. https://doi.org/10.31028/ji.v14.i1.17-24

Arunrat, N., & Pumijumnong, N. (2017). Practices for Reducing Greenhouse Gas Emissions from Rice Production in Northeast Thailand. 1–20. https://doi.org/10.3390/agriculture7010004

Arunrat, N., Sereenonchai, S., Chaowiwat, W., Wang, C., & Hatano, R. (2022). Carbon, Nitrogen and Water Footprints of Organic Rice and Conventional Rice Production over 4 Years of Cultivation: A Case Study in the Lower North of Thailand.

Attarod, P., Komori, D., Fukumura, K., & Thongdeenok, P. (2014). Estimation of Crop Coefficients and Evapotranspiration by Meteorological Parameters in a Rain-fed Paddy Rice Field, Cassava and Teak Plantations in Thailand. January 2006. https://doi.org/10.2480/agrmet.62.93

Azarpour E., Moraditochaee M., & Bozorgi, H. R. (2014). Effect of nitrogen fertilizer management on growth analysis of rice cultivars. International Journal of Biosciences, 4: 35–47.

Baas J, Schotten M, Plume A, Côté G, & Karimi R. (2020). Scopus as a curated, high-quality bibliometric data source for academic research in quantitative science studies. Quantitative Sci Stud 1(1):377–386. https://doi.org/10.1162/qss_a_00019

Bastviken, D., Sundgren, I., Natchimuthu, S., Reyier, H., & Gålfalk, M. (2015): Technical Note: Cost-efficient approaches to measure carbon dioxide fluxes and concentrations in terrestrial and aquatic environments using mini loggers, Biogeosciences, 12, 3849–3859, https://doi.org/10.5194/bg-12-3849-2015,

Belder, P., Bouman, B. A. M., Cabangon, R., Guoan, L., Quilang, E. J. P., Yuanhua, L., Spiertz, J. H. J., & Tuong, T. P. (2004). Effect of water-saving irrigation on rice yield and water use in typical lowland conditions in Asia. 65, 193–210. https://doi.org/10.1016/j.agwat.2003.09.002

Bhattacharyya, P., Neogi, S., Roy, K. S., & Rao, K. S. (2013). Gross primary production, ecosystem respiration and net ecosystem exchange in Asian rice paddy: an eddy covariance-based approach. January.

Blackstock, J. M., Covington, M. D., Perne, M., & Myre, J. M. (2019). Monitoring

Atmospheric, Soil, and Dissolved CO 2 Using a Low-Cost, Arduino Monitoring Platform (CO_2-LAMP): Theory , Fabrication , and Operation. 7(November), 1–19. https://doi.org/10.3389/feart.2019.00313

Blake, G. R., & Hartge, K. H. (1986). In Methods of soil analysis, part 1: Physical and mineralogical methods, 2nd ed., ed. A. Klute, 363–375. Madison, Wisc.: American Society of Agronomy and Soil Science Society of America

Boateng, K. K., Obeng, G. Y., & Mensah, E. (2017). Rice cultivation and greenhouse gas emissions: A review and conceptual framework with reference to ghana. Agriculture (Switzerland), 7(1). https://doi.org/10.3390/agriculture7010007

Bouman, B. A. M., Feng, L., Tuong, T. P., Lu, G., & Wang, H. (2007). Exploring options to grow rice using less water in northern China using a modelling approach II. Quantifying yield, water balance components, and water productivity. 88, 23–33. https://doi.org/10.1016/j.agwat.2006.10.005

Bouyoucos, G. J. (1951). Recalibration of the Hydrometer Method for Making Mechanical Analysis of Soils, A (AJ). 434–438.

Bowden, R. D., Davidson, E., Savage, K., Arabia, C., & Steudler, P. (2004). Chronic nitrogen additions reduce total soil respiration and microbial respiration in temperate forest soils at the Harvard Forest. 196(x), 43–56. https://doi.org/10.1016/j.foreco.2004.03.011

Brändle, J. & Kunert, N. (2019). A new automated stem CO_2 efflux chamber based on industrial ultra-low-cost sensors, Tree Physiology, tpz104, https://doi.org/10.1093/treephys/tpz104.

Bremner,J.M., & Mulvaney, C.S. (1982). Nitrogen-total., In: Methods of Soil Analysis Part 2 (Page, Miller and Kenly ed.). Amer. Soc. Agron., Inc. Publ., USA. pp. 595-624.

Buresh, R.J., & Haefele, S.M. (2010). Changes in paddy soils under transition to water-saving and diversified cropping systems. In: CD, 19th World Congress of SoilScience, 1–6 August 2010, Brisbane, Australia.

Cabangon, R. J., Tuong, T. P., Castillo, E. G., Bao, L. X., Lu, G., Wang, G., Cui, Y., Bouman, B. A. M., Li, Y., Chen, C., & Wang, J. (2004). Effect of irrigation method and N-fertilizer management on rice yield, water productivity and nutrient-use efficiencies in typical lowland rice conditions in China. Paddy and Water Environment, 2(4), 195–206. https://doi.org/10.1007/s10333-004-0062-3

Cao, X. C., Wu, L. L., Lu, R. H., Zhu, L. F., Zhang, J. H., & Jin, Q. Y. (2020). Irrigation and fertilization management to optimize rice yield, water productivity and nitrogen recovery efficiency. Irri. Sci. 39, 235–249. https://doi: 10.1007/s00271-020-00700-4

Capri, C., Gatti, M., Guadagna, P., Zozzo, F. Del, Magnanini, E., & Poni, S. (2021). Original papers A low-cost portable chamber based on Arduino micro-controller for measuring cover crops water use. Computers and Electronics in Agriculture, April, 106361. https://doi.org/10.1016/j.compag.2021.106361

Carrijo, D. R., Lundy, M. E., & Linquist, B. A. (2017). Field Crops Research Rice yields and water use under alternate wetting and drying irrigation: A meta-analysis. Field Crops Research, 203, 173–180. https://doi.org/10.1016/j.fcr.2016.12.002

Chahal, G. B. S., Sood, A., Jalota, S. K., Choudhury, B. U., & Sharma, P. K. (2007). Yield, evapotranspiration and water productivity of rice– wheat system in Punjab (India) as influenced by transplanting date of rice and weather parameters. 88, 14–22. https://doi.org/10.1016/j.agwat.2006.08.007

Curcoll, R., Morguí, J., Kamnang, A., Cañas, L., Vargas, A., & Grossi, C. (2022). Metrology for low-cost CO 2 sensors applications: the case of a steady-state through-flow (SS-TF) chamber for CO 2 fluxes observations. 2807–2818.

Dahlmann, A., Hoffmann, M., Verch, G., Schmidt, M., Sommer, M., & Dubbert, M. (2022). Measuring evapotranspiration on an eroded cropland by an automated and mobile chamber system: gap filling strategies and impact of soil type and topsoil removal., Hydrol. Earth Syst. Sci. Discuss. [preprint], https://doi.org/10.5194/hess-2022-323

Deng, Q.Q., Ashraf, U., Cheng, S.R., Sabir, S.R., Mo, Z.W. & Pan, S.G. (2018). Mild drought in interaction with additional nitrogen dose at grain filling stage modulates 2-acetyl-1-pyrrolidine biosynthesis and grain yield in fragerant rice. Appl. Ecol. Env. Res. 16,7741–7758

Detto, M., Verfaillie, J., Anderson, F., Xu, L., & Baldocchi, D. (2011). Agricultural and Forest Meteorology Comparing laser-based open- and closed-path gas analyzers to measure methane fluxes using the eddy covariance method. Agricultural and Forest Meteorology, 151(10), 1312–1324. https://doi.org/10.1016/j.agrformet.2011.05.014

Dill, J., Deichert, G., & Thu, L. N. (2013). Promoting the System of Rice Intensification, Lessons Learned from Trà Vinh Province, Vietnam. Deutsche Gesellschaft für Internationale Zusammenarbeit (GIZ) GmbH publishers, Viet Nam. Pp. 4 -10.

Djaman, K., Mel, V. C., Diop, L., Sow, A., El-Namaky, R., Manneh, B., Saito, K., Futakuchi, K., & Irmak, S. (2018). Effects of alternate wetting and drying irrigation regime and nitrogen fertilizer on yield and nitrogen use efficiency of irrigated rice in the Sahel. Water (Switzerland), 10(6). https://doi.org/10.3390/w10060711

Dong, N.M., Brandt, K.K., Sorensen, J., Hung, N.N., Hach, C.V., Tan, P.S. & Dalsgaard, T. (2012). Effects of alternating wetting and drying versus continuous flooding on fertilizer nitrogen fate in rice fields in the Mekong Delta, Vietnam. Soil Biol. Biochem. 47, 166–174. http://dx.doi.org/10.1016/j.soilbio.2011.12.028.

Dossou-Yovo, E. R., Brüggemann, N., Ampofo, E., Igue, A. M., Jesse, N., Huat, J., & Agbossou, E. K. (2016). Combining no-tillage, rice straw mulch and nitrogen fertilizer application to increase the soil carbon balance of upland rice field in northern Benin. Soil and Tillage Research, 163, 152–159. http://doi:10.1016/j.still.2016.05.019

Dossou-yovo, E. R., Vandamme, E., Dieng, I., & Johnson, J. (2020). Field Crops Research Decomposing rice yield gaps into efficiency, resource, and technology yield gaps in sub-Saharan Africa. Field Crops Research, 258(September), 107963. https://doi.org/10.1016/j.fcr.2020.107963

Drewitt, G. B., Black, T. A., Nesic, Z., Humphreys, E. R, Jork, E. M., Swanson, R., Ethier, G. J., Griffis, T., & Morgenstern, K. (2002). Measuring Forest floor CO_2 fluxes in a Douglasfir forest, Agric. For. Meteorol., 101, 299–317.

El-wahab, A. E., Mahrous, F. N., & Ghanem, S. A. (2007). Irrigation management and splitting of nitrogen application as affected on grain yield and water productivity of hybrid and inbred rice. Journal of Agriculture, Mansoura University. 8(1990): 45–52.

Enrique, A. G., Bruno, C., Christopher, A., Virgile, C., & Stéven, C. (2008). Effects of nitrogen availability on microbial activities, densities and functional diversities involved in the degradation of a Mediterranean evergreen oak litter. Soil Biology and Biochemistry,40(7), 1654–1661

Falagas, M. E., Pitsouni, E. I., Malietzis, G. A., & Pappas, G. (2008). Comparison of PubMed, Scopus, Web of Science, and Google Scholar: strengths and weaknesses. The FASEB Journal, 22(2), 338–342. https://doi.org/10.1096/fj.07-9492lsf

Fageria, N.K., Moreira, A. & Coelho, A.M. (2011). Yield and yield components of upland rice as influenced by nitrogen sources. J. Plant Nutr. 34, 361–370.

Fazli, P., Man, H. C., Shah, U. K., & Idris, A. (2013). Characteristics of Methanogens and Methanotrophs in Rice Fields: A Review.

Fohrer, N., Bormann, H.,Miegel, K., Casper, M., Schumann, A., Bronstert, A., & Weiler, M. (2016) .Hydrologie. 1. Auflage. Stuttgart: UTB GmbH; Haupt (Utb Basics, 4513)

Gao, Y., Wallach, D., Liu, B., Dingkuhn, M., Boote, K. J., Singh, U., Asseng, S., Kahveci, T., He, J., & Zhang, R. (2020). Agricultural and Forest Meteorology Comparison of three calibration methods for modeling rice phenology. Agricultural and Forest Meteorology, 280(September 2019), 107785. https://doi.org/10.1016/j.agrformet.2019.107785

Garnett, T., Conn, V., & Kaiser, B. N. (2009). Root based approaches to improving nitrogen use. 1272–1283. https://doi.org/10.1111/j.1365-3040.2009.02011.x

Gérardeaux, E., Falconnier, G., Gozé, E., Defrance, D., Kouakou, P., Loison, R., Sultan, B., Affholder, F., & Muller, B. (2021). Adapting rainfed rice to climate change: a case study in Senegal.,

Gilmanov, T. G., Wylie, B. K., Tieszen, L. L., Meyers, T. P., Baron, V. S., Bernacchi, C. J., Billesbach, D. P., Burba, G. G., Fischer, M. L., Glenn, A. J., Hanan, N. P., Hatfield, J. L., Heuer, M. W., Hollinger, S. E., Howard, D. M., Matamala, R., Prueger, J. H., Tenuta, M., & Young, D. G. (2013). Agriculture, Ecosystems and Environment CO_2 uptake and Eco physiological parameters of the grain crops of midcontinent North America: Estimates from flux tower measurements. “Agriculture, Ecosystems and Environment,” 164, 162–175. https://doi.org/10.1016/j.agee.2012.09.017

Greaver, T. L., Clark, C. M., Compton, J. E., Vallano, D., Talhelm, A. F., Weaver, C. P., & Band, L. E. (2016). Key ecological responses to nitrogen are altered by climate change. Nature Publishing Group, 6(9), 836–843. https://doi.org/10.1038/nclimate3088

GRISP (2010). Global Rice Science Partnership (GRiSP) full proposal., November, 746.

Hanjra, M. A., & Qureshi, M. E. (2010). Global water crisis and future food security in an era of climate change. Food Policy, 35(5). https://doi.org/10.1016/j.foodpol.2010

Haslwanter, A., Hammerle, A., & Wohlfahrt, G. (2009). Open-path vs. closed-path eddy covariance measurements of the net ecosystem carbon dioxide and water vapor exchange: perspective.149,291–302. https://doi.org/10.1016/j.agrformet.2008.08.011

Hoffmann, M., Jurisch, N., Albiac, E., Hagemann, U., Drösler, M., Sommer, M., & Augustin, J. (2015). Agricultural and Forest Meteorology Automated modeling of ecosystem CO_2 fluxes based on periodic closed chamber measurements: A standardized conceptual and practical approach. Agricultural and Forest Meteorology, 200, 30–45. https://doi.org/10.1016/j.agrformet.2014.09.005

Hoffmann, M., Pehle, N., Huth, V., Jurisch, N., Sommer, M., & Augustin, J. (2017). A simple method to assess the impact of sealing, headspace mixing and pressure vent on airtightness of manually closed chambers. Journal of Plant Nutrition and Soil Science, 181(1), 36–40. https://doi:10.1002/jpln.201600299

Hoogenboom, G., Jones, J.W., Wilkens, P.W., Porter, C.H., Boote, K.J., Hunt, L.A., Singh,U., Lizaso, J.L., White, J.W., Uryasev, O., Royce, F.S., Ogoshi, R., Gijsman, A.J.,& Tsuji,G.Y., (2010). Decision Support System for Agrotechnology Transfer (DSSAT) v. 4.5, vol. 4. Univ. of Hawaii, Honolulu.

Hoogenboom, G., Porter, C.H., Shelia, V., Boote, K.J., Singh, U., White, J.W., Hunt, L.A., Ogoshi, R., Lizaso, J.I., Koo, J., Asseng, S., Singels, A., Moreno, L.P., & Jones, J.W., (2017). Decision Support System for Agrotechnology Transfer (DSSAT) Version 4.7 (www.DSSAT.net). DSSAT Foundation, Gainesville, Florida, USA.

Horwath, W. R. (2011). Greenhouse Gas Emissions from Rice Cropping.

Hutchinson, G.L. & Rochette, P. (2003). Non-Flow-Through Steady-State chamber for measuring soil respiration: Numerical evaluation of their performance. Soil Sci. Soc. Am. J. 67, 166–180

IPCC (2007). Intergovernmental Panel on Climate Change, Fourth Assessment Report, Geneva, Switzerland: Inter-governmental Panel on Climate Change. Cambridge; UK: Cambridge University Press; 2007. Available from: www. ipcc.ch. In Intergovernmental Panel on Climate Change. https://doi. org/ 10. 1038/ 44672 7a

IPCC (2013). Climate change 2013: the physical science basis. Contribution of working group I to the fifth assessment report of the intergovernmental panel on climate change. Cambridge University Press, Cambridge, United Kingdom and New York, NY, USA

IPCC (2014). Climate Change 2014: Mitigation of Climate Change. Summary for Policymakers and Technical Summary. In Climate Change 2014: Mitigation of Climate Change. Part of the Working Group III Contribution to the Fifth Assessment Report of the Intergovernmental Panel on Climate Change. https://doi.org/10.1017/CBO9781107415416.005

Iqbal, J., Hu, R., Lin, S., Hatano, R., Feng, M., Lu, L., Ahamadou, B., & Du, L. (2009). Agriculture, Ecosystems and Environment CO_2 emission in a subtropical red paddy soil (Ultisol) as affected by straw and N-fertilizer applications: A case study in Southern China. 131, 292–302. https://doi.org/10.1016/j.agee.2009.02.001

Islam, S. F., de Neergaard, A., Sander, B. O., Jensen, L. S., Wassmann, R., & van Groenigen, J. W. (2020). Reducing greenhouse gas emissions and grain arsenic and lead levels without compromising yield in organically produced rice. Agriculture, Ecosystems and Environment, 295(January), 106922. https://doi.org/10.1016/j.agee.2020.106922

Islam, S. & Hasan, A. (2021). Determination of Upland Rice Cultivar Coefficient Specific Parameters for DSSAT (Version 4.7)-CERES-Rice Crop Simulation Model and Evaluation of the Crop Model under Different Temperature Treatments conditions. American Journal of Plant Sciences, 12, 782-795. https://doi: 10.4236/ajps.2021.125054.

Jahan, M. S., Nozulaidi, M. B. N., Moneruzzaman, M. K., Ainun, A., and Husna, N. (2014). Control of plant growth and water loss by a lack of light-harvesting complexes in photosystem-II in Arabidopsis thaliana ch1-1 mutant. Acta Physiol. Plant. 36, 1627–1635. https://doi: 10.1007/s11738-014-1538-4

Jain, N., Pathak, H., Mitra, S., & Bhatia, A. (2004). Emission of methane from rice fields -. 63(February), 101–115.

Jha, P. K., Athanasiadis, P., Gualdi, S., Trabucco, A., Mereu, V., Shelia, V., Hoogenboom, G., Sui, C. E., & Climatici, C. (2019). Agricultural and Forest Meteorology Using daily data from seasonal forecasts in dynamic crop models for yield prediction: A case study for rice in Nepal' s Terai. Agricultural and Forest Meteorology, 265(November 2018), 349–358. https://doi.org/10.1016/j.agrformet.2018.11.029

Jiang, L., Dai, T., Jiang, D., & Cao, W. (2004). Characterizing physiological N-use efficiency as influenced by nitrogen management in three rice cultivars. 88, 239–250. https://doi.org/10.1016/j.fcr.2004.01.023

Jones, J. W., Hoogenboom, G., Porter, C. H., Boote, K. J., Batchelor, W. D., Hunt, L. A., Wilkens, P. W., Singh, U., Gijsman, A. J., & Ritchie, J. T. (2003). The DSSAT cropping system model (Vol. 18).

Kadiyala, M. D. M., Jones, J. W., Mylavarapu, R. S., Li, Y. C., & Reddy, M. D. (2015). Identifying irrigation and nitrogen best management practices for aerobic rice – maize cropping system for semi-arid tropics using CERES-rice and maize models. 149, 23–32. https://doi.org/10.1016/j.agwat.2014.10.019

Keimel, A. (2019). Comparison of Low-Cost CO 2 Non-Dispersive Infrared (NDIR) Sensors for Ambient Greenhouse Gas Monitoring.

Khairi, M., Nozulaidi, M., Afifah, A., & Jahan, S. (2015). Effect of various water regimes on rice production in lowland irrigation Effect of various water regimes on rice production in lowland irrigation.

Khalil, M. A. K., Rasmussen, R. A., Shearer, M. J., Yao, H., & Yang, J. (1998). trace gases from rice fields in China. 103.

Kim, D., Thomas, A. D., Pelster, D., & Rosenstock, T. S. (2015). Reviews and syntheses: Greenhouse gas emissions in natural and agricultural lands in sub-Saharan Africa: synthesis of available data and suggestions for further studies. 16479–16526. https://doi.org/10.5194/bgd-12-16479-2015

Kim, G.W., Jeong, S.T., Kim, P.J., & Gwon, H.S. (2017). Influence of nitrogen fertilization on the net ecosystem carbon budget in a temperate mono-rice paddy. Geoderma, 306, 58–66.

Kimura, M., Murase, J., & Lu, Y. (2004). Carbon cycling in rice field ecosystems in the context of input, decomposition and translocation of organic materials and the fates of their end products. 36, 1399–1416. https://doi.org/10.1016/j.soilbio.2004.03.006

Komiya, S., Noborio, K., Katano, K., Pakoktom, T., Siangliw, M., & Toojinda, T. (2015). Contribution of Ebullition to Methane and Carbon Dioxide Emission from Water between Plant Rows in a Tropical Rice Paddy Field. 2015.

Kutzbach, L., Wille, C., & Pfeiffer, M. (2007).: The exchange of carbon dioxide between wet arctic tundra and the atmosphere at the Lena River Delta, Northern Siberia. Bio geosciences, 4, 869-890.

Lampayan, R. M., Rejesus, R. M., Singleton, G. R., & Bouman, B. A. M. (2015). Adoption and economics of alternate wetting and drying water management for irrigated lowland rice. Field Crops Research, 170, 95–108, https://doi:10.1016/j.fcr.2014.10.013

Le Mer, J. & Roger, P. (2001).: Production, Oxidation, Emission and Consumption of Methane by Soils: A Review. European Journal of Soil Biology, 37, 25-50. http://dx.doi.org/10.1016/S1164-5563(01)01067-6

Leiber-Sauheitl, K.., Fuß, R.., Voigt, C., & Freibauer, A. (2014). High CO_2 fluxes from grassland on histic Gleysol along soil carbon and drainage gradients, Biogeosciences, 11, 749–761, https://doi.org/10.5194/bg-11-749-2014.

Li, C., Kou, Z., Yang, J., Cai, M., Wang, J., & Cao, C. (2010). Soil CO 2 fluxes from direct seeding rice fields under two tillage practices in central China. Atmospheric Environment, 44(23), 2696–2704. https://doi.org/10.1016/j.atmosenv.2010.04.045

Li, T., Nie, T., Chen, P., Zhang, Z., Lan, J., Zhang, Z., Qi, Z., Han, Y., & Jiang, L. (2022). Carbon Budget of Paddy Fields after Implementing Water-Saving Irrigation in Northeast China. Ci, 1–14.

Liang, K., Zhong, X., Huang, N., Lampayan, R. M., Pan, J., Tian, K., & Liu, Y. (2016). Grain yield, water productivity and CH_4 emission of irrigated rice in response to water management in south China. Agricultural Water Management, 163, 319–331. https://doi.org/10.1016/j.agwat.2015.10.015

Linquist, B. A., Adviento-Borbe, M. A., Pittelkow, C. M., van Kessel, C., & van Groenigen, K. J. (2012). Fertilizer management practices and greenhouse gas emissions from rice systems: A quantitative review and analysis. In Field Crops Research (Vol. 135, pp. 10–21). Elsevier. https://doi.org/10.1016/j.fcr.2012.06.007

Liou, R. (2003). Methane emission from fields with differences in nitrogen fertilizers and rice varieties in Taiwan paddy soils. 50, 237–246.

Liu, G., & Si, B. C. (2009). Multi-layer diffusion model and error analysis applied to chamber-based gas fluxes measurements §. 149, 169–178. https://doi.org/10.1016/j.agrformet.2008.07.012

Liu, L., Chen, T., Wang, Z., Zhang, H., Yang, J., & Zhang, J. (2013). Field Crops Research Combination of site-specific nitrogen management and alternate wetting and drying irrigation increases grain yield and nitrogen and water use efficiency in super rice. Field Crops Research, 154, 226–235. https://doi.org/10.1016/j.fcr.2013.08.016

Liu, Y., Wan, K., Tao, Y., Li, Z., Zhang, G., Li, S., & Chen, F. (2013). Carbon Dioxide Flux from Rice Paddy Soils in Central China: Effects of Intermittent Flooding and Draining Cycles. 8(2). https://doi.org/10.1371/journal.,pone.0056562

Livingston, G.P., & Hutchinson, G.L. (1995). Enclosure-based measurement of trace gas exchange: applications and sources of error, In Matson, P.A., Harris, R.C. (Eds.), Methods in Ecology. Biogenic Trace Gases: Measuring Emissions from Soil and Water, Blackwell Sci, New York, pp. 14–51.

Lu, X., Wang, H., Xiang, Y., Wang, Q., Su, T., Gong, R., Zhang, H., Zhu, L., Li, E., & Abdelghany, A. E. (2022). Determination of Nitrogen Application Ratio and Sowing Time for Improving the Future Yield of Double-Harvest Rice in Nanchang Based on the DSSAT-CERES-Rice Model.

Ma, K. E., Qiu, Q., & Lu, Y. (2010). Microbial mechanism for rice variety control on methane emission from rice field soil. Global Change Biology, 16(11), 3085–3095. https://doi.org/10.1111/j.1365-2486.2009.02145.

Maeck, A., Hofmann, H., & Lorke, A. (2014). Pumping methane out of aquatic sediments – ebullition forcing mechanisms in an impounded river. 1, 2925–2938. https://doi.org/10.5194/bg-11-2925-2014

Mafakheri, A., Siosemardeh, A., Bahramnejad, B., Struik, P. C., & Sohrabi, Y. (2010). Effect of drought stress on yield, proline and chlorophyll contents in three chickpea cultivars. 4(8), 580–585.

Mannan, M. A., Bhuiya, M. S. U., Akhand, M. I. M., & Zaman, M. M. (2012). Growth and Yield of Basmati and Traditional Aromatic Rice as Influenced by Water Stress and Nitrogen Level. 10(2), 52–62.

Martin, C. R., Zeng, N., Karion, A., Dickerson, R. R., Ren, X., Turpie, B. N., & Weber, K. J. (2017). Evaluation and environmental correction of ambient CO_2 measurements from a low-cost NDIR sensor. 2383–2395.

Mboyerwa,P.A., Kibret, K., Mtakwa P., & Aschalew A. (2022).Lowering nitrogen rates under the system of rice intensification enhanced rice productivity and nitrogen use efficiency in irrigated lowland rice. Heliyon.8(3): e09140.

Min, S., & Rulík, M. (2020). Comparison of carbon dioxide (CO_2) fluxes between conventional and conserved irrigated rice paddy fields in Myanmar. Sustainability (Switzerland), 12(14), 1–19. https://doi.org/10.3390/su12145798

Miyata, A, Iwata, T., Yamada, T., Yoshikoshi, H., Mano, M., Harazono, Y., Ohtaki, E., Baten, M. A., Inohara, S., Takimoto, T., & Saito, M. (2005). Seasonal Variation of Carbon Dioxide and Methane Fluxes at Single Cropping Paddy Fields in Central and Western Japan. 45.

Miyata, Akira, Leuning, R., Thomas, O., Kim, J., & Harazono, Y. (2000). Carbon dioxide and methane fluxes from an intermittently flooded paddy field. 102, 287–303.

Moldrop P, Olesen T, Yamaguchi T, Schonning P, Rolaton DE (1999). Modeling diffusion and relation in soils IX. The Buckingham-Burdine-Campbell equation for gas diffusivity in undisturbed soil. Soil Sci. 164, 542–551

Moratiel, R. (2013). Evapotranspiration and crop coefficients of rice (Oryza sativa L.) under sprinkler irrigation in a semiarid climate determined by the surface renewal method. 411–422. https://doi.org/10.1007/s00271-011-0319-8

Moyano, F. E., Manzoni, S., & Chenu, C. (2013). Soil Biology & Biochemistry Responses of soil heterotrophic respiration to moisture availability: An exploration of processes and models Soil Moisture Organic Matter. Soil Biology and Biochemistry, 59, 72–85. https://doi.org/10.1016/j.soilbio.2013.01.002

Myklebust, M. C., Hipps, L. E., & Ryel, R. J. (2008). Comparison of eddy covariance, chamber, and gradient methods of measuring soil CO 2 efflux in an annual semi-arid grass. https://doi.org/10.1016/j.agrformet.2008.06.016

Nishimura, S., Yonemura, S., Minamikawa, K., & Yagi, K. (2014). Seasonal and diurnal variations in net carbon dioxide flux throughout the year from soil in paddy field. https://doi.org/10.1002/2014JG002746.

Nishimura, S., Yonemura, S., Sawamoto, T., Shirato, Y., Akiyama, H., Sudo, S., & Yagi, K. (2008). Effect of land use change from paddy rice cultivation to upland crop cultivation on soil carbon budget of a cropland in Japan. 125, 9–20. https://doi.org/10.1016/j.agee.2007.11.003

Nyambo, P., Cornelius, C., & Araya, T. (2020). Carbon Dioxide Fluxes and Carbon Stocks under Conservation agricultural practices in south Africa.

Nyang, W. O., Mati, B.M., Kalamwa, K., Wanjogu, R. K. & Kiplagat, L.K. (2014). Estimating rice yield under changing weather conditions in Kenya using CERES-rice model, International Journal of Agronomy, 1-12.

Oliver, V., Cochrane, N., Magnusson, J., Brachi, E., Volante, A., Courtois, B., Vale, G., Price, A., & Arn, Y. (2019). Science of the Total Environment Effects of water management and cultivar on carbon dynamics, plant productivity and biomass allocation in European rice systems. Science of the Total Environment, 685, 1139–1151. https://doi.org/10.1016/j.scitotenv.2019.06.110

Pakoktom, T., Aoki, M., Kasemsap, P., Boonyawat, S., & Attarod, P., (2009). CO_2 and H_2O fluxes ratio in paddy fields of Thailand and Japan. Hydrological Research Letters 3, 10–13. https://doi.org/10.3178/hrl.3.10.

Pan, J., Liu, Y., Zhong, X., Lampayan, R. M., Singleton, G. R., Huang, N., Liang, K., Peng, B., & Tian, K. (2017). Grain yield, water productivity and nitrogen use efficiency of rice under different water management and fertilizer-N inputs in South China. Agricultural Water Management, 184, 191–200. https://doi.org/10.1016/j.agwat.2017.01.013

Pandey, S. K., Kim, K., & Lee, S. (2007). Use of a Dynamic Enclosure Approach to Test the Accuracy of the NDIR Sensor: Evaluation Based on the CO_2 Equilibration Pattern. 3459–3471.

Patel, N. R., Dadhwal, V. K., & Saha, S. K. (2011). Measurement and Scaling of Carbon Dioxide Exchanges in Wheat Using Flux-Tower and Remote Sensing. 39(September), 383–391. https://doi.org/10.1007/s12524-011-0107-1

Peng, S., Hou, H., & Xu, J. (2011). Nitrous oxide emissions from paddy fields under different water managements in southeast China. 403–411. https://doi.org/10.1007/s10333-011-0275-1

Qi, L., Niu, H., Zhou, P., Jia, R., & Gao, M. (2018). Effects of Biochar on the Net Greenhouse Gas Emissions under Continuous Flooding and Water-Saving Irrigation Conditions in Paddy Soils. 16–18. https://doi.org/10.3390/su10051403

Quansah, E., Mauder, M., Balogun, A. A., Amekudzi, L. K., Hingerl, L., Bliefernicht, J., & Kunstmann, H. (2015). Carbon dioxide fluxes from contrasting ecosystems in the Sudanian Savanna in West Africa. 1–17. https://doi.org/10.1186/s13021-014-0011-4

Reddy, K.R. & Delaune, R.D. (2008). Biogeochemistry of Wetlands: Science and Applications. CRC Press, Boca Raton. http://dx.doi.org/10.1201/9780203491454

Ren, X., Wang, Q., Tong, C., Wu, J., Wang, K., Zhu, Y., Lin, Z., Watanabe, M. & Tang, G. (2007). Estimation of soil respiration in a paddy ecosystem in the subtropical region of China. Chinese Sci. Bull., 52, 2722–2730.

Rezaei, M., Vahed, H. S., Amiri, E., Motamed, M. K., & Azarpour, E. (2009). The Effects of Irrigation and Nitrogen Management on Yield and Water Productivity of Rice. World Applied Sciences Journal., 7(2): 203–210.

Richards, M. and Sander, B. O. (2014). Alternate wetting and drying in irrigated rice Implementation guidance for policymakers and investors. [https://cgspace.cgiar.org/rest/bitstreams/34363/retrieve] site visited on 24 Janv 2022.

Rothfuss, Y., Quade, M., Brüggemann, Nicolas., Graf, A., Vereecken, H., & Dubbert, M. (2021). Reviews and syntheses: Gaining insights into evapotranspiration partitioning with novel isotopic monitoring methods. In Biogeosciences 18 (12), pp. 3701–3732. https://doi: 10.5194/bg-18-3701-2021.

Sabbour M.M., & ShSI W. (2007). Efficiency of some bioinsecticides against broad bean beetle, Bruchus rufimanus (Coleoptera Bruchidae). Research Journal of Agriculture and Biological Science, 3(2): 67-72

Saidou, A., Gnakpenou, K., Balogoun I., Hounnahin S. R., Kindomihou M. V., (2014). Effet de l'urée et du NPK 15-15-15 perlés et super granulés sur la productivité des variétés de riz IR841 et NERICA-L14 en zone de bas-fond au Sud-Bénin, Journal of Applied Biosciences 77 :6575 – 6589. http://dx.doi.org/10.4314/jab.v77i1.13

Saito, M., Miyata, A., Nagai, H., & Yamada, T. (2005). Seasonal variation of carbon dioxide exchange in rice paddy field in Japan. 135, 93–109. https://doi.org/10.1016/j.agrformet.2005.10.007

Seck, P. A., & Diagne, A. (2012). Crops that feed the world 7: Rice. 7–24. https://doi.org/10.1007/s12571-012-0168-1

Seck, P.A., Touré, A.A., Coulibaly, J., Diagne, A., & Wopereis, M.C.S. (2013). Africa's rice economy before and after the 2008 rice crisis. In: Wopereis, M.C.S., Johnson, D. E., Ahmadi, N., Tollens, E., Jalloh, A. (Eds.), Realizing Africa's Rice Promise. CAB International, Wallingford, UK, pp. 24–34

Shpilyov, A. V., Vladislav, V. Z., Bernhard, G., & Lokstein, H. (2013). Chlorophyll a phytylation is required for the stability of photosystems I and II in the cyanobacterium Synechocystis PCC 6803. The Plant Journal 73:336-346.

Sintondji, O.L., Atidégla,S., Ayédéhin, A., Ahouansou, M. & Agbossou, K.E. (2017) . Characterization of irrigation techniques and typology of vegetable gardens in the districts of Covè and Zangnanado in center of Benin." International Journal of Engineering Research and Applications (IJERA), vol. 7, no. 10, pp. 40–51.

Smith, P., Martino, D., Cai, Z., Gwary, D., Janzen, H., Kumar, P., Mccarl, B., Ogle, S., Mara, F. O., Rice, C., Scholes, B. & Towprayoon, S. (2007). Policy and technological constraints to implementation of greenhouse gas mitigation options in agriculture. 118, 6–28. https://doi.org/10.1016/j.agee.2006.06.006

Soussana, J. F., Tallec, T., & Blanfort, V. (2009). Mitigating the greenhouse gas balance of ruminant production systems through carbon sequestration in grasslands. Animal, 4(03), 334–350. https://doi:10.1017/s1751731109990784

Sossa, C.L.G., Sanogo, S., Naab, J. B., & Sintondji, L. O. (2022). Trends and research features on greenhouse gas emissions from rice production: review based on bibliometric analysis. Environmental Science and Pollution Research. https://doi.org/10.1007/s11356-022-22921-0

Steduto, P., Hsiao, T.C., Fereres, E., &Raes, D. (2012). Crop yield response to water. FAO Irrigation and Drainage Paper No. 66. FAO: Rome. http:// www.fao.org/nr/water

Sun, Y., Ma, J., Sun, Y., Xu, H., Yang, Z., Liu, S., & Jia, X. (2012). Field Crops Research The effects of different water and nitrogen managements on yield and nitrogen use efficiency in hybrid rice of China. Field Crops Research, 127, 85–98. https://doi.org/10.1016/j.fcr.2011.11.015

Swain, C. K., Bhattacharyya, P., Singh, N. R., Neogi, S., Sahoo, R. K., Nayak, A. K., Zhang, G., & Leclerc, M. Y. (2016). Net ecosystem methane and carbon dioxide exchange in relation to heat and carbon balance in lowland tropical rice. Ecological Engineering, 95, 364–374. https://doi.org/10.1016/j.ecoleng.2016.06.053

Sys, C., Van Ranst, E., Debaveye, J., & Beernaert, F. (1993). Land Evaluation. Part III: crop requirements. Agricultural Publications n° 7, G.A.D.C., Brussels, Belgium, 1993, 191 p.

Tabbal, D. F., Bouman, B. A. M., & Bhuiyan, S. I. (2002). On-farm strategies for reducing water input in irrigated rice; case studies in the Philippines. 56, 93–112.

Tadesse, T. F., Nigussie, D. R., Wondimu, B., & Setegn, G. (2013). Impact of rainwater management on growth and yield of rainfed lowland rice. Wudpecker Journal of Agricultural Research, 2, 108–114.

Tan, X., Shao, D., & Liu, H. (2013). Effects of alternate wetting and drying irrigation on percolation and nitrogen leaching in paddy fields. 381–395. https://doi.org/10.1007/s10333-012-0328-0

Tang, J., Liang, S., Li, Z., Zhang, H., Wang, S., & Zhang, N. (2016). Emission Laws and Influence Factors of Greenhouse Gases in Saline-Alkali Paddy Fields. https://doi.org/10.3390/su8020163

Thakur, A. K., & Rath, S. (2013). Differential responses of system of rice intensification (SRI) and conventional flooded-rice management methods to applications of nitrogen fertilizer. https://doi.org/10.1007/s11104-013-1612-5

Tizon-Salazar, B.U., Cruz, P.C.S., Salazar, B.M., Aguilar, E.A. & Badayos, R.B. (2015). Grain-filling process in lowland rice (Oryza sativa L. 'PSB Rc18') under water deficit is enhanced by nitrogen fertilization. Asia Life Sci. 24, 715–725.

Trajkovic, S. (2009). Comparison of radial basis function networks and empirical equations for converting from pan evaporation to reference evapotranspiration. 880(January), 874–880. https://doi.org/10.1002/hyp

Tuong, P., Bouman, B. A. M., Mortimer, M., Bouman, B. A. M., Mortimer, M., Rice, M., Tuong, T. P., Bouman, B. A. M., & Mortimer, M. (2015). More Rice, Less Water Integrated Approaches for Increasing Water Productivity in Irrigated Rice- Based Systems in Asia More Rice, Less Water — Integrated Approaches for Increasing Water Productivity in Irrigated Rice-Based Systems in Asia. 1008. https://doi.org/10.1626/pps.8.231

Uphoff, N., Bouman, B. A. M. & Mortimer, M. (2015). The System of Rice Intensification (SRI) as a System of Agricultural Innovation. 1–18.

Vatananan-Thesenvitz, R., Schaller, A. A., & Shannon, R. (2019). A bibliometric review of the knowledge base for innovation in sustainable development. Sustainability (Switzerland), 11(20), 1–22. https://doi.org/10.3390/su11205783

Wang, Z.Q., Zhang, W.Y., Beebout, S.S., Zhang, H., Liu, L.J., Yang, J.C. & Zhang, J.H., (2016). Grain yield, water and nitrogen use efficiencies of rice as influenced by irrigation.

Wang, C., Lai, D. Y. F., Sardans, J., Wang, W., Zeng, C., & Pe, J. (2017). Factors Related with CH 4 and N 2 O Emissions from a Paddy Field: Clues for Management implications. 1–23. https://doi.org/10.1371/journal.,pone.0169254

Wang, K., Liu, C., Zheng, X., Pihlatie, M., Li, B., Haapanala, S., Vesala, T., Liu, H., Wang, Y., Liu, G., & Hu, F. (2013). Comparison between eddy covariance and automatic chamber techniques for measuring net ecosystem exchange of carbon dioxide in cotton and wheat fields. 6865–6877. https://doi.org/10.5194/bg-10-6865-2013

Wang, R., Hu, Y., Wang, Y., Ali, S., Liu, Q., & Guo, S. (2019). Nitrogen application increases soil respiration but decreases temperature sensitivity: Combined effects of crop and soil properties in a semiarid agroecosystem. Geoderma, 353, 320–330. https://doi:10.1016/j.geoderma.2019.07.019

Wassmann, R., Hosen, Y., & Sumfleth, K. (2009). Reducing Methane Emissions from Irrigated Rice. International Food Policy Research Institute

Wastine, B., Hummelgård, C., Bryzgalov, M., Rödjegård, H., Martin, H., & Schröder, S. (2022). Compact Non-Dispersive Infrared Multi-Gas Sensing Platform for Large Scale Deployment with Sub-ppm Resolution.

Webb, E. K., Pearman, G. I., & Leuning, R. (1980). Correction of flux measurements for density effects due to heat and water vapour transfer, Quarterly Journal of the Royal Meteorological Society, 106(447), 85–100, https://doi.org/10.1002/qj.49710644707

Wild, J., Kopecký, M., Macek, M., Šanda, M., Jankovec, J., & Haase, T. (2019). Climate at ecologically relevant scales: A new temperature and soil moisture logger for long-term microclimate measurement. Agricultural and Forest Meteorology, 268, 40–47. https://doi:10.1016/j.agrformet.2018.12.018

Wik, M., Crill, P. M., Varner, R. K., & Bastviken, D. (2013). Multiyear measurements of ebullitive methane flux from three subarctic lakes. 118(July), 1307–1321. https://doi.org/10.1002/jgrg.20103

Willmott, C.J., Ackleson, S.G., Davis, R.E., Feddema, J.J., Klink, K.M., Legates, D.R.,O'Connell, J., & Rowe, C.M. (1985). Statistics for the evaluation and comparison ofmodels. J. Geophys. Res. 90, 8995–9005.

Wohlfahrt, G., & Gu, L. (2015). The many meanings of gross photosynthesis and their implication for photosynthesis research from leaf to globe. Plant, Cell & Environment, 38(12), 2500–2507. https://doi:10.1111/pce.12569

Xu, Y., Gu, D., Li, K., Zhang, W., Zhang, H., Wang, Z., & Yang, J. (2019). Response of Grain Quality to Alternate Wetting and Moderate Soil Drying Irrigation in Rice. 1272(june), 1261–1272. https://doi.org/10.2135/cropsci2018.11.0700

Xue, L.H., Yang, L.Z., Shi, W.M., & Wang, S.Q. (2013). Reduce–Retain–Reuse–Restore technology for controlling the agricultural non-point pollution in countryside in China: source reduction technology. J. Agro-Environ. Sci. 32 (5), 881–888 (In Chinese with English abstract).

Yakubu, A., Ofori, J., Amoatey, C., & Kadyampakeni, D. M. (2019). Agronomic, Water Productivity and Economic Analysis of Irrigated Rice under Different Nitrogen and Water Management Methods. 92–109. https://doi.org/10.4236/as.2019.101008

Yan, X., Ohara, T., & Akimoto, H. (2003). Development of region-specific emission factors and estimation of methane emission from rice fields in the East, Southeast and South Asian countries. Global Change Biology, 9(2), 237–254. https://doi.org/10.1046/j.1365-2486.2003.00564.x

Yang, C., Du, Y., & Zhang, J. (2012). Technologies to Improve Water Management for Rice Cultivation to Cope with Climate Change. 193–207.

Yang, J.M., Yang, J.Y., Liu, S., & Hoogenboom, G., (2014). An evaluation of the statistical methods for testing the performance of crop models with observed data. Agric. Syst. 127, 81–89. http://dx.doi.org/10.1016/j.agsy.2014.01.008.

Yang, J., Liu, K., Wang, Z., Du, Y., & Zhang, J. (2007). Water-Saving and High-Yielding Irrigation for Lowland Rice by Controlling Limiting Values of Soil Water Potential., 49(10), 1445–1454. https://doi.org/10.1111/j.1672-9072.2007.00555.x

Yang, J., & Zhang, J. (2016). by irrigation regimes and their interaction with nitrogen rates. Field Crops Research. https://doi.org/10.1016/j.fcr.2016.03.006

Yang, J., Zhou, Q., & Zhang, J. (2016). ScienceDirect Moderate wetting and drying increases rice yield and reduces water use, grain arsenic level, and methane emission. CJ. https://doi.org/10.1016/j.cj.2016.06.002

Yang, S., Liu, X., Liu, X., & Xu, J. (2017). Effect of water management on soil respiration and NEE of paddy fields in Southeast China. Paddy and Water Environment. https://doi.org/10.1007/s10333-017-0591-1

Yao, F., Huang, J., Cui, K., Nie, L., Xiang, J., Liu, X., & Wu, W. (2012). Field Crops Research Agronomic performance of high-yielding rice variety grown under alternate wetting and drying irrigation. Field Crops Research, 126, 16–22. https://doi.org/10.1016/j.fcr.2011.09.018

Yasuda, T. (2012). Comparison of the Characteristics of Small Commercial NDIR. 3641–3655. https://doi.org/10.3390/s120303641

Ye, Q., Yang, X., Dai, S., & Chen, G. (2015). Effects of climate change on suitable rice cropping areas, cropping systems and crop water requirements in southern China. Agricultural Water Management, 159, 35–44. https://doi.org/10.1016/j.agwat.2015.05.022

Youssouf I. & Lawani M. (2000). Les sols béninois : Classification dans la Base de Reference mondiale : 29-50. In : FAO (eds), Rapport sur les ressources en sols du monde, Quatorzième réunion du souscomité Ouest et Centre africain de corrélation des sols pour la mise en valeur des terres.

Yoshida, S. (1981). Fundamentals of crop science. The Rice Research Institute, 268, 22–23

Zare, N., Khaledian, M., Pirmoradian, N., & Rezaei, M. (2014). Simulation of rice yield under different irrigation and nitrogen application managements by CropSyst model. Acta Agriculturae Slovenica, 103(2), 181–190. https://doi:10.14720/aas.2014.103.2.3

Zhang, H., Xue, Y., Wang, Z., Yang, J., & Zhang, J. (2009). An Alternate Wetting and Moderate Soil Drying Regime Improves Root and Shoot Growth in Rice. December. https://doi.org/10.2135/cropsci2009.02.0099

Zhang, H., Zhang, S., Yang, J., Zhang, J., & Wang, Z. (2008). Postanthesis Moderate Wetting Drying Improves Both Quality and Quantity of Rice Yield. 726–734. https://doi.org/10.2134/agronj2007.0169

Zhang, J. K., Cheng, M. T., Ji, D. S., Liu, Z. R., Hu, B., Sun, Y., & Wang, Y. S. (2016). Characterization of submicron particles during biomass burning and coal combustion periods in Beijing, China. Science of The Total Environment, 562, 812–821. https://doi:10.1016/j.scitotenv.2016.04.015

Zhang, J., Miao, Y., Batchelor, W. D., Lu, J., & Wang, H. (2018). Improving High-Latitude Rice Nitrogen Management with the CERES-Rice Crop Model. 1–14. https://doi.org/10.3390/agronomy8110263

Zhang, W., Yu, J., Xu, Y., Wang, Z., Liu, L., & Zhang, H. (2021). Field Crops Research Alternate wetting and drying irrigation combined with the proportion of polymer-coated urea and conventional urea rates increases grain yield, water and nitrogen use efficiencies in rice. Field Crops Research, 268(April), 108165. https://doi.org/10.1016/j.fcr.2021.108165

Zhao, Q.M., Li, X.L. (1993). Effects of temperature and light on crop yield. Terr. Nat.Resour. Stud. 1, 44–47 (In Chinese with English abstract).

Zhao, C., Chen, M., Li, X., Dai, Q., Xu, K., Guo, B., Hu, Y., Wang, W., & Huo, Z. (2021). Effects of Soil Types and Irrigation Modes on Rice Root Morphophysiological Traits and Grain Quality.

Zheng, H., Huang, H., Yao, L., Liu, J., He, H., & Tang, J. (2014). Impacts of rice varieties and management on yield-scaled greenhouse gas emissions from rice fields in China: A meta-analysis. Bio geosciences, 11(13), 3685–3693. https://doi.org/10.5194/bg-11-3685-2014

Zhou, Lijie, Liang, S., Ponce, K., Marundon, S., Ye, G., & Zhao, X. (2015). Field Crops Research Factors affecting head rice yield and chalkiness in indica rice. Field Crops Research, 172, 1–10. https://doi.org/10.1016/j.fcr.2014.12.004

Zhou, Lingyan, Zhou, X., Shao, J., & Nie, Y. (2016). Interactive effects of global change factors on soil respiration and its components: a meta-analysis. 1–13. https://doi.org/10.1111/gcb.13253

Zou, J., Huang, Y., Jiang, J., Zheng, X., & Sass, R. L. (2005). A 3-year field measurement of methane and nitrous oxide emissions from rice paddies in China: Effects of water regime, crop residue, and fertilizer application. Global Biogeochemical Cycles, 19(2), 1–9. https://doi.org/10.1029/2004GB002401

Zou, J., Huang, Y., Zheng, X., & Wang, Y. (2007). Quantifying direct N_2O emissions in paddy fields during rice growing season in mainland China: Dependence on water regime. 41, 8030–8042. https://doi.org/10.1016/j.atmosenv.2007.06.049

ANNEXES

ANNEXE 1: List of the conferences

Oral presentation

- Effect of N fertilizer amount and water management on CO_2 exchange and water productivity of rice cultivation in Southern Benin, World PhD Climate Change Students Summit 2022, University of Hamburg, Germany, March 10,2022.

- Effect of N fertilizer amount and water management on CO_2 exchange and Net Ecosystem C balance of rice cultivation in Southern Benin, The European Geosciences Union (EGU) General Assembly 2022, Vienna, Austria, May 24, 2022.

- Moderate N fertilizer inputs under proper water management enhance irrigated rice production in southern Benin, International Scientific Colloquium of the National University of Agriculture of Kétou, Benin, November 28,2022

Poster presentation

Effect of N fertilizer amount and water management on CO_2 exchange and net ecosystem C balance of rice cultivation in Southern Benin, Tropentag 2022, Czech University of Life Sciences, Prague, September 16, 2022

ANNEXE 2: the developed script for the low-cost device

```
#include "cactus_io_DHT22.h"
#include <DallasTemperature.h>
#include <Adafruit_Sensor.h>  // include Adafruit sensor library
#include <Adafruit_BMP280.h>  // include adafruit library for BMP280 sensor
#include <SD.h>
#include <SPI.h>
#include "RTClib.h"
#include <Wire.h>
#include <OneWire.h>
#include <LiquidCrystal_I2C.h>
//#include <Adafruit_SCD30.h>
#include "kSeries.h" //include kSeries Library

//Constants
#define DHTPIN 5     // what pin we're connected to
//#define DHTTYPE DHT22   // DHT 22  (AM2302)
#define ONE_WIRE_BUS 2
#define BMP280_I2C_ADDRESS  0x76

kSeries K_30(6,7); //Initialize a kSeries Sensor with pin 12 as Rx and 13 as Tx
Adafruit_BMP280 bmp280;
//Adafruit_SCD30  scd30;
DHT22 dht(DHTPIN); //// Initialize DHT sensor for normal 16mhz Arduino
OneWire oneWire(ONE_WIRE_BUS);
DallasTemperature sensors(&oneWire);
RTC_DS1307 rtc;
LiquidCrystal_I2C lcd(0x27, 16, 2);

const int chipSelect = 10; //10 is default by shield, but normally on Pin 4
int interval = 5;  //Log to SD Card every 5 seconds
int chk;
float air_temp_BMP280;
float pressure;
float altitude;
float ppm_final;
float air_temp_DHT;
float hum_DHT;
//byte cmd[9] = {0xFF,0x01,0x86,0x00,0x00,0x00,0x00,0x00,0x79};
//unsigned char response[9];
long timer;
String timestring;

void setup() {
  Serial.,begin(9600);
  dht.begin();
  rtc.begin();
  bmp280.begin(BMP280_I2C_ADDRESS);
  lcd.init();      // initialize the lcd
  lcd.backlight();  //lcd.setCursor(0, 0);
  lcd.print("MonksHillLab");
```

```
//Serial.,println("Initializing SD card...");
  if (!SD.begin(chipSelect)) {
    Serial.,println("SD Card error");
    return;
  }
  Serial.,println("card initialized");
  if (! rtc.begin()) {
    Serial.,println("No RTC found");
  } else {
    Serial.,println("RTC clock found");
  }
  if (! rtc.isrunning()) {
    Serial.,println("RTC is not configured");
    }

}

void loop(){

  DateTime now = rtc.now();
  timestring = now.day();
  timestring += "-";
  timestring += now.month();
  timestring += "-";
  timestring += now.year();
  timestring += " ";
  timestring += now.hour();
  timestring += ":";
  timestring += now.minute();
  timestring += ":";
  timestring += now.second();
  Serial.,print(timestring);
  Serial.,print(",");

  air_temp_BMP280 = bmp280.readTemperature();  // get temperature
  pressure    = bmp280.readPressure();     // get pressure

  if (isnan(dht.humidity)|| isnan(dht.temperature_C)) {
  Serial.,println("DHT sensor read failure!");
  return;
  }

  dht.readHumidity();
  dht.readTemperature();

  double co2 = K_30.getCO2('p'); //returns co2 value in ppm ('p') or percent ('%')
  Serial.,print(co2); //print value
  delay(2000);

  //sensors.requestTemperatures();
  //scd30.read(); //from test file
  //scd30.dataReady(); //from test file
```

```
   //Print temp and humidity values to serial monitor
   //print the temperature in Celsius
   Serial.,print(",");
   Serial.,print(air_temp_BMP280);
   Serial.,print(",");
   Serial.,print(pressure);
   Serial.,print(",");
   Serial.,print(dht.temperature_C);
   Serial.,print(",");
   Serial.,println(dht.humidity);

  //Serial.,println(scd30.CO2, 3); //added from test script

  lcd.clear();
   //check if any reads failed
   lcd.setCursor(0, 0);  // start to print at the first row
   lcd.print("T:");
   lcd.print(dht.temperature_C);     // print the temperature
   lcd.print(",P:");
   lcd.print(pressure);     // print the temperature

   lcd.setCursor(0, 1);  // start to print at the second row
   lcd.print("H:");
   lcd.print(dht.humidity);      // print the humidity
   lcd.print(",C:");
   lcd.print(co2);      // print the CO2; change from t est script

  File dataFile = SD.open("datalog.txt", FILE_WRITE);
  if (dataFile) {
   dataFile.print(timestring);
       dataFile.print(";");
   dataFile.print(air_temp_BMP280);
       dataFile.print(";");
   dataFile.print(pressure);
        dataFile.print(";");
   dataFile.print(dht.temperature_C);
     dataFile.print(";");
   dataFile.print(dht.humidity);
     dataFile.print(";");
   dataFile.println(co2);

 dataFile.close();
  }
  else {
   Serial.,println("error writing datalog.txt");
  }

delay (1000);

}
```

ANNEXE 3: summary of the daily cumulative CO_2 emissions

- CFN90

DOY	Reco_cum	GPP_cum	NEE_cum	Temp_air	PAR	NEE_cum_all
17.11.2022	2.121983	-3.77425	-1.65227	34.33619	737.2469	-1.65227
18.11.2022	3.054971	-4.19611	-1.14114	32.39498	353.3646	-2.79341
19.11.2022	3.2662	-4.23983	-0.97363	32.69825	460.45	-3.76704
20.11.2022	3.396051	-4.55697	-1.16092	32.31654	467.5792	-4.92797
21.11.2022	3.706179	-4.43339	-0.72721	32.60385	350.9375	-5.65518
22.11.2022	3.929746	-4.73672	-0.80697	32.5495	434.8625	-6.46215
23.11.2022	4.430634	-5.1359	-0.70527	33.43465	467.2063	-7.16742
24.11.2022	4.968689	-5.01481	-0.04612	33.95129	439.9938	-7.21354
25.11.2022	5.362376	-5.61045	-0.24808	34.11842	463.7104	-7.46162
26.11.2022	5.823479	-5.88173	-0.05825	34.16477	455.9542	-7.51987
27.11.2022	5.282372	-6.21648	-0.93411	33.75563	530.4604	-8.45398
28.11.2022	6.051064	-6.25479	-0.20372	34.09098	476.2333	-8.6577
29.11.2022	4.336056	-5.53414	-1.19809	32.2944	323.1979	-9.85578
30.11.2022	3.654916	-6.06837	-2.41345	31.33044	343.7563	-12.2692
01.12.2022	4.073166	-6.44809	-2.37492	31.32883	403.1042	-14.6442
02.12.2022	4.893588	-6.68856	-1.79498	32.06329	351.4417	-16.4391
03.12.2022	5.053672	-6.74113	-1.68746	31.9616	350.3083	-18.1266
04.12.2022	4.764062	-7.27773	-2.51367	31.63819	397.3354	-20.6403
05.12.2022	5.66429	-7.67829	-2.014	31.96156	415.0208	-22.6543
06.12.2022	6.711873	-7.82635	-1.11447	33.13598	381.4396	-23.7687
07.12.2022	4.096478	-7.88996	-3.79348	31.59619	371.5729	-27.5622
08.12.2022	6.235209	-8.43334	-2.19813	32.95629	442.5521	-29.7603
09.12.2022	7.258262	-9.51639	-2.25813	32.86906	490.7792	-32.0185
10.12.2022	6.900177	-9.36198	-2.46181	32.12348	462.9167	-34.4803
11.12.2022	6.167758	-9.05625	-2.88849	32.27442	375.3979	-37.3688
12.12.2022	6.719053	-8.67881	-1.95976	32.29308	308.0833	-39.3285
13.12.2022	4.095185	-9.41303	-5.31785	31.21808	361.5792	-44.6464
14.12.2022	4.816907	-9.75801	-4.9411	31.69275	345.4896	-49.5875
15.12.2022	5.702003	-10.1875	-4.4855	31.99769	356.9688	-54.073
16.12.2022	4.953005	-10.7172	-5.76416	30.86283	377.8125	-59.8371

17.12.2022	4.839377	-10.7346	-5.89523	30.43738	363.2479	-65.7324
18.12.2022	3.968189	-11.6916	-7.72339	28.27348	374.3083	-73.4558
19.12.2022	3.952923	-11.5921	-7.6392	27.0076	387.6833	-81.095
20.12.2022	4.468038	-12.2086	-7.74057	27.46944	432.3063	-88.8355
21.12.2022	5.883507	-11.928	-6.04447	28.43029	396.8104	-94.88
22.12.2022	5.811094	-13.5547	-7.74365	28.6376	485.8646	-102.624
23.12.2022	3.664543	-12.4957	-8.83112	27.68644	349.9896	-111.455
24.12.2022	4.610482	-12.1696	-7.55909	28.12631	341.449	-119.014
25.12.2022	6.122188	-13.6271	-7.50496	30.52881	473.6255	-126.519
26.12.2022	6.580084	-14.8853	-8.30522	31.21283	492.4063	-134.824
27.12.2022	6.81578	-13.1405	-6.32468	31.09127	326.4208	-141.149
28.12.2022	6.06419	-13.9845	-7.92028	30.4314	347.5896	-149.069
29.12.2022	7.013229	-13.8814	-6.8682	31.4046	334.5604	-155.937
30.12.2022	7.885485	-13.7249	-5.83945	31.44523	311.4188	-161.777
31.12.2022	8.074891	-15.1611	-7.08625	31.55704	344.375	-168.863
01.01.2023	8.331317	-16.5648	-8.23348	32.04063	384.8625	-177.096
02.01.2023	8.570742	-15.671	-7.10025	31.78942	359.4604	-184.197
03.01.2023	8.053406	-16.3464	-8.29301	31.4395	358.4458	-192.49
04.01.2023	3.85156	-16.9392	-13.0876	28.84898	362.7021	-205.577
05.01.2023	4.279283	-16.8955	-12.6162	28.57669	361.4208	-218.193
06.01.2023	5.179856	-17.356	-12.1761	28.47479	357.6563	-230.37
07.01.2023	7.164327	-17.1993	-10.035	30.74685	340.7188	-240.405
08.01.2023	7.326323	-16.1823	-8.85594	31.37035	302.2938	-249.261
09.01.2023	5.779992	-16.0273	-10.2473	29.58152	329.3375	-259.508
10.01.2023	5.372335	-15.8021	-10.4297	27.80879	336.5646	-269.938
11.01.2023	6.017499	-15.2749	-9.25737	29.65225	318.8667	-279.195
12.01.2023	7.609278	-14.2759	-6.66667	31.85888	301.5896	-285.862
13.01.2023	8.029168	-13.6085	-5.57936	32.2361	295.6396	-291.441
14.01.2023	9.392115	-13.0741	-3.68199	32.8626	304.6125	-295.123
15.01.2023	8.182873	-13.1047	-4.92184	32.01827	310.5917	-300.045
16.01.2023	5.511626	-12.0305	-6.51888	29.50381	312.775	-306.564
17.01.2023	5.679594	-12.266	-6.58644	29.61488	375.1021	-313.15
18.01.2023	6.004414	-11.3432	-5.33877	30.53413	318.5875	-318.489
19.01.2023	5.121745	-12.4453	-7.32354	28.55096	398.8208	-325.812

20.01.2023	5.925955	-12.1517	-6.2257	28.6774	478.7792	-332.038
21.01.2023	5.336991	-9.7245	-4.38751	27.47842	297.0792	-336.426
22.01.2023	5.913457	-9.74663	-3.83318	28.53206	347.6167	-340.259
23.01.2023	5.970826	-8.16768	-2.19686	28.66075	265.8875	-342.456
24.01.2023	5.855807	-8.04832	-2.19251	29.11075	263.0146	-344.648
25.01.2023	5.605401	-7.73826	-2.13286	27.86719	321.9438	-346.781
26.01.2023	5.209177	-7.8211	-2.61193	27.37675	374.65	-349.393
27.01.2023	5.078532	-7.20336	-2.12482	28.98729	468.0833	-351.518
28.01.2023	5.309829	-6.6907	-1.38087	30.59581	397.6521	-352.899
29.01.2023	5.207931	-5.79193	-0.584	30.68152	290.3813	-353.483
30.01.2023	4.865688	-5.68004	-0.81435	28.85869	387.9063	-354.297
31.01.2023	4.548289	-5.16034	-0.61205	27.10127	449.4292	-354.909
01.02.2023	4.379633	-4.12844	0.251193	26.3945	281.8083	-354.658
02.02.2023	4.270536	-3.90198	0.368557	26.9674	354.6333	-354.289
03.02.2023	4.156599	-3.47012	0.686477	29.18827	367.5417	-353.603
04.02.2023	4.167035	-3.6416	0.52543	31.30246	500.9063	-353.077
05.02.2023	4.167035	-3.45721	0.709824	31.84896	388.9396	-352.368
06.02.2023	4.167035	-3.47165	0.695387	30.72683	389.0875	-351.672
07.02.2023	4.167035	-3.51096	0.656077	31.48002	342.4854	-351.016
08.02.2023	4.167035	-3.56618	0.600851	32.00558	448.85	-350.415
09.02.2023	4.167035	-3.4481	0.718939	32.6674	426.0833	-349.696
10.02.2023	4.167035	-3.26683	0.900205	32.88525	312.0333	-348.796
11.02.2023	4.167035	-3.34231	0.824725	32.97631	314.6917	-347.971
12.02.2023	4.167035	-3.59435	0.572685	33.05181	390.8333	-347.399
13.02.2023	4.167035	-3.42618	0.740854	32.91769	371.625	-346.658
14.02.2023	4.167035	-3.27804	0.888995	32.9804	321.8146	-345.769
15.02.2023	4.167035	-3.47426	0.69278	33.13471	418.3125	-345.076
16.02.2023	4.038587	-3.07689	0.961692	33.16733	322.2438	-344.114
17.02.2023	3.237899	-0.14725	3.090651	34.27698	438.2167	-341.024
18.02.2023	3.01521	0	3.01521	33.96498	232.3708	-338.009
19.02.2023	2.948441	0	2.948441	33.97988	291.1729	-335.06
20.02.2023	2.898141	0	2.898141	34.74063	384.3	-332.162
21.02.2023	2.809848	0	2.809848	33.45021	286.7958	-329.352
22.02.2023	2.752072	0	2.752072	33.97513	375.6063	-326.6

23.02.2023	2.686351	0	2.686351	33.82021	443.6042	-323.914
24.02.2023	2.62564	0	2.62564	34.36217	258.1479	-321.288
25.02.2023	2.557566	0	2.557566	34.14473	339.4479	-318.73
26.02.2023	2.493384	0	2.493384	34.5584	341.5729	-316.237
27.02.2023	2.424897	0	2.424897	32.61679	465.375	-313.812
28.02.2023	1.729299	0	1.729299	31.18263	339.6343	-312.083

- CFN120

DOY	Reco_cum	GPP_cum	NEE_cum	Temp_air	PAR	NEE_cum_all
17.11.2022	2.333951	-4.15161	-1.81766	34.33619	737.2469	-1.81766
18.11.2022	3.346835	-4.59103	-1.24419	32.39498	353.3646	-3.06186
19.11.2022	3.559949	-4.61116	-1.05121	32.69825	460.45	-4.11307
20.11.2022	3.684936	-4.92967	-1.24473	32.31654	467.5792	-5.3578
21.11.2022	4.000642	-4.7698	-0.76916	32.60385	350.9375	-6.12696
22.11.2022	4.226168	-5.07452	-0.84836	32.5495	434.8625	-6.97531
23.11.2022	4.741911	-5.47996	-0.73805	33.43465	467.2063	-7.71336
24.11.2022	5.300778	-5.32964	-0.02886	33.95129	439.9938	-7.74222
25.11.2022	5.702364	-5.94252	-0.24016	34.11842	463.7104	-7.98238
26.11.2022	6.174768	-6.20952	-0.03475	34.16477	455.9542	-8.01713
27.11.2022	5.597513	-6.54551	-0.948	33.75563	530.4604	-8.96512
28.11.2022	6.390371	-6.56331	-0.17294	34.09098	476.2333	-9.13807
29.11.2022	4.5837	-5.77942	-1.19572	32.2944	323.1979	-10.3338
30.11.2022	3.8569	-6.32291	-2.46601	31.33044	343.7563	-12.7998
01.12.2022	4.283585	-6.71125	-2.42767	31.32883	403.1042	-15.2275
02.12.2022	5.131626	-6.93402	-1.8024	32.06329	351.4417	-17.0299
03.12.2022	5.289366	-6.97892	-1.68955	31.9616	350.3083	-18.7194
04.12.2022	4.979142	-7.52886	-2.54972	31.63819	397.3354	-21.2691
05.12.2022	5.921275	-7.94923	-2.02795	31.96156	415.0208	-23.2971
06.12.2022	7.018853	-8.11284	-1.09398	33.13598	381.4396	-24.3911
07.12.2022	4.285414	-8.18566	-3.90025	31.59619	371.5729	-28.2913
08.12.2022	6.52485	-8.76882	-2.24396	32.95629	442.5521	-30.5353
09.12.2022	7.597713	-9.90377	-2.30605	32.86906	490.7792	-32.8413

10.12.2022	7.225175	-9.75033	-2.52516	32.12348	462.9167	-35.3665
11.12.2022	6.460274	-9.42946	-2.96918	32.27442	375.3979	-38.3357
12.12.2022	7.039734	-9.03527	-1.99554	32.29308	308.0833	-40.3312
13.12.2022	4.292063	-9.81236	-5.52029	31.21808	361.5792	-45.8515
14.12.2022	5.049815	-10.1776	-5.1278	31.69275	345.4896	-50.9793
15.12.2022	5.979208	-10.6343	-4.65507	31.99769	356.9688	-55.6344
16.12.2022	5.195192	-11.1941	-5.99894	30.86283	377.8125	-61.6333
17.12.2022	5.0773	-11.2166	-6.13933	30.43738	363.2479	-67.7726
18.12.2022	4.164288	-12.2277	-8.06344	28.27348	374.3083	-75.8361
19.12.2022	4.149227	-12.1311	-7.98189	27.0076	387.6833	-83.818
20.12.2022	4.690938	-12.7843	-8.09339	27.46944	432.3063	-91.9114
21.12.2022	6.178222	-12.4901	-6.31187	28.43029	396.8104	-98.2232
22.12.2022	6.103526	-14.2087	-8.1052	28.6376	485.8646	-106.328
23.12.2022	3.849912	-13.0973	-9.24744	27.68644	349.9896	-115.576
24.12.2022	4.844649	-12.7583	-7.91367	28.12631	341.449	-123.49
25.12.2022	6.4343	-14.3006	-7.86625	30.52881	473.6255	-131.356
26.12.2022	6.916831	-15.6284	-8.71152	31.21283	492.4063	-140.067
27.12.2022	7.165921	-13.7929	-6.62699	31.09127	326.4208	-146.694
28.12.2022	6.37692	-14.6863	-8.30942	30.4314	347.5896	-155.004
29.12.2022	7.376199	-14.5813	-7.20514	31.4046	334.5604	-162.209
30.12.2022	8.294931	-14.4206	-6.12571	31.44523	311.4188	-168.335
31.12.2022	8.495604	-15.9352	-7.43958	31.55704	344.375	-175.774
01.01.2023	8.766856	-17.4174	-8.65057	32.04063	384.8625	-184.425
02.01.2023	9.020204	-16.4818	-7.46157	31.78942	359.4604	-191.886
03.01.2023	8.477102	-17.1978	-8.7207	31.4395	358.4458	-200.607
04.01.2023	4.054892	-17.826	-13.7711	28.84898	362.7021	-214.378
05.01.2023	4.505853	-17.7846	-13.2788	28.57669	361.4208	-227.657
06.01.2023	5.454875	-18.2739	-12.819	28.47479	357.6563	-240.476
07.01.2023	7.545761	-18.1133	-10.5675	30.74685	340.7188	-251.043
08.01.2023	7.716947	-17.0457	-9.32874	31.37035	302.2938	-260.372
09.01.2023	6.082783	-16.8774	-10.7947	29.58152	329.3375	-271.167
10.01.2023	5.646173	-16.6341	-10.9879	27.80879	336.5646	-282.155
11.01.2023	6.31856	-16.0727	-9.75411	29.65225	318.8667	-291.909
12.01.2023	7.988075	-15.0147	-7.02666	31.85888	301.5896	-298.935

13.01.2023	8.423169	-14.3061	-5.8829	32.2361	295.6396	-304.818
14.01.2023	9.851642	-13.7379	-3.88623	32.8626	304.6125	-308.705
15.01.2023	8.570673	-13.7628	-5.19211	32.01827	310.5917	-313.897
16.01.2023	5.749685	-12.6274	-6.87775	29.50381	312.775	-320.774
17.01.2023	5.919414	-12.8685	-6.94913	29.61488	375.1021	-327.724
18.01.2023	6.254364	-11.8897	-5.63538	30.53413	318.5875	-333.359
19.01.2023	5.317394	-13.0393	-7.72189	28.55096	398.8208	-341.081
20.01.2023	6.157316	-12.7239	-6.56654	28.6774	478.7792	-347.647
21.01.2023	5.529723	-10.1676	-4.63792	27.47842	297.0792	-352.285
22.01.2023	6.129747	-10.1823	-4.05256	28.53206	347.6167	-356.338
23.01.2023	6.182975	-8.52158	-2.3386	28.66075	265.8875	-358.676
24.01.2023	6.054618	-8.38484	-2.33023	29.11075	263.0146	-361.007
25.01.2023	5.783648	-8.0524	-2.26875	27.86719	321.9438	-363.275
26.01.2023	5.359079	-8.1287	-2.76962	27.37675	374.65	-366.045
27.01.2023	5.214261	-7.47458	-2.26032	28.98729	468.0833	-368.305
28.01.2023	5.450698	-6.92609	-1.47539	30.59581	397.6521	-369.781
29.01.2023	5.336161	-5.97561	-0.63945	30.68152	290.3813	-370.42
30.01.2023	4.968454	-5.84723	-0.87877	28.85869	387.9063	-371.299
31.01.2023	4.626916	-5.29241	-0.6655	27.10127	449.4292	-371.964
01.02.2023	4.442059	-4.20938	0.232679	26.3945	281.8083	-371.732
02.02.2023	4.319939	-3.95698	0.362963	26.9674	354.6333	-371.369
03.02.2023	4.19408	-3.49645	0.697635	29.18827	367.5417	-370.671
04.02.2023	4.204539	-3.67023	0.534307	31.30246	500.9063	-370.137
05.02.2023	4.204539	-3.48354	0.720996	31.84896	388.9396	-369.416
06.02.2023	4.204539	-3.49811	0.706429	30.72683	389.0875	-368.709
07.02.2023	4.204539	-3.53764	0.666903	31.48002	342.4854	-368.043
08.02.2023	4.204539	-3.59372	0.610815	32.00558	448.85	-367.432
09.02.2023	4.204539	-3.47422	0.730321	32.6674	426.0833	-366.701
10.02.2023	4.204539	-3.2909	0.913638	32.88525	312.0333	-365.788
11.02.2023	4.204539	-3.36724	0.8373	32.97631	314.6917	-364.95
12.02.2023	4.204539	-3.62215	0.58239	33.05181	390.8333	-364.368
13.02.2023	4.204539	-3.4522	0.752343	32.91769	371.625	-363.616
14.02.2023	4.204539	-3.30232	0.902216	32.9804	321.8146	-362.714
15.02.2023	4.204539	-3.50093	0.703611	33.13471	418.3125	-362.01

16.02.2023	4.071598	-3.10009	0.971506	33.16733	322.2438	-361.038
17.02.2023	3.242782	-0.14825	3.094533	34.27698	438.2167	-357.944
18.02.2023	3.01521	0	3.01521	33.96498	232.3708	-354.929
19.02.2023	2.948441	0	2.948441	33.97988	291.1729	-351.98
20.02.2023	2.898141	0	2.898141	34.74063	384.3	-349.082
21.02.2023	2.809848	0	2.809848	33.45021	286.7958	-346.272
22.02.2023	2.752072	0	2.752072	33.97513	375.6063	-343.52
23.02.2023	2.686351	0	2.686351	33.82021	443.6042	-340.834
24.02.2023	2.62564	0	2.62564	34.36217	258.1479	-338.208
25.02.2023	2.557566	0	2.557566	34.14473	339.4479	-335.651
26.02.2023	2.493384	0	2.493384	34.5584	341.5729	-333.157
27.02.2023	2.424897	0	2.424897	32.61679	465.375	-330.732
28.02.2023	1.729299	0	1.729299	31.18263	339.6343	-329.003

- AWD15N90

DOY	Reco_cum	GPP_cum	NEE_cum	Temp_air	PAR	NEE_cum_all
17.11.2022	1.534585	-3.72556	-2.19097	34.33619	810.9716	-2.19097
18.11.2022	2.204749	-4.08629	-1.88155	32.39498	388.701	-4.07252
19.11.2022	2.222585	-3.86889	-1.6463	32.69825	506.495	-5.71882
20.11.2022	2.214086	-3.92126	-1.70718	32.31654	514.3371	-7.42599
21.11.2022	2.22773	-3.75893	-1.5312	32.60385	386.0313	-8.9572
22.11.2022	2.246254	-3.77735	-1.53109	32.5495	478.3488	-10.4883
23.11.2022	2.275718	-3.89548	-1.61977	33.43465	513.9269	-12.1081
24.11.2022	2.719332	-4.08914	-1.3698	33.95129	483.9931	-13.4779
25.11.2022	3.196271	-4.91516	-1.71889	34.11842	510.0815	-15.1967
26.11.2022	3.719198	-5.49356	-1.77436	34.16477	501.5496	-16.9711
27.11.2022	3.820948	-6.16923	-2.34828	33.75563	583.5065	-19.3194
28.11.2022	4.495308	-6.53694	-2.04163	34.09098	523.8567	-21.361
29.11.2022	3.74829	-5.99063	-2.24234	32.2944	355.5177	-23.6034
30.11.2022	3.489259	-6.82846	-3.33921	31.33044	378.1319	-26.9426
01.12.2022	3.943916	-7.58469	-3.64077	31.32883	443.4146	-30.5833
02.12.2022	4.749675	-8.02536	-3.27568	32.06329	386.5858	-33.859

03.12.2022	5.009483	-8.37477	-3.36529	31.9616	385.3392	-37.2243
04.12.2022	4.944896	-9.2993	-4.35441	31.63819	437.069	-41.5787
05.12.2022	5.607301	-9.53991	-3.93261	31.96156	456.5229	-45.5113
06.12.2022	6.412768	-9.93343	-3.52066	33.13598	503.5003	-49.032
07.12.2022	4.519502	-9.74656	-5.22706	31.59619	490.4763	-54.259
08.12.2022	6.107155	-10.1576	-4.05043	32.95629	584.1688	-58.3095
09.12.2022	6.626832	-11.1747	-4.54786	32.86906	647.8285	-62.8573
10.12.2022	6.324085	-10.7303	-4.40619	32.12348	611.05	-67.2635
11.12.2022	5.949776	-10.1888	-4.23899	32.27442	495.5253	-71.5025
12.12.2022	6.305187	-9.62056	-3.31537	32.29308	406.67	-74.8179
13.12.2022	4.607017	-10.1924	-5.58537	31.21808	477.2845	-80.4032
14.12.2022	5.153988	-10.3819	-5.22788	31.69275	456.0463	-85.6311
15.12.2022	5.781405	-10.6232	-4.84182	31.99769	471.1988	-90.4729
16.12.2022	5.241014	-10.9847	-5.74373	30.86283	498.7125	-96.2167
17.12.2022	5.167815	-10.855	-5.68716	30.43738	479.4873	-101.904
18.12.2022	4.368555	-11.5542	-7.1856	28.27348	494.087	-109.089
19.12.2022	4.260347	-11.2537	-6.99333	27.0076	511.742	-116.083
20.12.2022	4.603162	-11.6271	-7.0239	27.46944	570.6443	-123.107
21.12.2022	5.439433	-11.344	-5.90458	28.43029	523.7898	-129.011
22.12.2022	5.463674	-12.4556	-6.99193	28.6376	641.3413	-136.003
23.12.2022	4.282004	-11.5295	-7.24752	27.68644	461.9863	-143.251
24.12.2022	4.984349	-11.178	-6.19369	28.12631	450.7127	-149.444
25.12.2022	6.050622	-12.0156	-5.96498	30.52881	625.1857	-155.409
26.12.2022	6.431192	-12.8502	-6.41902	31.21283	649.9763	-161.828
27.12.2022	6.615244	-11.6243	-5.00904	31.09127	430.8755	-166.837
28.12.2022	6.154076	-12.0932	-5.93916	30.4314	458.8183	-172.777
29.12.2022	6.829888	-11.9841	-5.15422	31.4046	441.6198	-177.931
30.12.2022	7.158009	-11.8157	-4.6577	31.44523	411.0728	-182.589
31.12.2022	7.215295	-12.8833	-5.66798	31.55704	454.575	-188.256
01.01.2023	7.472466	-13.7853	-6.31287	32.04063	508.0185	-194.569
02.01.2023	7.353483	-13.0046	-5.65115	31.78942	474.4878	-200.221
03.01.2023	7.169336	-13.3119	-6.14261	31.4395	473.1485	-206.363
04.01.2023	5.039726	-13.7276	-8.68786	28.84898	478.7668	-215.051
05.01.2023	5.337864	-13.5721	-8.23421	28.57669	477.0755	-223.285

06.01.2023	5.761755	-13.851	-8.08926	28.47479	472.1063	-231.374
07.01.2023	7.128505	-13.7706	-6.64209	30.74685	449.7488	-238.017
08.01.2023	7.291676	-12.9484	-5.6567	31.37035	399.0278	-243.673
09.01.2023	6.33836	-12.8737	-6.53531	29.58152	434.7255	-250.209
10.01.2023	5.793822	-12.7425	-6.94871	27.80879	444.2653	-257.157
11.01.2023	6.431197	-12.4832	-6.05197	29.65225	420.904	-263.209
12.01.2023	7.505496	-11.8738	-4.36826	31.85888	398.0983	-267.578
13.01.2023	7.584708	-11.3807	-3.79604	32.2361	390.2443	-271.374
14.01.2023	8.050128	-10.9574	-2.90727	32.8626	402.0885	-274.281
15.01.2023	7.421547	-11.0644	-3.64283	32.01827	409.981	-277.924
16.01.2023	6.160735	-10.2652	-4.1045	29.50381	412.863	-282.028
17.01.2023	6.257245	-10.3281	-4.07081	29.61488	495.1348	-286.099
18.01.2023	6.555596	-9.95944	-3.40385	30.53413	420.5355	-289.503
19.01.2023	5.961522	-10.6719	-4.71036	28.55096	526.4435	-294.213
20.01.2023	6.242478	-10.337	-4.09448	28.6774	631.9885	-298.308
21.01.2023	5.854006	-8.9159	-3.0619	27.47842	392.1445	-301.37
22.01.2023	6.182388	-8.94153	-2.75914	28.53206	458.854	-304.129
23.01.2023	6.219912	-7.7682	-1.54829	28.66075	350.9715	-305.677
24.01.2023	6.202873	-7.90736	-1.70449	29.11075	347.1793	-307.381
25.01.2023	6.049913	-7.62169	-1.57178	27.86719	424.9658	-308.953
26.01.2023	5.903552	-7.71144	-1.80789	27.37675	494.538	-310.761
27.01.2023	6.007731	-7.21033	-1.20259	28.98729	617.87	-311.964
28.01.2023	6.175891	-7.00516	-0.82927	30.59581	524.9008	-312.793
29.01.2023	6.12458	-6.31285	-0.18827	30.68152	319.4194	-312.981
30.01.2023	5.956498	-6.26832	-0.31182	28.85869	426.6969	-313.293
31.01.2023	5.841606	-5.98106	-0.13946	27.10127	494.3721	-313.433
01.02.2023	5.798986	-5.25861	0.540373	26.3945	309.9892	-312.892
02.02.2023	5.80248	-5.22672	0.575761	26.9674	390.0967	-312.316
03.02.2023	5.797383	-5.01245	0.784938	29.18827	404.2958	-311.531
04.02.2023	5.804481	-5.19905	0.605435	31.30246	550.9969	-310.926
05.02.2023	5.804481	-4.98239	0.822088	31.84896	427.8335	-310.104
06.02.2023	5.804481	-5.0032	0.801277	30.72683	427.9963	-309.303
07.02.2023	5.804481	-5.06133	0.743152	31.48002	376.734	-308.559
08.02.2023	5.804481	-5.11881	0.685667	32.00558	493.735	-307.874

09.02.2023	5.804481	-4.97875	0.825727	32.6674	468.6917	-307.048
10.02.2023	5.804481	-4.75631	1.048174	32.88525	343.2367	-306
11.02.2023	5.804481	-4.8484	0.956084	32.97631	346.1608	-305.044
12.02.2023	5.804481	-5.15337	0.651108	33.05181	429.9167	-304.393
13.02.2023	5.804481	-4.94515	0.859328	32.91769	408.7875	-303.533
14.02.2023	5.804481	-4.76567	1.038808	32.9804	353.996	-302.495
15.02.2023	5.804481	-4.99659	0.80789	33.13471	460.1438	-301.687
16.02.2023	5.486073	-4.44909	1.036983	33.16733	354.4681	-300.65
17.02.2023	3.538502	-0.21924	3.319258	34.27698	482.0383	-297.33
18.02.2023	3.107263	0	3.107263	33.96498	255.6079	-294.223
19.02.2023	3.104831	0	3.104831	33.97988	320.2902	-291.118
20.02.2023	3.167507	0	3.167507	34.74063	422.73	-287.951
21.02.2023	3.049248	0	3.049248	33.45021	315.4754	-284.902
22.02.2023	3.095374	0	3.095374	33.97513	413.1669	-281.806
23.02.2023	3.071046	0	3.071046	33.82021	487.9646	-278.735
24.02.2023	3.119144	0	3.119144	34.36217	283.9627	-275.616
25.02.2023	3.108003	0	3.108003	34.14473	373.3927	-272.508
26.02.2023	3.13251	0	3.13251	34.5584	375.7302	-269.376
27.02.2023	2.936883	0	2.936883	32.61679	511.9125	-266.439
28.02.2023	1.953858	0	1.953858	30.78306	382.2	-264.485

- AWD15N120

DOY	Reco_cum	GPP_cum	NEE_cum	Temp_air	PAR	NEE_cum_all
17.11.2022	1.534585	-3.68958	-2.15499	34.33619	737.2469	-2.15499
18.11.2022	2.204749	-4.02506	-1.82031	32.39498	353.3646	-3.97531
19.11.2022	2.222585	-3.81786	-1.59527	32.69825	460.45	-5.57058
20.11.2022	2.214086	-3.87512	-1.66103	32.31654	467.5792	-7.23161
21.11.2022	2.22773	-3.69873	-1.471	32.60385	350.9375	-8.70261
22.11.2022	2.246254	-3.72388	-1.47762	32.5495	434.8625	-10.1802
23.11.2022	2.275718	-3.84483	-1.56912	33.43465	467.2063	-11.7493
24.11.2022	2.719332	-4.02464	-1.30531	33.95129	439.9938	-13.0547
25.11.2022	3.196271	-4.83267	-1.6364	34.11842	463.7104	-14.6911

26.11.2022	3.719198	-5.39409	-1.67489	34.16477	455.9542	-16.3659
27.11.2022	3.820948	-6.05746	-2.23651	33.75563	530.4604	-18.6025
28.11.2022	4.495308	-6.4004	-1.90509	34.09098	476.2333	-20.5075
29.11.2022	3.74829	-5.82559	-2.0773	32.2944	323.1979	-22.5848
30.11.2022	3.489259	-6.64081	-3.15155	31.33044	343.7563	-25.7364
01.12.2022	3.943916	-7.39783	-3.45391	31.32883	403.1042	-29.1903
02.12.2022	4.749675	-7.78868	-3.03901	32.06329	351.4417	-32.2293
03.12.2022	5.009483	-8.13825	-3.12877	31.9616	350.3083	-35.3581
04.12.2022	4.952842	-9.05574	-4.10289	31.63819	397.3354	-39.461
05.12.2022	5.668417	-9.31983	-3.65142	31.96156	415.0208	-43.1124
06.12.2022	6.539458	-9.28645	-2.74699	33.13598	381.4396	-45.8594
07.12.2022	4.669643	-9.13483	-4.46519	31.59619	371.5729	-50.3246
08.12.2022	6.345302	-9.65295	-3.30764	32.95629	442.5521	-53.6322
09.12.2022	6.928186	-10.6641	-3.73588	32.86906	490.7792	-57.3681
10.12.2022	6.669303	-10.273	-3.6037	32.12348	462.9167	-60.9718
11.12.2022	6.338729	-9.69706	-3.35833	32.27442	375.3979	-64.3301
12.12.2022	6.763525	-9.11046	-2.34694	32.29308	308.0833	-66.6771
13.12.2022	5.020772	-9.74042	-4.71964	31.21808	361.5792	-71.3967
14.12.2022	5.646941	-9.93994	-4.293	31.69275	345.4896	-75.6897
15.12.2022	6.364512	-10.224	-3.85952	31.99769	356.9688	-79.5492
16.12.2022	5.822307	-10.609	-4.78668	30.86283	377.8125	-84.3359
17.12.2022	5.78232	-10.4896	-4.70732	30.43738	363.2479	-89.0432
18.12.2022	4.927095	-11.2545	-6.32738	28.27348	374.3083	-95.3706
19.12.2022	4.831801	-11.0105	-6.17869	27.0076	387.6833	-101.549
20.12.2022	5.243657	-11.4377	-6.19407	27.46944	432.3063	-107.743
21.12.2022	6.207983	-11.1	-4.89206	28.43029	396.8104	-112.635
22.12.2022	6.276363	-12.3628	-6.08642	28.6376	485.8646	-118.722
23.12.2022	4.978629	-11.3632	-6.38455	27.68644	349.9896	-125.106
24.12.2022	5.813633	-10.9985	-5.18484	28.12631	341.449	-130.291
25.12.2022	7.076633	-12.0142	-4.93752	30.52881	473.6255	-135.229
26.12.2022	7.557948	-12.9323	-5.37439	31.21283	492.4063	-140.603
27.12.2022	7.812126	-11.539	-3.72688	31.09127	326.4208	-144.33
28.12.2022	7.309191	-12.0963	-4.7871	30.4314	347.5896	-149.117
29.12.2022	8.145242	-11.9669	-3.82162	31.4046	334.5604	-152.939

30.12.2022	8.566983	-11.7902	-3.22317	31.44523	311.4188	-156.162
31.12.2022	8.674586	-12.9022	-4.22762	31.55704	344.375	-160.39
01.01.2023	9.025841	-13.8931	-4.86727	32.04063	384.8625	-165.257
02.01.2023	8.918267	-13.0984	-4.18016	31.78942	359.4604	-169.437
03.01.2023	8.735074	-13.4884	-4.75331	31.4395	358.4458	-174.19
04.01.2023	6.165966	-13.9172	-7.75119	28.84898	362.7021	-181.941
05.01.2023	6.553307	-13.7866	-7.2333	28.57669	361.4208	-189.175
06.01.2023	7.100301	-14.0892	-6.98888	28.47479	357.6563	-196.164
07.01.2023	8.824033	-13.9822	-5.15815	30.74685	340.7188	-201.322
08.01.2023	9.051924	-13.1488	-4.09685	31.37035	302.2938	-205.419
09.01.2023	7.820875	-13.0637	-5.24284	29.58152	329.3375	-210.661
10.01.2023	7.090492	-12.9317	-5.84125	27.80879	336.5646	-216.503
11.01.2023	7.829593	-12.6435	-4.81386	29.65225	318.8667	-221.317
12.01.2023	9.11766	-11.978	-2.86039	31.85888	301.5896	-224.177
13.01.2023	9.164542	-11.4851	-2.32052	32.2361	295.6396	-226.498
14.01.2023	9.696429	-11.0725	-1.37608	32.8626	304.6125	-227.874
15.01.2023	8.855078	-11.1789	-2.32382	32.01827	310.5917	-230.197
16.01.2023	7.219924	-10.3529	-3.13294	29.50381	312.775	-233.33
17.01.2023	7.286632	-10.483	-3.1964	29.61488	375.1021	-236.527
18.01.2023	7.604197	-10.0014	-2.39722	30.53413	318.5875	-238.924
19.01.2023	6.807896	-10.8296	-4.02169	28.55096	398.8208	-242.946
20.01.2023	7.107937	-10.5381	-3.4302	28.6774	478.7792	-246.376
21.01.2023	6.568773	-8.92151	-2.35273	27.47842	297.0792	-248.729
22.01.2023	6.925226	-8.9714	-2.04617	28.53206	347.6167	-250.775
23.01.2023	6.917896	-7.73812	-0.82023	28.66075	265.8875	-251.595
24.01.2023	6.841634	-7.83741	-0.99577	29.11075	263.0146	-252.591
25.01.2023	6.596671	-7.58016	-0.98349	27.86719	321.9438	-253.574
26.01.2023	6.358394	-7.70708	-1.34869	27.37675	374.65	-254.923
27.01.2023	6.431668	-7.20345	-0.77178	28.98729	468.0833	-255.695
28.01.2023	6.58708	-6.96156	-0.37448	30.59581	397.6521	-256.069
29.01.2023	6.468542	-6.39685	0.071688	30.68152	290.3813	-255.998
30.01.2023	6.203979	-6.34884	-0.14486	28.85869	387.9063	-256.142
31.01.2023	6.005355	-6.02674	-0.02138	27.10127	449.4292	-256.164
01.02.2023	5.897081	-5.23972	0.657362	26.3945	281.8083	-255.506

02.02.2023	5.84628	-5.19127	0.655005	26.9674	354.6333	-254.851
03.02.2023	5.79814	-4.94995	0.848187	29.18827	367.5417	-254.003
04.02.2023	5.804505	-5.14796	0.65655	31.30246	500.9063	-253.347
05.02.2023	5.804505	-4.92351	0.880997	31.84896	388.9396	-252.466
06.02.2023	5.804505	-4.94384	0.860664	30.72683	389.0875	-251.605
07.02.2023	5.804505	-5.00154	0.802964	31.48002	342.4854	-250.802
08.02.2023	5.804505	-5.06263	0.741874	32.00558	448.85	-250.06
09.02.2023	5.804505	-4.9176	0.886905	32.6674	426.0833	-249.173
10.02.2023	5.804505	-4.68918	1.115322	32.88525	312.0333	-248.058
11.02.2023	5.804505	-4.78389	1.020613	32.97631	314.6917	-247.037
12.02.2023	5.804505	-5.09867	0.705831	33.05181	390.8333	-246.332
13.02.2023	5.804505	-4.88454	0.91997	32.91769	371.625	-245.412
14.02.2023	5.804505	-4.69982	1.104685	32.9804	321.8146	-244.307
15.02.2023	5.804505	-4.93947	0.865037	33.13471	418.3125	-243.442
16.02.2023	5.486094	-4.39301	1.093089	33.16733	322.2438	-242.349
17.02.2023	3.538505	-0.21508	3.323421	34.27698	438.2167	-239.025
18.02.2023	3.107263	0	3.107263	33.96498	232.3708	-235.918
19.02.2023	3.104831	0	3.104831	33.97988	291.1729	-232.813
20.02.2023	3.167507	0	3.167507	34.74063	384.3	-229.646
21.02.2023	3.049248	0	3.049248	33.45021	286.7958	-226.596
22.02.2023	3.095374	0	3.095374	33.97513	375.6063	-223.501
23.02.2023	3.071046	0	3.071046	33.82021	443.6042	-220.43
24.02.2023	3.119144	0	3.119144	34.36217	258.1479	-217.311
25.02.2023	3.108003	0	3.108003	34.14473	339.4479	-214.203
26.02.2023	3.13251	0	3.13251	34.5584	341.5729	-211.07
27.02.2023	2.936883	0	2.936883	32.61679	465.375	-208.133
28.02.2023	1.953858	0	1.953858	30.78306	347.4545	-206.18

- AWD25N90

DOY	Reco_cum	GPP_cum	NEE_cum	Temp_air	PAR	NEE_cum_all
17.11.2022	1.461579	-3.66855	-2.20697	34.33619	737.2469	-2.20697
18.11.2022	2.100951	-4.00205	-1.9011	32.39498	353.3646	-4.10807

19.11.2022	2.117743	-3.79606	-1.67831	32.69825	460.45	-5.78638
20.11.2022	2.109727	-3.85301	-1.74328	32.31654	467.5792	-7.52966
21.11.2022	2.122561	-3.67757	-1.55501	32.60385	350.9375	-9.08467
22.11.2022	2.139995	-3.7026	-1.5626	32.5495	434.8625	-10.6473
23.11.2022	2.177395	-3.82283	-1.64543	33.43465	467.2063	-12.2927
24.11.2022	2.476183	-3.80518	-1.32899	33.95129	439.9938	-13.6217
25.11.2022	2.793166	-4.33531	-1.54215	34.11842	463.7104	-15.1638
26.11.2022	3.111731	-4.63618	-1.52445	34.16477	455.9542	-16.6883
27.11.2022	3.410574	-4.96794	-1.55737	33.75563	530.4604	-18.2457
28.11.2022	3.719087	-5.14801	-1.42892	34.09098	476.2333	-19.6746
29.11.2022	3.989894	-4.79289	-0.80299	32.2944	323.1979	-20.4776
30.11.2022	4.251581	-5.29066	-1.03908	31.33044	343.7563	-21.5167
01.12.2022	4.561392	-5.58999	-1.0286	31.32883	403.1042	-22.5453
02.12.2022	4.883728	-6.00327	-1.11954	32.06329	351.4417	-23.6648
03.12.2022	5.203326	-6.06157	-0.85825	31.9616	350.3083	-24.523
04.12.2022	5.459439	-6.51819	-1.05875	31.63819	397.3354	-25.5818
05.12.2022	5.533427	-6.8098	-1.27637	31.96156	415.0208	-26.8582
06.12.2022	5.618234	-6.80169	-1.18345	33.13598	381.4396	-28.0416
07.12.2022	5.555323	-6.76764	-1.21232	31.59619	371.5729	-29.2539
08.12.2022	5.719008	-6.97837	-1.25936	32.95629	442.5521	-30.5133
09.12.2022	5.792336	-7.75318	-1.96084	32.86906	490.7792	-32.4741
10.12.2022	5.799035	-7.52838	-1.72934	32.12348	462.9167	-34.2035
11.12.2022	5.809445	-7.33256	-1.52311	32.27442	375.3979	-35.7266
12.12.2022	5.907146	-7.07864	-1.17149	32.29308	308.0833	-36.8981
13.12.2022	5.60568	-7.49804	-1.89236	31.21808	361.5792	-38.7905
14.12.2022	5.739432	-7.7045	-1.96507	31.69275	345.4896	-40.7555
15.12.2022	5.911007	-7.91924	-2.00824	31.99769	356.9688	-42.7638
16.12.2022	5.756126	-8.24739	-2.49127	30.86283	377.8125	-45.255
17.12.2022	5.725349	-8.23268	-2.50734	30.43738	363.2479	-47.7624
18.12.2022	5.369307	-8.77379	-3.40449	28.27348	374.3083	-51.1668
19.12.2022	5.26055	-8.59816	-3.33761	27.0076	387.6833	-54.5045
20.12.2022	5.356664	-8.92914	-3.57247	27.46944	432.3063	-58.0769
21.12.2022	5.659248	-8.81328	-3.15403	28.43029	396.8104	-61.231
22.12.2022	5.669247	-9.67975	-4.01051	28.6376	485.8646	-65.2415

23.12.2022	5.115298	-9.05395	-3.93865	27.68644	349.9896	-69.1801
24.12.2022	5.492762	-8.83716	-3.3444	28.12631	341.449	-72.5245
25.12.2022	5.94973	-9.52638	-3.57665	30.52881	473.6255	-76.1012
26.12.2022	6.212496	-10.2498	-4.0373	31.21283	492.4063	-80.1385
27.12.2022	6.314701	-9.32931	-3.0146	31.09127	326.4208	-83.1531
28.12.2022	6.01636	-9.75898	-3.74262	30.4314	347.5896	-86.8957
29.12.2022	6.442578	-9.71207	-3.26949	31.4046	334.5604	-90.1652
30.12.2022	6.618813	-9.6099	-2.99108	31.44523	311.4188	-93.1563
31.12.2022	6.645766	-10.5293	-3.88355	31.55704	344.375	-97.0398
01.01.2023	6.837256	-11.3353	-4.49805	32.04063	384.8625	-101.538
02.01.2023	6.718494	-10.724	-4.00551	31.78942	359.4604	-105.543
03.01.2023	6.575668	-11.0499	-4.47423	31.4395	358.4458	-110.018
04.01.2023	4.871912	-11.4307	-6.55876	28.84898	362.7021	-116.576
05.01.2023	5.040549	-11.3462	-6.3057	28.57669	361.4208	-122.882
06.01.2023	5.323291	-11.6183	-6.29502	28.47479	357.6563	-129.177
07.01.2023	6.46028	-11.5543	-5.094	30.74685	340.7188	-134.271
08.01.2023	6.574549	-10.8798	-4.30521	31.37035	302.2938	-138.576
09.01.2023	5.713388	-10.8281	-5.11472	29.58152	329.3375	-143.691
10.01.2023	5.234648	-10.7424	-5.5078	27.80879	336.5646	-149.199
11.01.2023	5.81963	-10.5272	-4.70759	29.65225	318.8667	-153.906
12.01.2023	6.797842	-9.99854	-3.2007	31.85888	301.5896	-157.107
13.01.2023	6.880477	-9.6123	-2.73183	32.2361	295.6396	-159.839
14.01.2023	7.310699	-9.2911	-1.9804	32.8626	304.6125	-161.819
15.01.2023	6.75632	-9.40721	-2.65089	32.01827	310.5917	-164.47
16.01.2023	5.632935	-8.73853	-3.10559	29.50381	312.775	-167.576
17.01.2023	5.731138	-8.87282	-3.14169	29.61488	375.1021	-170.718
18.01.2023	6.010998	-8.50034	-2.48934	30.53413	318.5875	-173.207
19.01.2023	5.487676	-9.22866	-3.74099	28.55096	398.8208	-176.948
20.01.2023	5.75188	-9.01076	-3.25888	28.6774	478.7792	-180.207
21.01.2023	5.4136	-7.67211	-2.25851	27.47842	297.0792	-182.465
22.01.2023	5.720487	-7.74638	-2.02589	28.53206	347.6167	-184.491
23.01.2023	5.765603	-6.71704	-0.95144	28.66075	265.8875	-185.443
24.01.2023	5.761612	-6.84147	-1.07986	29.11075	263.0146	-186.522
25.01.2023	5.635293	-6.65058	-1.01529	27.86719	321.9438	-187.538

26.01.2023	5.514912	-6.79689	-1.28198	27.37675	374.65	-188.82
27.01.2023	5.620018	-6.39337	-0.77336	28.98729	468.0833	-189.593
28.01.2023	5.782706	-6.22562	-0.44291	30.59581	397.6521	-190.036
29.01.2023	5.74787	-5.77393	-0.02606	30.68152	290.3813	-190.062
30.01.2023	5.607941	-5.77315	-0.16521	28.85869	387.9063	-190.227
31.01.2023	5.515882	-5.5348	-0.01892	27.10127	449.4292	-190.246
01.02.2023	5.488869	-4.87084	0.618025	26.3945	281.8083	-189.628
02.02.2023	5.503357	-4.88217	0.621186	26.9674	354.6333	-189.007
03.02.2023	5.507352	-4.70244	0.804912	29.18827	367.5417	-188.202
04.02.2023	5.514256	-4.89054	0.623711	31.30246	500.9063	-187.578
05.02.2023	5.514256	-4.67732	0.836936	31.84896	388.9396	-186.741
06.02.2023	5.514256	-4.69664	0.81762	30.72683	389.0875	-185.924
07.02.2023	5.514256	-4.75145	0.762805	31.48002	342.4854	-185.161
08.02.2023	5.514256	-4.80949	0.704769	32.00558	448.85	-184.456
09.02.2023	5.514256	-4.67171	0.842549	32.6674	426.0833	-183.614
10.02.2023	5.514256	-4.45471	1.059545	32.88525	312.0333	-182.554
11.02.2023	5.514256	-4.54468	0.969572	32.97631	314.6917	-181.585
12.02.2023	5.514256	-4.84373	0.670528	33.05181	390.8333	-180.914
13.02.2023	5.514256	-4.6403	0.87396	32.91769	371.625	-180.04
14.02.2023	5.514256	-4.46482	1.049439	32.9804	321.8146	-178.991
15.02.2023	5.514256	-4.69248	0.821774	33.13471	418.3125	-178.169
16.02.2023	5.230615	-4.17334	1.057271	33.16733	322.2438	-177.112
17.02.2023	3.500712	-0.20433	3.296383	34.27698	438.2167	-173.815
18.02.2023	3.107263	0	3.107263	33.96498	232.3708	-170.708
19.02.2023	3.104831	0	3.104831	33.97988	291.1729	-167.603
20.02.2023	3.167507	0	3.167507	34.74063	384.3	-164.436
21.02.2023	3.049248	0	3.049248	33.45021	286.7958	-161.386
22.02.2023	3.095374	0	3.095374	33.97513	375.6063	-158.291
23.02.2023	3.071046	0	3.071046	33.82021	443.6042	-155.22
24.02.2023	3.119144	0	3.119144	34.36217	258.1479	-152.101
25.02.2023	3.108003	0	3.108003	34.14473	339.4479	-148.993
26.02.2023	3.13251	0	3.13251	34.5584	341.5729	-145.86
27.02.2023	2.936883	0	2.936883	32.61679	465.375	-142.923
28.02.2023	1.953858	0	1.953858	30.78306	347.4545	-140.969

- AWD25N120

DOY	Reco_cum	GPP_cum	NEE_cum	Temp_air	PAR	NEE_cum_all
17.11.2022	1.534585	-3.68958	-2.15499	34.33619	737.2469	-2.15499
18.11.2022	2.204749	-4.02506	-1.82031	32.39498	353.3646	-3.97531
19.11.2022	2.222585	-3.81786	-1.59527	32.69825	460.45	-5.57058
20.11.2022	2.214086	-3.87512	-1.66103	32.31654	467.5792	-7.23161
21.11.2022	2.22773	-3.69873	-1.471	32.60385	350.9375	-8.70261
22.11.2022	2.246254	-3.72388	-1.47762	32.5495	434.8625	-10.1802
23.11.2022	2.284849	-3.84477	-1.55992	33.43465	467.2063	-11.7402
24.11.2022	2.5804	-3.82422	-1.24382	33.95129	439.9938	-12.984
25.11.2022	2.887571	-4.35361	-1.46604	34.11842	463.7104	-14.45
26.11.2022	3.19646	-4.65254	-1.45609	34.16477	455.9542	-15.9061
27.11.2022	3.484304	-4.98235	-1.49804	33.75563	530.4604	-17.4041
28.11.2022	3.782502	-5.16011	-1.37761	34.09098	476.2333	-18.7818
29.11.2022	4.040541	-4.80185	-0.76131	32.2944	323.1979	-19.5431
30.11.2022	4.288943	-5.2981	-1.00916	31.33044	343.7563	-20.5522
01.12.2022	4.588511	-5.59549	-1.00698	31.32883	403.1042	-21.5592
02.12.2022	4.901374	-6.00694	-1.10556	32.06329	351.4417	-22.6648
03.12.2022	5.21133	-6.06315	-0.85182	31.9616	350.3083	-23.5166
04.12.2022	5.463246	-6.52249	-1.05925	31.63819	397.3354	-24.5758
05.12.2022	5.558528	-6.85069	-1.29217	31.96156	415.0208	-25.868
06.12.2022	5.670119	-6.87796	-1.20784	33.13598	381.4396	-27.0758
07.12.2022	5.617578	-6.87746	-1.25988	31.59619	371.5729	-28.3357
08.12.2022	5.816811	-7.1265	-1.30969	32.95629	442.5521	-29.6454
09.12.2022	5.915647	-7.95362	-2.03798	32.86906	490.7792	-31.6834
10.12.2022	5.940452	-7.75677	-1.81632	32.12348	462.9167	-33.4997
11.12.2022	5.969379	-7.58417	-1.61479	32.27442	375.3979	-35.1145
12.12.2022	6.095297	-7.3476	-1.2523	32.29308	308.0833	-36.3668
13.12.2022	5.777695	-7.81429	-2.0366	31.21808	361.5792	-38.4034
14.12.2022	5.943669	-8.05849	-2.11482	31.69275	345.4896	-40.5182
15.12.2022	6.151669	-8.31326	-2.1616	31.99769	356.9688	-42.6798
16.12.2022	5.99694	-8.68636	-2.68942	30.86283	377.8125	-45.3692

17.12.2022	5.980103	-8.69788	-2.71778	30.43738	363.2479	-48.087
18.12.2022	5.601862	-9.30179	-3.69993	28.27348	374.3083	-51.7869
19.12.2022	5.498381	-9.14367	-3.64529	27.0076	387.6833	-55.4322
20.12.2022	5.622536	-9.5234	-3.90086	27.46944	432.3063	-59.3331
21.12.2022	5.976101	-9.42322	-3.44712	28.43029	396.8104	-62.7802
22.12.2022	6.004572	-10.3826	-4.37804	28.6376	485.8646	-67.1582
23.12.2022	5.406433	-9.73395	-4.32752	27.68644	349.9896	-71.4858
24.12.2022	5.837608	-9.52357	-3.68596	28.12631	341.449	-75.1717
25.12.2022	6.373532	-10.2965	-3.923	30.52881	473.6255	-79.0947
26.12.2022	6.677625	-11.1065	-4.42888	31.21283	492.4063	-83.5236
27.12.2022	6.808547	-10.1277	-3.31917	31.09127	326.4208	-86.8428
28.12.2022	6.494417	-10.6198	-4.12534	30.4314	347.5896	-90.9681
29.12.2022	6.985355	-10.5907	-3.60534	31.4046	334.5604	-94.5735
30.12.2022	7.198532	-10.5007	-3.30219	31.44523	311.4188	-97.8756
31.12.2022	7.245841	-11.5296	-4.28374	31.55704	344.375	-102.159
01.01.2023	7.475968	-12.4386	-4.96262	32.04063	384.8625	-107.122
02.01.2023	7.361372	-11.7905	-4.4291	31.78942	359.4604	-111.551
03.01.2023	7.220036	-12.1725	-4.9525	31.4395	358.4458	-116.504
04.01.2023	5.344333	-12.6149	-7.2706	28.84898	362.7021	-123.774
05.01.2023	5.549068	-12.5443	-6.99523	28.57669	361.4208	-130.769
06.01.2023	5.880588	-12.8675	-6.98695	28.47479	357.6563	-137.756
07.01.2023	7.16127	-12.8185	-5.65719	30.74685	340.7188	-143.414
08.01.2023	7.302649	-12.0882	-4.78552	31.37035	302.2938	-148.199
09.01.2023	6.338361	-12.0225	-5.68409	29.58152	329.3375	-153.883
10.01.2023	5.793823	-11.9166	-6.12282	27.80879	336.5646	-160.006
11.01.2023	6.4312	-11.6669	-5.23571	29.65225	318.8667	-165.242
12.01.2023	7.5055	-11.0695	-3.56403	31.85888	301.5896	-168.806
13.01.2023	7.584713	-10.6306	-3.04588	32.2361	295.6396	-171.852
14.01.2023	8.050134	-10.2646	-2.21448	32.8626	304.6125	-174.066
15.01.2023	7.421553	-10.3809	-2.95936	32.01827	310.5917	-177.025
16.01.2023	6.160743	-9.63123	-3.47049	29.50381	312.775	-180.496
17.01.2023	6.257253	-9.7685	-3.51125	29.61488	375.1021	-184.007
18.01.2023	6.555605	-9.34273	-2.78712	30.53413	318.5875	-186.794
19.01.2023	5.961532	-10.1326	-4.17107	28.55096	398.8208	-190.965

20.01.2023	6.242489	-9.88004	-3.63755	28.6774	478.7792	-194.603
21.01.2023	5.854018	-8.39291	-2.53889	27.47842	297.0792	-197.142
22.01.2023	6.182401	-8.46053	-2.27813	28.53206	347.6167	-199.42
23.01.2023	6.219926	-7.32082	-1.1009	28.66075	265.8875	-200.521
24.01.2023	6.202888	-7.43989	-1.237	29.11075	263.0146	-201.758
25.01.2023	6.049929	-7.21789	-1.16796	27.86719	321.9438	-202.926
26.01.2023	5.903569	-7.3618	-1.45823	27.37675	374.65	-204.384
27.01.2023	6.007749	-6.9075	-0.89975	28.98729	468.0833	-205.284
28.01.2023	6.17591	-6.70639	-0.53048	30.59581	397.6521	-205.814
29.01.2023	6.124599	-6.19742	-0.07282	30.68152	290.3813	-205.887
30.01.2023	5.956519	-6.17895	-0.22243	28.85869	387.9063	-206.11
31.01.2023	5.841628	-5.90135	-0.05973	27.10127	449.4292	-206.169
01.02.2023	5.799009	-5.16938	0.629626	26.3945	281.8083	-205.54
02.02.2023	5.802503	-5.15869	0.643817	26.9674	354.6333	-204.896
03.02.2023	5.797407	-4.94995	0.847457	29.18827	367.5417	-204.048
04.02.2023	5.804505	-5.14796	0.65655	31.30246	500.9063	-203.392
05.02.2023	5.804505	-4.92351	0.880997	31.84896	388.9396	-202.511
06.02.2023	5.804505	-4.94384	0.860664	30.72683	389.0875	-201.65
07.02.2023	5.804505	-5.00154	0.802964	31.48002	342.4854	-200.847
08.02.2023	5.804505	-5.06263	0.741874	32.00558	448.85	-200.105
09.02.2023	5.804505	-4.9176	0.886905	32.6674	426.0833	-199.218
10.02.2023	5.804505	-4.68918	1.115322	32.88525	312.0333	-198.103
11.02.2023	5.804505	-4.78389	1.020613	32.97631	314.6917	-197.082
12.02.2023	5.804505	-5.09867	0.705831	33.05181	390.8333	-196.377
13.02.2023	5.804505	-4.88454	0.91997	32.91769	371.625	-195.457
14.02.2023	5.804505	-4.69982	1.104685	32.9804	321.8146	-194.352
15.02.2023	5.804505	-4.93947	0.865037	33.13471	418.3125	-193.487
16.02.2023	5.486094	-4.39301	1.093089	33.16733	322.2438	-192.394
17.02.2023	3.538505	-0.21508	3.323421	34.27698	438.2167	-189.07
18.02.2023	3.107263	0	3.107263	33.96498	232.3708	-185.963
19.02.2023	3.104831	0	3.104831	33.97988	291.1729	-182.858
20.02.2023	3.167507	0	3.167507	34.74063	384.3	-179.691
21.02.2023	3.049248	0	3.049248	33.45021	286.7958	-176.642
22.02.2023	3.095374	0	3.095374	33.97513	375.6063	-173.546

23.02.2023	3.071046	0	3.071046	33.82021	443.6042	-170.475
24.02.2023	3.119144	0	3.119144	34.36217	258.1479	-167.356
25.02.2023	3.108003	0	3.108003	34.14473	339.4479	-164.248
26.02.2023	3.13251	0	3.13251	34.5584	341.5729	-161.116
27.02.2023	2.936883	0	2.936883	32.61679	465.375	-158.179
28.02.2023	1.953858	0	1.953858	30.78306	347.4545	-156.225